Faculté des Sciences
Département de Géographie
Unité de recherches SPHERES
Laboratoire de Climatologie et Topoclimatologie

Polar Surface Mass Balance in a Changing Climate: Reconstructions, Drivers, and Coupled Modeling Advances

A thesis submitted for the partial fulfilment
of the requirements for the academic degree of

Philosophiae Doctor in Sciences
at the University of Liège (College of Geography)
by

Damien Maure

Academic year 2025–2026

Jury members:

Brice Noël	President	Associate Professor FRS-FNRS, ULiège
Xavier Fettweis	Promoter	Professor, ULiège
Christoph Kittel	Co-promoter & Secretary	Postdoctoral Researcher FRS-FNRS, ULiège
Cécile Agosta		Researcher, CEA, LSCE, Paris Saclay
Charles Amory		Researcher, CNRS, IGE, UGA
Nicolas Jourdain		Senior Researcher, CNRS, IGE, UGA

List of abbreviations

20CRv3	20th Century Reanalysis v3
AIS	Antarctic Ice Sheet
AMO	Atlantic Multi-decadal Oscillation
AO	Arctic Oscillation
ASC	Antarctic Slope Current
ASL	Amundsen Sea Low
AWS	Automatic Weather Station
CDW	Circumpolar Deep Water
CRMSE	Centered Root Mean Squared Error
DJF	December-October-February
DU	Dobson Unit
EAWR	East Atlantic western Russia index
ECMWF	European Centre for Medium-Range Weather Forecasts
ERA5	ECMWF Reanalysis 5th generation
GBI	Greenland Blocking Index
GrIS	Greenland Ice Sheet
HPC	High Performance Computing
JJA	June-July-August
LWD	Longwave downwelling radiation
MAM	March-April-May
MAR	Modèle Atmosphérique Régional
ME	Surface Melt
MSLP	Mean sea level pressure
NAO	North Atlantic Oscillation
NEMO	Nucleus for European Modelling of the Ocean
NP	North Pacific Index
ODS	Ozone Depleting Substances
P2m	2-meters Pressure
PDO	Pacific Decadal Oscillation
PNA	Pacific North American index
POL	Polar Eurasian pattern
PR	Liquid Precipitation
r	Correlation Coefficient
R^2	Determination Coefficient
RMSE	Root Mean Squared Error
SAM	Southern Annular Mode
SCA	Scandinavian Pattern

SF	Solid Precipitation
SI3	Sea Ice modelling Integrated Initiative
SIA	Sea Ice Area
SIC	Sea Ice Concentration
SIE	Sea Ice Extent
SISVAT	Soil Ice Snow Vegetation Atmosphere Transfer
SLE	Sea Level Equivalent
SLR	Sea Level Rise
SMB	Surface Mass Balance
SO	Southern Oceans
SON	September-October-November
SP	Surface Pressure
SSC	Sea Surface Conditions
SST	Sea Surface Temperature
SU	Sublimation
SWD	Shortwave downwelling radiation
T2m	2-meters temperature
WP	West Pacific Pattern
WS	Windspeed

Contents

Part I

Polar regional modeling in a changing climate

CHAPTER 1

General introduction

1.1 General context

Humankind has already substantially altered the climate system, by rising the average temperature of the planet by 1.1°C (IPCC, 2023). While changes led by anthropogenic carbon emissions in Earth's radiative budget have been known for centuries (Arrhenius, 1896), and their consequences for decades, climate change has started to be a recurrent concern for the general population only a few years ago. The successive reports of the Intergovernmental Panel on Climate Change (IPCC) have synthesized and highlighted the strong link between human activity and the observed changes in the Earth's energy balance. The Sixth Assessment Report (AR6) confirms with high confidence that the current warming of 1.1 °C is entirely driven by anthropogenic greenhouse gas emissions, mainly carbon dioxide (CO_2), methane (CH_4), and nitrous oxide (N_2O). These gasses alter the radiative balance of the planet by trapping heat in the atmosphere, amplifying the greenhouse effect that naturally keeps Earth habitable - a process called 'Radiative Forcing'.

The carbon dioxide molecule (and all other green-house effect molecules) has an absorption band inside the black-body thermal emission radiative spectrum of the Earth. Consequently, with other atmospheric gasses, such as water vapor or methane, they absorb part of the outgoing photons from the surface, retaining energy. The molecules then de-excite themselves by re-emitting a photon in a random direction, including downwards, effectively "trapping" energy in the atmosphere (the process we call "Greenhouse effect"). This natural process is necessary for the emergence of life on Earth and keeping an habitable temperature at the surface. However, the problem lies in the imbalance of the energy budget when more of those greenhouse effect gasses are emitted into the atmosphere. Since the beginning of the industrial revolution, our societies have emitted 1.5 trillion tons of CO_2(Ritchie, 2019), increasing the concentration from 280 to 442 ppmv (Lan et al., 2023), effectively rising the radiative forcing by already 2.1 $W.m^2$.

Among many substantial threats to human societies caused by this added energy in the climate system, Sea Level Rise (SLR) is one of the slowest to appear and one of the processes with the most inertia. As of today, more than 600 million people live in low elevation costal zones (McMichael et al., 2020) and are prone to more intense flooding events or even total submersion, as we have already committed to 2.5 m of SLR (2.3mSLR.°C^{-1}) within the next 2000 years (Levermann et al., 2013). Consequently, understanding the rate at which the sea level will rise in the future comes from understanding the water budget and melting from continental ice - glaciers, ice caps and ice sheets - that account for more than 50% of this increase along with thermal expansion (IPCC, 2023).

In that regard, more than 99% of all continental ice on the planet is located at high latitudes - above (below) 70°N(S). The two major ice sheets of Greenland and Antarctica, hold a potential Sea Level Equivalent (SLE) of 7.42m and 57.9m, respectively. Understanding and monitoring the dynamics that governs polar climates, in link with the evolution of those ice giants is then crucial for human societies.

1.2 Polar climatology

The Arctic (respectively the Antarctic) is usually defined as the region North (South) of 66°34'N (S), a latitude defining the Arctic (Antarctic) polar circle. With no sunlight in winter and a very low incidence angle in summer, the polar regions receive 170Wm^2 of incoming shortwave radiation on average. This is less than half of the planet average, making them inherently the coldest places on Earth. Moreover, they are called "poles" because they are located around the Earth's axis of rotation. This has a strong influence on the polar climate, as the global atmospheric circulation is structured around strong zonal currents in between atmospheric cells. At the junction between the polar (between 90° and 60°) and the Ferrel (between 60° and 30°) lies the polar vortex, a very strong tropospheric and stratospheric eastward current that helps insulating the polar regions from the lower latitudes heat, enhancing their cold (and dry) climates. However, the two polar regions are very different, both from their geography and climate. As such, while the Antarctic can be defined as a continent surrounded by a zonally uninterrupted ocean, the Arctic is more of the opposite, with an ocean surrounded by land - a property illustrated by the Spilhaus Projection in Fig.1.1.

1.2.1 Arctic

The Arctic region is an ocean almost entirely surrounded by land, including Greenland, the Canadian Archipelago, Alaska, and the northern parts of Eurasia (Fig.1.2). It is connected to the Pacific through the narrow Bering Strait and to the Atlantic through the Fram Strait and the Barents Sea. This semi-enclosed ocean receives significant freshwater input from large rivers such as the Ob, Yenisei, and Mackenzie, which strongly influence its salinity and stratification. Sea ice covers much of the Arctic Ocean, especially in winter, and plays a central role in its climate system.

The Arctic climate is cold and highly seasonal, with long, dark winters and short, cool summers. Because of the surrounding land and oceanic gateways, the Arctic is strongly influenced by ocean–atmosphere interactions. Warm water inflow from the Atlantic through the Barents and Fram Straits, a process referred to as Arctic Atlantification, has intensified in recent decades, contributing to regional warming (Polyakov et al., 2023). This heat input works together with atmospheric circulation patterns to shape the variability of the region. The Arctic

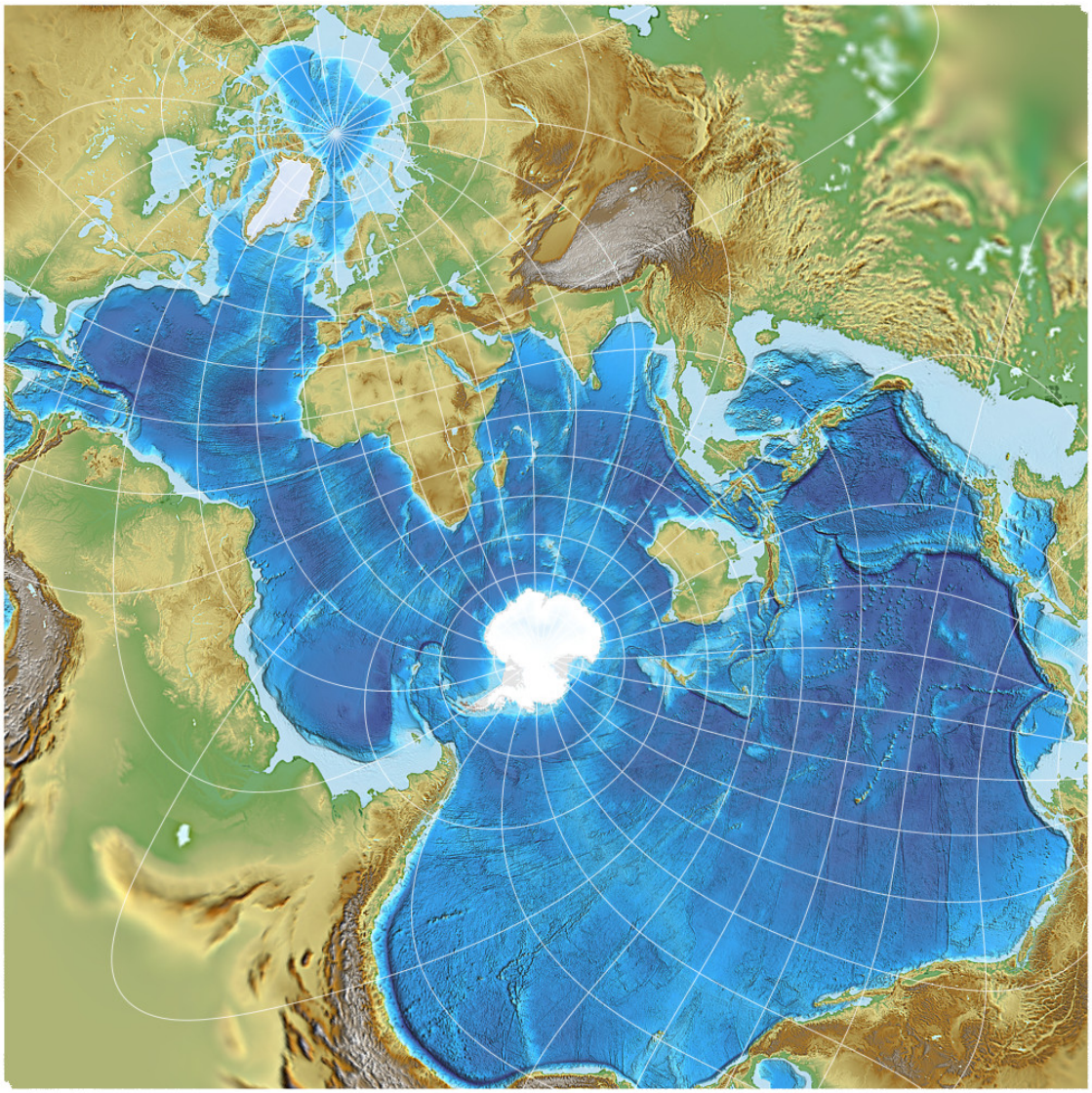

Figure 1.1: World oceans represented in the Spilhaus projection. The Antarctic can be seen surrounded by ocean in the middle while the Arctic Ocean is surrounded by land in the top left corner.

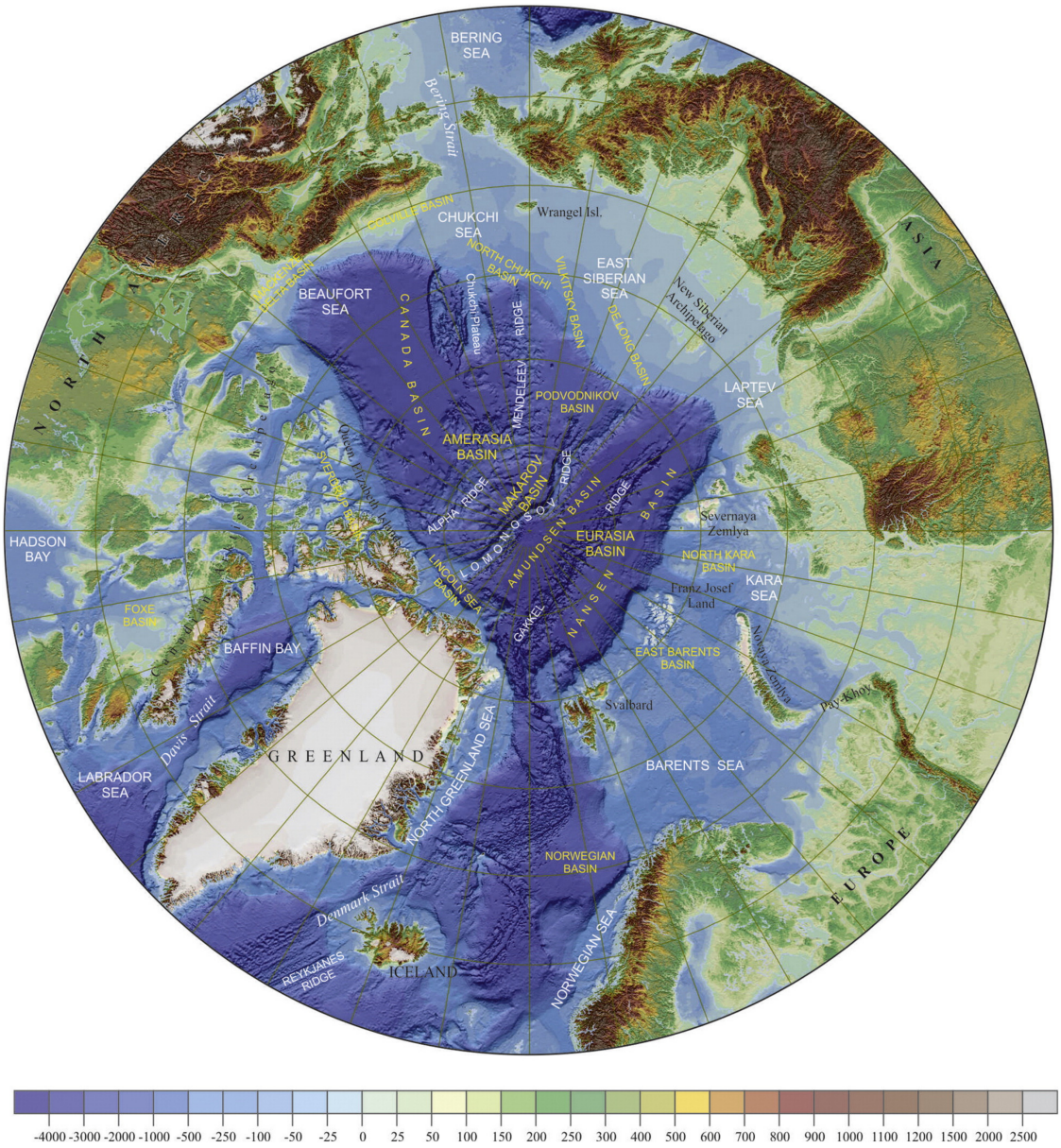

Figure 1.2: Physical map of the Arctic, with major sea names and points of interest. Colorscale shown topography and bathymetry in meters. Adapted from Petrov et al. (2016).

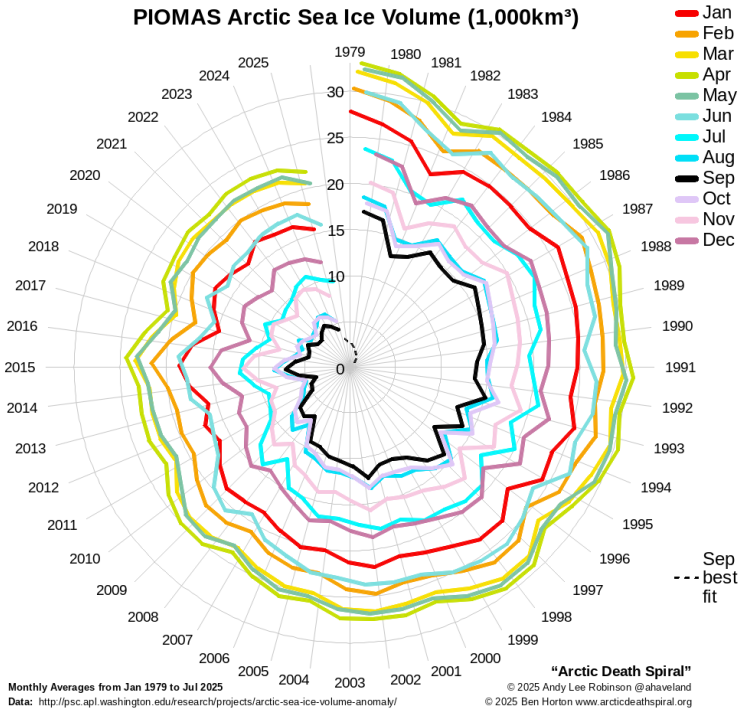

Figure 1.3: Monthly evolution of Arctic sea-ice volume (from PIOMASS) from 1979 to 2025. Color lines shows evolution for different months from 1979 to 2025. The decrease of sea-ice volume is remarkable across all seasons.

Oscillation (AO) is the dominant mode, controlling the strength of the polar vortex. In its positive phase, it traps cold air in the Arctic, while its negative phase allows cold air outbreaks at lower latitudes (Thompson and Wallace, 1998). Other large-scale patterns, such as the North Atlantic Oscillation (NAO), and teleconnections like ENSO and the AMO, also influence Arctic temperatures and precipitation (Overland et al., 2016).

Sea ice is a key component of the Arctic system because it reflects sunlight and reduces heat absorption. Over the last 40 years, sea ice extent has declined significantly, especially in late summer. The September minimum has decreased by about 13.5% per decade, while the winter maximum in March has dropped by around 2.8% per decade (Serreze and Meier, 2019). Ice thickness has also decreased (See Fig.1.3 for total volume evolution), with more than 95% of the oldest multi-year ice disappearing since the 1980s (Perovich et al., 2020). The loss of reflective ice surface exposes darker ocean water, which absorbs more solar energy and accelerates warming (a mechanism known as the ice–albedo feedback) (Pithan and Mauritsen, 2014).

One of the most prominent features of recent climate change is the Arctic amplification: the Arctic warms much faster than the global average. Between 1971 and 2017, the Arctic warmed by about 3.1°C in the cold season, over three times the global mean (Box et al., 2019). In some regions, such as the Barents Sea, the warming rate is up to seven times higher than the global average (Isaksen

et al., 2022). The main drivers of this amplification include the loss of sea ice and snow, increased ocean heat transport, and changes in atmospheric dynamics. These changes lead to faster melting of the Greenland Ice Sheet, permafrost thaw, and can influence weather extremes in mid-latitudes through altered jet stream patterns (Screen and Simmonds, 2010; Overland and Wang, 2018).

1.2.2 Antarctic

Antarctica lies at the opposite end of the Earth from the Arctic, and its geography is completely different. It is a vast continent surrounded by ocean, rather than an ocean surrounded by land. With a surface area of about 14 million km^2, it is more than 40% larger than Europe and is by far the highest continent on Earth, with an average elevation of 2,500 m due to its thick ice cover. The Antarctic Ice Sheet contains enough ice to raise global sea level by about 58 m if fully melted (Fretwell et al., 2013b). The ice is up to 4 km thick in places, and it flows outwards from the center towards the coast, where it forms floating ice shelves that fringe much of the continent. Antarctica is divided into three main regions: East Antarctica, which is the largest and most stable part; West Antarctica, which is smaller, lower, and more vulnerable to ocean-driven melting; and the Antarctic Peninsula, which extends north toward South America and experiences the mildest climate. These two major sectors, East and West Antarctica, are separated by the Transantarctic Mountains.

Antarctica was the last continent to be explored due to its remoteness and harsh conditions. In 1895, the 6th International Geographical Congress called for its scientific exploration, and expeditions continued until Roald Amundsen reached the South Pole in 1911. Today, more than 70 permanent research stations from 29 countries operate under the Antarctic Treaty System, which protects the continent for peaceful scientific purposes.

The Antarctic atmosphere is dominated by extreme cold, making it the coldest place on Earth. This is mainly due to the high albedo of its ice surface, which reflects most solar radiation, and the long polar night in winter. The isolation of the Antarctic climate is reinforced by strong circumpolar westerly winds and the polar vortex, which act as a barrier limiting the exchange of heat and moisture with lower latitudes (Marshall and Connolley, 2006). Over the ice sheet, strong radiative cooling creates a permanent surface-based temperature inversion, which in turn drives powerful katabatic winds. These winds flow downslope from the high plateau toward the coast, reaching average speeds of 10 m.s^{-1} and up to 20 m.s^{-1} during winter storms (Parish and Bromwich, 2007). They transport large amounts of snow toward the coast, enhancing blowing snow processes (Amory et al., 2020). Katabatic winds also play a major role in the ocean system by maintaining coastal polynyas, open-water areas that produce vast amounts of sea ice. When sea ice forms, it rejects brine, creating dense water that contributes to Antarctic Bottom Water formation and thus to global ocean circulation (Orsi et al., 1999).

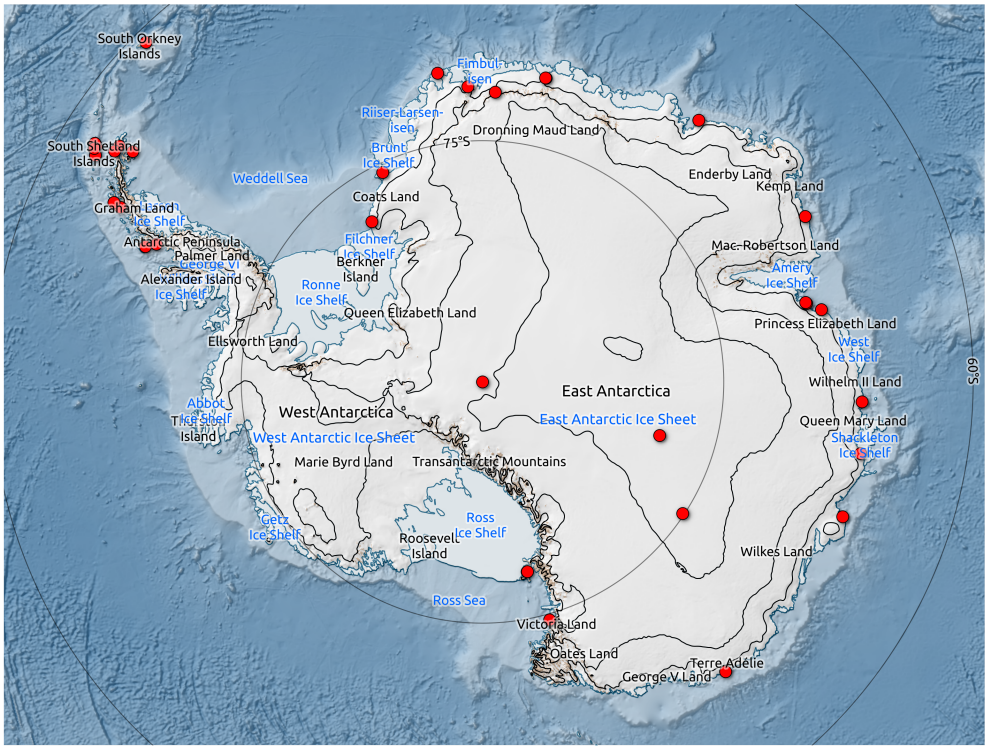

Figure 1.4: Geographical map of the Antarctic continent. Permanent research stations are shown as red dots. In black (blue) are written notable regions (Ice Shelves) names.

Antarctica is generally very dry, particularly in the interior, where precipitation can be less than 50 mm water equivalent per year (mmWE.yr), making it a polar desert. In contrast, coastal regions and the Peninsula receive much higher precipitation, often exceeding 500 mmWE.yr^{-1} (Arthern et al., 2006). The Peninsula has a milder and more humid climate because of its proximity to the Southern Ocean and frequent cyclonic systems. These depressions bring strong winds and heavy snowfall to the western side, while the eastern side often experiences foehn winds, causing rapid warming and occasional surface melting events (Cape et al., 2015). Although precipitation mainly falls as snow, rare rainfall events have been reported in coastal areas and the Peninsula, and they may become more frequent in a warming climate (Vignon et al., 2021).

Overall, the Antarctic climate is shaped by its isolation, strong winds, and very low temperatures. The continent plays a key role in the global climate system by influencing ocean circulation and acting as the planet's largest freshwater reservoir.

1.3 Ice Mass balance and Sea level rise

The total volume of land ice on Earth has been evolving and fluctuating over the course of thousands of years since their first appearance. It used to be mainly driven by millennial climate fluctuations, from Earth orbital parameters natural fluctuations that led to glacial and inter-glacial cycles. For any given ice mass, long term changes are the cumulated result of yearly anomalies - positive or negative - in its total ice Mass Balance (MB).

Over the course of a year, the MB of an ice body is the sum (Eq.1.1) of its 1) Surface Mass Balance (SMB), encompassing all positive and negative contributions occurring at the top layer of the ice mass, 2) discharge (D) - happening when the ice overflows from the continent over ocean and eventually breaks up - and 3) basal melting (M_{basal}) - mainly from ocean underneath the ice. The two latter parts of the MB are specific to floating ice-tongues and ice-shelves. In particular, they are the main source of negative contribution to MB in Antarctica. Thus:

$$MB = SMB - D - M_{basal} \tag{1.1}$$

M_{basal} also accounts for some refreezing below floating ice; and melting at the basal rocks / ice interface by geothermal heating and friction due to glacier dynamics. The latter is less impactfull and relevant than D and SMB, being orders of magnitude smaller (Mankoff et al., 2021). The MB evolution of all land ice on earth is linked with the sea level height (SLH), as MB loss (gain) results in more (less) water in the oceans. The exact computation is different for SLH as ice overflowing from the continent to the ocean at grounding lines immediately impacts SLH as soon as it starts to float (before melting or breaking up).

The SMB in itself (Eq.1.2) - what we will mainly be interested in part II of this manuscript - is composed of a positive, accumulation part; from solid (SF) and liquid (RF) precipitations (also deposition (DE) from blowing snow), and a negative part from snow erosion (ER), sublimation (SU) and meltwater runoff (RU). The latter is the whole meltwater (ME) production that does not refreeze as ice (RZ) or retained in the snowpack (RE), following:

$$SMB = SF + RF + DE - ER - SU - RU \tag{1.2}$$

and

$$RU = ME - RZ - RE \tag{1.3}$$

Historically, the Greenland Ice Sheet maintained near-equilibrium SMB, with snowfall compensating for surface melt and associated runoff. However, since the late 20th century, SMB has become increasingly negative. Regional climate model reconstructions indicate a strong downward trend in SMB from 1990 onward, driven by enhanced melt and runoff linked to atmospheric warming and persistent anticyclonic circulation anomalies (Mankoff et al., 2021; Fettweis et al., 2020). Post-2000, SMB loss has accelerated, contributing significantly to mass imbalance, as summer melt and runoff outpaced accumulation. As such, the Greenland SMB decreased from +450 Gt.yr^{-1} in the 1950s to +250 Gt.yr^{-1} in the 2010s.

Dynamic discharge—ice flux through outlet glaciers—has also increased since the 1990s. Glacier acceleration and retreat, particularly at Jakobshavn Isbræ, Helheim, and Kangerdlugssuaq, contributed substantially to the early 2000s mass loss peak (IMBIE, 2020). The relative importance of discharge has declined compared to SMB losses in the past decade, but still accounts for over 60% of Greenland's net mass loss (King et al., 2020), by rising from -375 Gt.yr^{-1} in the 1950s to -490 Gt.yr^{-1} in the 2010s (Mankoff et al., 2021) (Fig.1.5).

The Antarctic SMB is overwhelmingly positive, with very low melting rates. Recent SMB estimates are +2,329 ± 94 Gt.yr^{-1} (1987–2015) (Mottram et al., 2021). Melting mainly occurs over the Ice Shelves of the Peninsula, with 150 Gt.yr^{-1}, though the majority of the melt refreezes every year. This melting proportion is projected to increase over the Ice Shelves with future anthropic warming (Kittel et al., 2021a), while precipitation rates will also be rising over the continent. No clear consensus is found for the SMB prior to 1979, though studies point towards a continent-wide SMB increase over the 20$^{\text{th}}$ century (Thomas et al., 2008, 2017; Wang et al., 2021; Ekaykin et al., 2024; Philippe et al., 2016).

Antarctica's dominant mass loss mechanism is dynamic discharge, driven by basal melting beneath ice shelves and grounding line retreat (Fig.1.6). Observations from satellite altimetry and gravimetry show that West Antarctica (especially the Amundsen and Bellingshausen sectors) accounts for most dynamic losses, triggered by intrusions of warm Circumpolar Deep Water (Rignot et al., 2019). East Antarctica remains closer to balance but exhibits localized discharge accelerations (e.g. Totten Glacier, Li et al., 2015). These processes are sensitive to ocean forcing and are subject to tipping points. They lie at the interface

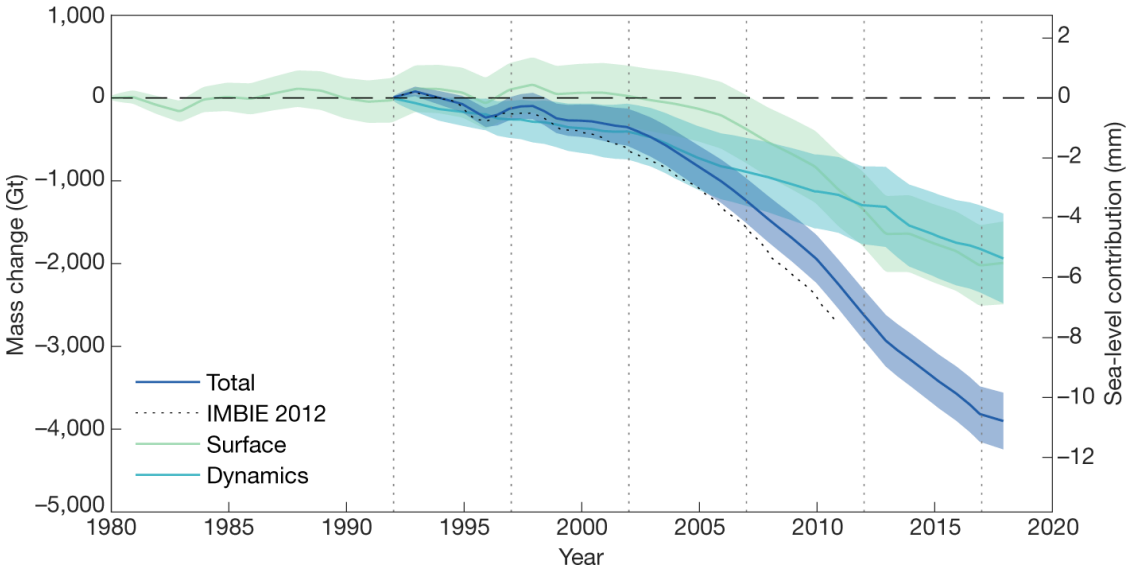

Figure 1.5: Cumulative Greenland MB evolution from surface (SMB) and dynamical (D) contributions estimates. (From IMBIE, 2020)

between ice-dynamics, oceanic projections of warm water intrusions below the shelves, and future atmospheric forcings guiding those oceanic currents; making future projections of MB highly uncertain.

Combined, Greenland and Antarctica contributed ∼1.3 mm.yr^{-1} to global mean SLR over 2012–2017, representing more than half of observed sea-level rise during this period (Rignot et al., 2011). Greenland's contribution is dominated by negative SMB, whereas Antarctica's is dominated by dynamic losses. Despite improved observations since the satellite era (post-1979), major uncertainties remain:

Historical Gaps: Sparse reconstructions of SMB before 1979, especially for Antarctica, limit the ability to quantify long-term variability and separate natural vs. anthropogenic drivers.

Regional Coverage: Arctic regions outside Greenland remain underrepresented in SMB reconstructions.

Process Representation: Future projections of MB are highly sensitive to oceanic forcings and Ice discharge.

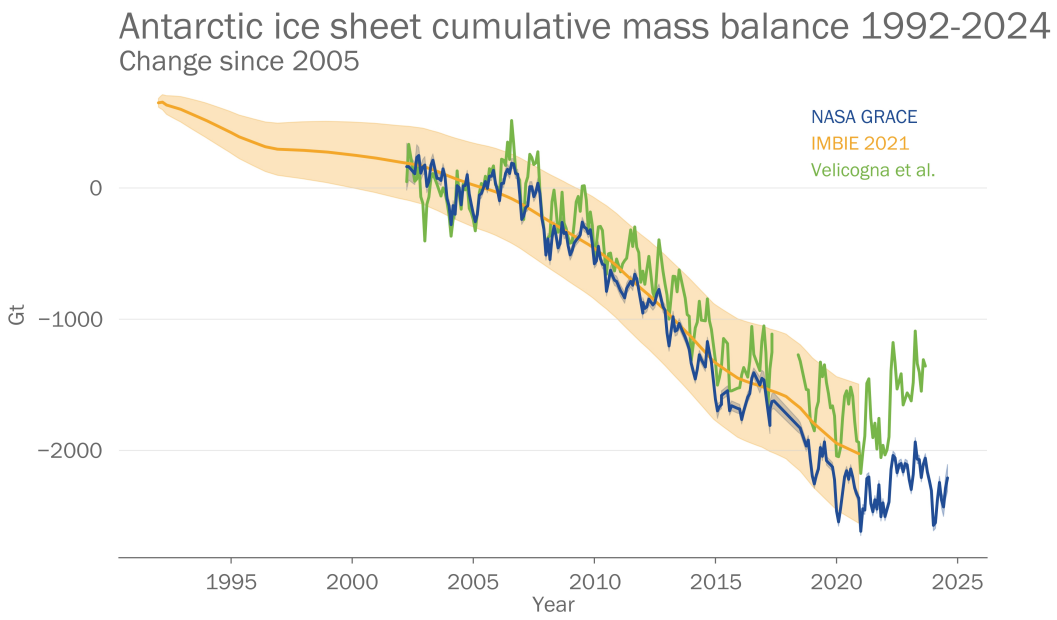

Figure 1.6: Monthly Antarctic ice sheet cumulative mass balance (Gt, difference from the 2005-2005 average) from 1992-2024. Data are from the following three data sets: NASA GRACE, IMBIE 2021, Velicogna et al.

1.4 Numerical modelling tools in the context of climate change

To understand and predict how the climate is changing, we use models. At the largest scale, Global Climate Models (GCMs) simulate the whole Earth system, including atmosphere, ocean, sea ice, and land. They are mainly used in two ways. First, in the form of reanalyses, where the model is constrained by observations (from satellites, weather stations, and other measurements) to produce a continuous and consistent picture of past climate - outputs that will be used throughout this manuscript. Second, in the form of projections, where the model is run forward in time using greenhouse gas concentration pathways, such as the Shared Socioeconomic Pathways (SSP) scenarios defined by the IPCC, to explore possible futures depending on hunmankind choices. However, GCMs usually have a coarse resolution and little snow/ice physics representation, making them less suitable for capturing regional processes.

For this reason, Regional Climate Models (RCMs) are used. These models take boundary conditions from GCMs and simulate the climate at higher resolution over a specific region, allowing a better representation of small-scale processes. This is particularly important for the polar regions, where the surface mass balance (SMB) of ice sheets depends on processes such as snowfall, melt, and refreezing that need fine spatial details. The outputs from RCMs, such as SMB fields, can then be used as inputs for Ice Sheet Models (ISMs), which simulate the flow of ice and its response to climate forcing. In the case of Antarctica, atmospheric

models (directly in GCMs or on a regional configuration) can also provide surface and atmospheric forcing for ocean models that are needed to estimate the melt of floating ice shelves. When combined, these tools allow us to assess how much water from the polar regions will eventually reach (or has reached) the oceans, giving estimates and projections of Sea Level Rise.

1.5 Challenges and contributions

Research in polar climatology—and particularly in regional climate modeling—faces a number of long-standing challenges that shape how we design simulations, interpret results, and understand the climate system.

Past uncertainties. Our view of past climate conditions is still limited by sparse and uneven observations, especially in high-latitude regions. Before the satellite era, measurements of snowfall, temperature, or wind were patchy and often inconsistent. Multiple reanalysis datasets helps filling these gaps, but they still inherit the limitations of the underlying observations. As a result, a key task is to evaluate how well our models reproduce past conditions and to distinguish real climate signals from artefacts linked to data scarcity or assimilation methods.

Physical representation. Modern RCMs and GCMs simulate large-scale circulation reasonably well, but several important local processes remain difficult to represent. These include interactions between the ocean, sea ice, and atmosphere; the formation and breakup of polynyas; and the behaviour of near-surface atmospheric layers under very stable conditions. Regional models provide flexibility to test new parameterizations, but they are still evolving. In particular, MAR is not interactively coupled to the ocean or sea ice: it is forced over the ocean using external datasets for sea-surface temperature and sea-ice concentration. As a result, MAR cannot represent the two-way feedbacks that occur between the atmosphere, the ocean, and the sea ice, which can influence coastal heat fluxes and surface mass balance.

Resolution constraints. Even with modern computing resources, spatial resolution remains a compromise. Many processes that strongly influence surface mass balance—such as local wind channeling, blowing-snow redistribution, small-scale melt–refreeze cycles, and sharp topographic gradients—occur at scales finer than those resolved by typical regional climate grids. Increasing resolution is therefore not just a technical improvement: it is often necessary to capture the processes that shape SMB and to provide more realistic boundary conditions for ice-sheet models.

Understanding system behaviour. Even when data and model performance improve, the climate system remains complex. Teleconnections, feedback loops, and nonlinear responses make it difficult to assign simple causes to observed changes. Producing realistic simulations is only part of the goal; understanding the processes that create variability across regions, seasons, and decades is important.

Guided by these challenges, the contributions of this thesis aim to improve both the reconstruction and understanding of polar surface mass balance, while also advancing the modeling tools used to investigate it. The following sections summarize these contributions.

Hindcast products developed

Dynamically reconstructed SMB products are constantly improving, and discrepancies between studies remain among the community. These products remain crucial for precise forcings of the ice-dynamics models and for sea level rise attribution.

Contributions

- The SMB of numerous Russian Arctic Islands is dynamically reconstructed for the first time
- A unified product of all the Arctic land ice SMB at a 6km resolution from 1958 to 1979 is proposed
- A reconstruction of the Antarctic SMB before the satellite era is presented, at a 4 km resolution

Surface Mass Balance evolution analysis

Starting from the hindcast datasets mentioned above, properly assessing and understanding the SMB evolutions of those land ice is crucial for a clear representation of what they are experiencing.

Contributions

- Documented a clear geographical contrast in the past SMB evolution of the Arctic land-ice
- Highlighted a strong increase in the Antarctic SMB during the 1970s.

Mechanism and teleconnections

In a complex, multi-disciplinary domain such as climate sciences, identifying drivers of changes and links between variables is a way to better understand the system. It is essential to improve our understanding of how the climate can react to systemic future changes, say anthropogenic warming, for example.

Contributions

- Highlighted the influence of stratospheric ozone depletion in the SMB of the Antarctic ice sheet.
- Identified an anthropogenic warming melting compensation by increased snowfall rates over the Russian Arctic
- Identified different correlated drives of the SMB evolution heterogeneity over the Arctic

Numerical modelling

Numerical modeling is constantly evolving and improved. In particular, the models used during this PhD have changed substantially since its beginning. The contributions of this thesis in filling the model-improvement barrel of the Danaids are not fully developed in this manuscript, but are mentioned below.

Contributions

- Identified a latent heat bias near the oceanic borders of MAR
- Participated in a RCM intercomparison over Antarctica under the PolarRES poject
- Corrected a handful of bugs in the MAR-NEMO coupling interface
- Managed to setup a working framework on the Walloon Tier-1 HPCs for non-domain dependent MAR-NEMO coupling
- Participated in a model inter-comparison of Antarctic sea-ice albedo representation with MAR and NEMO

1.6 Structure of the Thesis and Research Questions

This thesis is organized into three main parts. This first one is an introduction to polar climatology, the importance of polar regions in the global system, as well as an introduction to regional atmosphere modeling in those areas. The two other parts each address a complementary aspect of polar SMB and its controlling processes. The overarching objective is to improve our understanding of the mechanisms driving past and present SMB variability in the Arctic and Antarctic, and to advance modeling capabilities for projections. The second part (Part II) focuses on quantifying and explaining historical SMB changes across polar regions during the second half of the 20th century and early 21st century, whereas the third part (Part III) explores the physical processes at the ocean–sea ice–atmosphere interface and lays the ground to a fully coupled modeling framework to better capture these interactions.

Part I – Polar regional modeling in a changing climate

This **Chapter 1** aims to present the context of this thesis. It describes the importance of polar climates in the global system and their recent changes, emphasizing the importance of SMB past and future evolutions in light of sea level rise.

Chapter 2 then details the modeling framework adopted throughout the thesis. It provides a technical description of the Modèle Atmosphérique Régional (MAR), a regional climate model optimized for polar applications. The chapter covers MAR physical parameterizations, snow and energy balance schemes, treatment of atmosphere–surface interactions, and boundaries forcing using reanalysis products.

Part II – Quantifying and Understanding Past SMB Variability

The second half of the 20th century and the early 21st century have witnessed profound changes in the polar cryosphere, but these changes have not occurred uniformly across regions. Part II investigates how Arctic and Antarctic SMB have evolved over the past decades, what processes explain these changes, and how robustly they can be reconstructed from available data and models.

Chapter 3 examines the Arctic, a region that has warmed nearly four times faster than the global average since 1979 (Box et al., 2019). This amplified warming has intensified glacier and ice cap melt, yet the magnitude and drivers of SMB changes vary markedly across Arctic sub-regions (Noël et al., 2018, 2022). Using high-resolution (6 km) simulations with the Modèle Atmosphérique Régional (MAR), this chapter provides a unified SMB dataset from 1950 to the present for all major Arctic land ice domains, including Greenland, Svalbard, the Canadian Arctic, and the Russian High Arctic. The analysis addresses several questions:

- How has SMB evolved since 1950 across these regions - especially the Russian High Arctic, where no similar study is available - and to what extent does Arctic amplification translate into regional variability?
- How reliable are these reconstructions in regions with sparse observational data, and how do they compare with analogous studies?
- Which large-scale circulation patterns, such as persistent blocking highs or North Atlantic cooling, explain the heterogeneity in observed trends?

Chapter 4 shifts the focus to Antarctica, where the SMB response to climate forcing is less intuitive. Contrary to the widespread expectation that anthropogenic warming accelerates mass loss, the Antarctic ice sheet seems to have experienced a SMB increase during the late 20th century (Thomas et al., 2008; Medley and Thomas, 2019a). This chapter reconstructs Antarctic SMB from 1958 to 2020 using MAR forced by multiple atmospheric reanalysis datasets,

assessing uncertainties before the satellite era and identifying dominant drivers of its variability. A particular emphasis is placed on the role of stratospheric ozone depletion, which intensified the Southern Annular Mode, deepening the Amundsen Sea Low and changing precipitation patterns. This raises several questions:

- How robust is the SMB increase reconstructed, and how does it compare with ice core observations?
- What is the relative importance of ozone depletion versus other potential drivers such as sea-ice changes or ocean variability?
- How did these circulation changes enable Antarctica to act as a transient buffer of global sea-level rise?

Part III – Constraining Climate Processes Controlling SMB

Building on the historical reconstructions of Part II, Part III explores the coupled processes that can control SMB and their representation in regional models. The atmosphere, ocean, and sea ice form an interconnected system in which feedbacks can amplify or dampen SMB changes. Yet, these feedbacks remain poorly resolved in standalone models, which lack the ability to simulate interactive energy and moisture exchanges across components.

Chapter 5 addresses this gap by developing and evaluating a fully coupled regional modeling framework that links MAR with the NEMO–SI³ ocean–sea ice system through the OASIS3-MCT coupler. This chapter documents the implementation, sensitivity tests, and challenges encountered in reproducing stable coupled simulations for Antarctica, with parallel development for the Arctic. It seeks to answer key questions such as:

- Why is a coupled system necessary to accurately capture polar feedbacks?
- How do biases in individual components (e.g., MAR radiative fluxes) propagate into coupled simulations, and what mechanisms drive energy imbalances?
- What lessons can be drawn from contrasting results in the Arctic (stable) and Antarctic (unstable) configurations?

Chapter 6 adds complementary elements on the Ocean-Ice system of Antarctica, as a preliminary for more complete studies in the future using the coupled system of the previous chapter.

Finally, **Part IV - Chapter 7** summarizes the conclusions of each chapter and examines doorways for future research.

CHAPTER 2

Methods and data

This chapter consists of a general description of the regional climate model MAR and its main components (Section 2.1) that was used in this thesis. This chapter also describes the data sets that were used to force MAR, from large-scale forcing to sea surface conditions.

Throughout this manuscript, different versions of MAR are used, MARv.3.11 and MARv3.13-3.14 notably. The specifications of every version are detailed inside each concerned chapter. For clarity, we use the abbreviation MAR for every version of the model.

2.1 MAR regional climate model

RCMs are numerical tools designed to simulate atmospheric and surface processes over a limited spatial domain at higher resolution than GCMs, while being driven at their lateral boundaries by large-scale meteorological fields. By nesting a high-resolution model within coarser GCM or reanalysis data, RCMs can explicitly resolve finer-scale topography, coastlines, and land–atmosphere interactions, and can apply more detailed parameterizations for processes such as cloud microphysics, radiation, and surface fluxes. This makes them particularly valuable for investigating regional climate variability, extreme events, and detailed surface–atmosphere coupling in cryospheric regions.

The Modèle Atmosphérique Régional (MAR) is an RCM specifically developed for polar and mountainous environments, with a strong emphasis on coupling between atmospheric dynamics and detailed snow and ice surface processes (Gallée and Schayes, 1994; Fettweis et al., 2017). Originally designed to study the Greenland and Antarctic ice sheets, MAR has also been applied to high-altitude glaciers and other cold climate systems (Damseaux et al., 2019; Beaumet et al., 2021). It combines a hydrostatic dynamical core with physically based parameterizations tailored for cold regions, including explicit treatment of snow metamorphism, surface albedo evolution, and interactions between wind, temperature, and surface mass balance.

MAR operates on a limited-area grid using terrain-following vertical coordinates, with atmospheric boundary conditions provided by GCMs or reanalyses. Its architecture allows for flexible horizontal resolutions (typically 5–25 km) and vertical layering optimized for polar boundary layers. The model is composed of distinct yet interacting modules, including the atmospheric dynamical core, cloud microphysics, shortwave and longwave radiative transfer, and the surface module (SISVAT) that handles snow, ice, vegetation, and soil processes (See Fig.2.1). These modules are coupled at each time step, enabling two-way interactions between the atmosphere and the underlying surface.

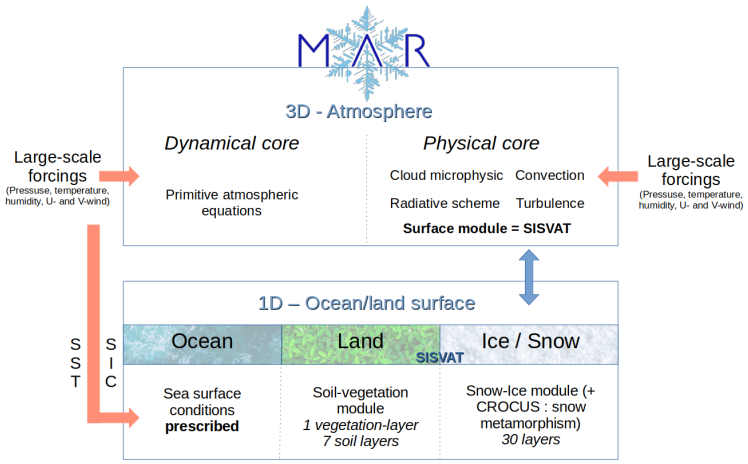

Figure 2.1: MAR - SISVAT diagram representing modules and interactions (Courtesy of A. Delhasse).

In the following subsections, we detail the governing equations and parameterizations used in MAR, focusing on the physical schemes most relevant to polar climate applications. For extensive details, we refer to Kittel (2021), Chapter 2.

2.1.1 Dynamical Core

The primitive equations driving MAR, that are directly derived from Navier-Stokes equations are described in Gallée and Schayes (1994). It is based on the hydrostatic approximation, meaning that the vertical pressure gradient force is assumed to be exactly balanced by the weight of overlying air:

$$\frac{\partial p}{\partial z} = -\rho g$$

where p is pressure, z is height, ρ is the air density and g the gravitational acceleration. It solves the momentum conservation equation along terrain-flowing vertical coordinates - pressure based normalized σ levels, where $\sigma = (p - p_{top})/(p_s - p_{top})$, p_{top} and p_s being respectively the pressure at the top and the surface of the domain. In such a framework, the vertical velocity w of air masses (in σ coordinates) is neglected in the equations, and is only diagnosed indirectly from the continuity equations of the horizontal fields. This approximation is not suitable as soon as vertical uplift becomes significant because of convection. Fortunately, this is managed by a separated module that implicitly represents convective events.

Numerically, the scheme used is a leap-frog (second order) integration in time space, and a centered fourth-order scheme in space. The advection of air masses properties is achieved by a semi-Lagrangian scheme by Seibert and Morariu (1991).

2.1.2 Surface and snow module

One of the main strengths of MAR is its ability to represent complex snow-pack representation and evolution. This surface layer is represented the 1-D scheme SISVAT (Soil Ice Snow Vegetation Atmosphere Transfer) module, containing sub-modules for soil and vegetation (Ridder and Schayes, 1997), snow (Gallée et al., 2001) and ice (Lefebre et al., 2003).

Every sub-module can be called at every MAR pixel: the mass and energy fluxes computed for each surface type are balanced as a function of the area percentage of each surface type in the corresponding pixel. Oceanic pixels have two sub-pixels, open-ocean and ice-covered. The polar configurations used in this manuscript are of two types for continental pixels: ice and tundra (Fettweis et al., 2013) for Arctic domains, ice and permanent rocks for the Antarctic.

SISVAT is forced by the lowest atmospheric layer of MAR, with temperature, humidity, precipitation, wind speed and radiative energy fluxes to compute downwards and upwards mass and energy fluxes from every sub-pixels. Its snow and ice module is made from a former version of CROCUS (Brun et al., 1989) that includes snow metamorphism on top of temperature, on top of which liquid water content and density evolution were added.

2.1.3 Microphysics module

MAR employs a detailed cloud microphysics scheme that solves conservation equations for five water species—cloud droplets (q_w), ice crystals (q_i), raindrops (q_r), snow particles (q_s), and water vapor (q_v)—as well as the ice crystal number concentration (n_i) (Gallée et al., 1995). These equations are solved at every horizontal grid point and vertical σ-level according to:

$$\frac{\partial q_\alpha}{\partial t} = -u\frac{\partial q_\alpha}{\partial x} - v\frac{\partial q_\alpha}{\partial y} + \dot{\sigma}\frac{\partial q_\alpha}{\partial \sigma} + F_{q_\alpha} + P_{q_\alpha}(+P_{\text{sed}}), \tag{2.1}$$

where the first three terms represent advection in the x, y, and σ directions, F_{q_α} denotes turbulent flux divergence, and P_{q_α} represents microphysical source/sink processes. The additional term P_{sed} accounts for sedimentation of precipitating hydrometeors (rain, snow, and ice) based on their fall velocities.

The microphysical scheme considers 21 processes, including condensation, evaporation, nucleation, aggregation, and accretion. These processes, originally based on the parameterizations of Kessler (1969) and later adapted by Gallée et al. (1995), govern interactions among the different hydrometeor species. Since graupel is not explicitly represented, processes that would normally form graupel instead produce snowflakes, assuming a Marshall–Palmer size distribution (Marshall and Palmer, 1948).

Several improvements have been introduced since the original scheme. The ice nucleation parameterization by Lin et al. (1983), which tended to overestimate

Table 2.1: Main microphysical processes represented in MAR (adapted from Gallée et al. (1995))

- Phase changes: condensation, evaporation, sublimation, freezing, and melting
- Droplet autoconversion and rain formation
- Aggregation and accretion among hydrometeors
- Deposition and sublimation on ice and snow
- Sedimentation of rain, snow, and ice particles

ice crystal numbers and underestimate downwelling solar radiation, CAPE, and rainfall (Messager et al., 2004), has been replaced by the approach of Meyers et al. (1992) and refined by Prenni et al. (2007). Ice crystal sedimentation is now explicitly modeled with a prognostic equation for n_i following Levkov and Rockel (1992). The autoconversion of cloud droplets to rain adopts the Sundqvist parameterization, which uses a critical cloud water mixing ratio (q_{w0}) and an autoconversion timescale (C_0). In MARv3.11, these are set to $q_{w0} = 10^{-3}$ kg kg^{-1} and $C_0 = 10^{-4}$. Additional tuning, such as adjustments to snowfall sedimentation velocity and cloud lifetime, has improved the model's ability to simulate cloud processes over polar ice sheets (Fettweis et al., 2017, 2020).

2.1.4 Radiative Scheme

MAR simulates the exchange of energy between the atmosphere and the surface through radiation. It treats shortwave (solar) and longwave (thermal) radiation separately, using a two-stream approach first described in Gallée and Schayes (1994). This method follows the upward and downward radiation through the atmosphere.

Radiation is absorbed and scattered by atmospheric gases, clouds, and aerosols. Water vapor, carbon dioxide, and ozone absorb part of the energy, while clouds both reflect and emit radiation. Their optical properties depend on the amount of cloud water and ice, and these are provided by the microphysics module. Surface albedo comes from SISVAT and changes with snow grain size, impurities, meltwater, and illumination. In this way, the radiative scheme interacts with both the atmosphere and the surface. The heating rates it produces directly affect air temperature and surface energy balance at each time step.

Since MAR v3.14, the ecRad radiation scheme from ECMWF has been included as an alternative option (Grailet et al., 2025). ecRad offers a more modern treatment of gas absorption and cloud–radiation interactions, with an increased spectral resolution at a lighter computational cost.

2.1.5 Boundaries & nudging

Being a limited-area model, MAR has to be forced at its lateral boundaries by GCMs output fields. To transition from prescribed large scale forcings (where the RCM is fixed) to a freely evolving model, a transition area of (usually) 7 pixels - the relaxation zone - progressively decreases the influence of the forcing inwards. This lateral nudging process is described in Marbaix et al. (2003).

MAR is also forced at its top boundary: because of larger and larger integration domains, it is now able to create its own synoptic circulation and drift away from prescribed large-scale fields. To prevent this, u,v and temperature fields of the few top σ layers are nudged towards forcing fields following van de Berg and Medley (2016) - the exact number of nudged layers depends on the size of the MAR grid.

Reanalyses combine observations with numerical weather prediction models through data assimilation to produce a physically consistent estimate of past atmospheric states. Despite major improvements in observational systems since the introduction of satellite data in 1979, the Antarctic Ice Sheet (AIS) remains one of the most poorly observed regions on Earth. Harsh environmental conditions, logistical challenges for station maintenance, polar night, and the difficulty of distinguishing clouds over snow-covered surfaces limit the availability and accuracy of observations. This results in sparse assimilation data and contributes to large uncertainties in reanalyses over Antarctica, especially prior to the satellite era.

In this study, we use two state-of-the-art reanalyses: ERA5 from the European Centre for Medium-Range Weather Forecasts (ECMWF) and 20th Century Reanalysis version 3 (20CRv3) from NOAA. ERA5 (Hersbach et al., 2020b) is the latest ECMWF reanalysis and successor to ERA-Interim. It provides global coverage at ∼0.3°horizontal resolution (≈ 9 km × 27 km at 70°S) with 137 vertical levels up to 0.01 hPa, and hourly output. ERA5 uses a 4D-Var data assimilation system and ingests a wider range of observations than its predecessor, including improved satellite data streams. It is available from 1950 to near-real time; however, 6-hourly fields needed to force regional climate models are considered most reliable after 1979. Studies have shown ERA5 improves the representation of Antarctic climate compared to ERA-Interim (Gossart et al., 2019; Vignon et al., 2019), particularly for atmospheric circulation and moisture transport, though some regional biases remain (e.g., Antarctic Peninsula, Hillebrand et al., 2021).

20CRv3 (Slivinski et al., 2019a) provides the longest global reanalysis available, spanning 1836 to the present. Unlike ERA5, it assimilates only surface pressure observations along with monthly sea-surface temperature and sea ice distributions, using an ensemble Kalman filter to generate a 80-member ensemble and quantify uncertainties. Its coarse horizontal resolution (∼1°) and reliance on sparse surface data in the high southern latitudes make it less constrained over Antarctica. Nevertheless, 20CRv3 is widely used for long-term climate variability studies due to its century-long coverage and uncertainty estimates.

ERA5 is used to force MAR in Chapter 3 and 4. It is also used to force NEMO and MAR in Chapter 5 and 6. 20CRv3 is used in Chapter 4 as a satellite-free alternative to ERA5.

Part II

Quantify and understand past surface mass balances of polar ice caps and their variability

CHAPTER 3

Contrasting effect of climate warming on the Arctic land ice

Following: **Maure, D.**, Kittel, C., Lambin, C., Delhasse, A., and Fettweis, X.: Spatially heterogeneous effect of climate warming on the Arctic land ice, The Cryosphere, published, 2023.

Abstract Global warming has already substantially altered the Arctic cryosphere. Due to the Arctic warming amplification, the temperature is increasing more strongly leading to pervasive changes in this area. Recent years were notably marked by melt records over the Greenland Ice Sheet while other regions such as Svalbard seem to remain less influenced. This raises the question of the current state of the Greenland Ice Sheet and the various ice caps in the Arctic for which few studies are available. We here run the Regional Climate Model (RCM) Modèle Atmosphérique Régional (MAR) at a resolution of 6 km over 4 different domains covering all Arctic land ice to produce a unified Surface Mass Balance product from 1950 to present day. We also compare our results to large-scale indices to better understand the heterogeneity of the evolutions across the Arctic and their links to recent climate change. We find a sharp decrease of Surface Mass Balance (SMB) over the western Arctic (Canada and Greenland), in relationship with the atmospheric blocking situations that have become more frequent in summer, resulting in a 41% increase of the melt rate since 1950. This increase is not seen over the Russian Arctic permanent ice areas, where melt rates have increased by only 3% on average, illustrating a heterogeneity in the Arctic SMB response to global warming.

3.1 Introduction

The warming amplification of the Arctic has led to a temperature rise of +3.8 degrees on average poleward of 66.5°N since 1979, 4 times larger than the global average (Rantanen et al., 2022). While this warming contributes to a higher melting rate of glaciers and ice caps (e.g., Fettweis et al., 2017; Noël et al., 2018), it has also raised the atmospheric humidity leading to more solid precipitation in winter (Przybylak, 2002; Førland et al., 2002). In combination with large-scale atmospheric circulation variations, changes in average melting and precipitation rates modify the surface mass balance (SMB) of the Arctic land ice i.e the Greenland Ice Sheet, Arctic ice caps and major perificial glaciers.

The SMB is the difference between the total amount of precipitation (solid and liquid) plus condensation/riming and the ablation by meltwater runoff and evaporation/sublimation. It is a component of the total ice mass budget of

permanent ice areas together with the ice discharge driven by the ice dynamics. Note that the definition we use as SMB is formerly defined as Climatic Mass Balance in Cogley et al. (2010). However, the Arctic SMB is more sensitive to seasonal climate variations and its importance in the total mass budget is expected to increase relative to the ice discharge, at least over the Greenland Ice Sheet (Fürst et al., 2015). Furthermore, the combined Arctic permanent ice areas (excluding the Greenland Ice Sheet) are the major contributor to sea level rise after the ice sheets (Gardner et al., 2013; Moon et al., 2020).

While the warming trend is global, the different studies carried over the Arctic indicate a regional heterogeneity in the response of SMB to the climate of the last decade. The higher frequency of blocking anticyclonic events has increased the summer melt rate over the Greenland Ice Sheet or Canadian ice caps (Fettweis et al., 2013; Lenaerts et al., 2013; Noël et al., 2018; Fettweis et al., 2017; Topál et al., 2022; Rajewicz and Marshall, 2014). On the contrary, recent North Atlantic cooling has decreased glacier mass loss rates in Iceland (Noël et al., 2022). In Svalbard, most studies indicate a significant negative mass balance trend in recent decades (e.g. Schuler et al., 2020; Van Pelt et al., 2019), although Lang et al. (2015) found a stable mass balance instead.

High-resolution dynamical downscaling has enhanced the estimations of SMB across the Arctic by providing continuous results in space and time compared to in situ observations (and satellite data). However, a unified estimate is still lacking over all the permanent land ice areas of the Arctic using the same method. Moreover, SMB estimates over the Russian High Arctic remain very scarce. Here, we present the results from a series of dynamical downscaling simulations, at high resolution (6km), covering all the Arctic regions with permanent Arctic land ice (Baffin, Devon, Ellesmere, Iceland, Svalbard, Greenland, Franz Joseph Land, Novaya Zemlya and the Russian High Arctic Islands), using the Modèle Atmosphérique Régional (MAR) Regional Climate Model (RCM). Aims of the study are to 1) present a unified SMB product derived through the same method over all the Arctic, and to 2) highlight the links between SMB changes over different regions and general climate patterns.

3.2 Methods

3.2.1 MAR

MAR is a 3D atmosphere-snowpack RCM initially designed for polar regions (Gallée and Schayes, 1994). It has been used in multiple studies and proven to be reliable to reconstruct the recent SMB changes over the Greenland (Fettweis et al., 2017, 2020) and Antarctic (Agosta et al., 2019a) ice sheets or smaller ice caps (Svalbard, Lang et al., 2015).

MAR resolves the primitive equations using the hydrostatic approximation and has a vertical sigma coordinate system. MAR also includes the 1D surface scheme SISVAT (Soil Ice Snow Vegetation Atmosphere Transfer; De Ridder and Gallée, 1998; Ridder and Schayes, 1997; Gallée and Duynkerke, 1997; Gallée et al., 2001; Lefebre et al., 2003) which describes the surface properties and their evolution through their interactions with the atmosphere. The snow/ice module of SISVAT describes the snowpack metamorphism and properties (such as temperature, liquid water content and density) of the 20 first meters of permanent ice areas divided into 30 layers of snow, firn or ice. Since MAR is here not coupled with an ice sheet model, the topography and ice extent are fixed in the model throughout the entire simulations. Pixels are considered as ice-covered only if they have at least 50% of their area covered by ice.

In this study, MAR version 3.11.5 (hereafter MARv3.11.5) is used to reconstruct SMB changes over the Arctic ice caps and ice sheet. The improvements of this version are described in Kittel et al. (2021b). A general summary of the modules and schemes used in MAR can also be found in Fettweis et al. (2017). Fig.3.1 presents the 4 integration domains (without the relaxation zone) used to run MAR over all the permanent Arctic ice areas, at a 6-km horizontal resolution using 24 vertical layers in atmosphere with a first level at 2 meters above surface. We used 4 different integration domains in order to reduce the computational cost of a 70-years-long simulation, enabling for such a high horizontal resolution. The model parameters and set-up are kept the same over all the domains. While a 6km resolution might be too low to fully resolve the elevation of the smaller ice areas, the average hypsometry of the model grid ice pixels remains close to observations on every sub-region (see Fig.S1). The biggest discrepancy can be seen in Franz Joseph sub-region where our grid is on average underestimating the real ice elevation, though it remains a relatively small bias and most likely does not

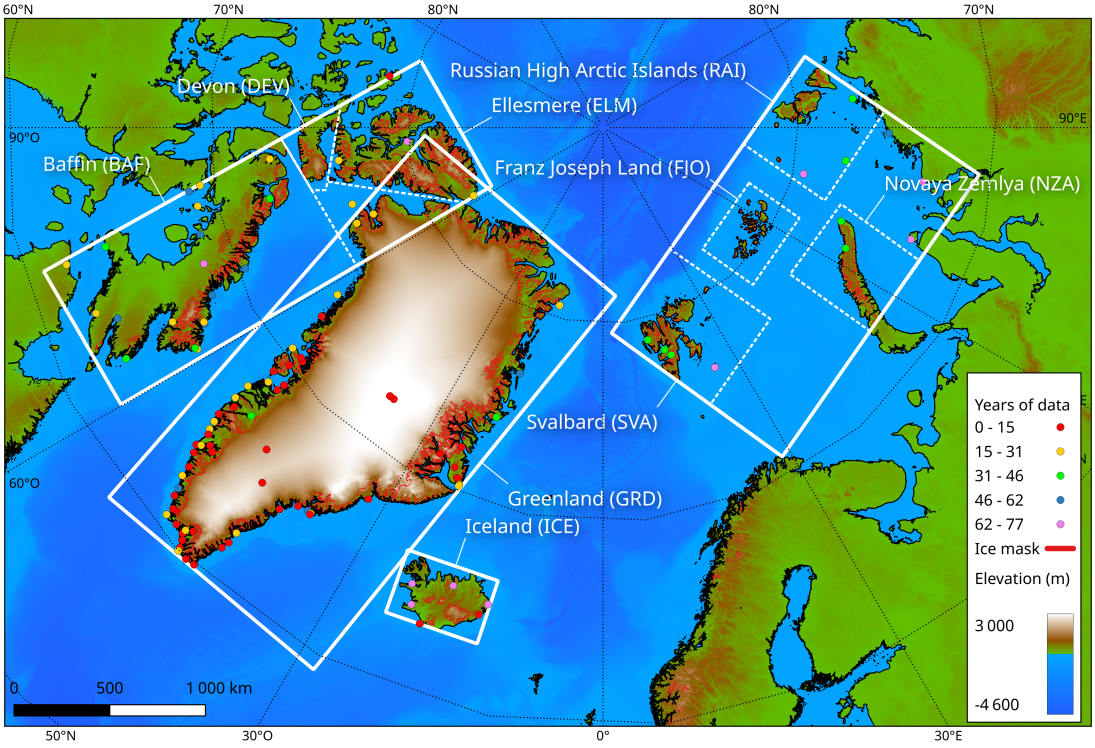

Figure 3.1: MAR domains used over the Arctic (white solid boxes) and integration sub-regions for analysis (dashed boxes). AWS locations are shown with a dot colored as a function of the years of data they provide.

have a major influence on the results. Even though the hyspometries do agree, the model resolution can still affect the surface mass balance in strong topographic variations areas, affecting shading, wind drift and precipitation.

3.2.2 Reanalysis

The ERA-5 reanalysis (Hersbach et al., 2020a) is used as forcing fields to prescribe MAR boundary conditions every 6 hours at each vertical level and over the ocean (temperature, u- and v-components of the wind, humidity, surface pressure, sea ice concentration and sea surface temperature). We chose ERA-5 because it has the advantage to be continuous from 1950 to present day, and is performing well over Greenland (Delhasse et al., 2020).

3.2.3 Data & evaluation methods

MAR has been often used over Greenland (e.g., Fettweis et al., 2020; Lambin et al., 2022) and Svalbard (Lang et al., 2015) but less frequently over Canada,

Iceland or the Russian Arctic. As our study deals with 3 new MAR domains, more attention is given to the evaluation of the results against field observations. First, the simulations are evaluated for their performance in reproducing real atmospheric conditions (in particular the 2m temperature, pressure and wind speed). Then, the reconstructed SMB is compared to the few observations available: satellite altimetry (from Hugonnet et al., 2021) to compare the regionally-integrated SMB from 2000 to 2020 over land-terminating glaciers, along with the SMB dataset from Machguth et al. (2016) over the Greenland Ice Sheet, available on the PROMICE website.

3.2.3.1 Evaluation of the atmosphere

Over the different domains, 102 automatic weather stations (AWSs) were used to evaluate the MAR simulations. The localisation of the AWSs is shown in Figure 3.1. Daily average values were used to compare observations to MAR simulations. For the modeled values, daily means were extracted as a distance-weighted mean between the 4 nearest MAR pixels. To avoid bias coming from ocean pixels (where the SST is prescribed into MAR from ERA5), only land MAR pixels were considered for the evaluation. Finally, the AWSs with an elevation difference of more than 200m with the 4-nearest-pixels average were excluded to avoid artificial biases driven by the elevation difference (16 excluded in total). Mean bias, root mean squared error (RMSE), centered root mean squared error (CRMSE), and correlation (r) between observed and modeled values were computed.

3.2.3.2 SMB evaluation

As precipitation and snow surface processes are the most challenging variables to represent in climate models, large biases can arise between models and observations when simulating the SMB. It is crucial to evaluate the modeled SMB over the different regions, although direct observations remain scarce, especially over the Russian Arctic.

Hugonnet et al. (2021) developed a global product of glacier elevation change from 2000 to 2019, using NASA's Advanced Spaceborne Thermal Emission and Reflection Radiometer (ASTER). Their glacier mass change product consists of monthly mass loss estimates integrated over sub-regions of the Randolph Glacier Inventory (RGI). It contains Mass Balance (MB) estimates for all the land ice in

Canada, Iceland, Svalbard, Russian Archipelagoes and the Greenland periphery. Because the MB is the difference between the SMB and the dynamical iceberg discharge (in the case of marine terminating glaciers), we selected data for only land-terminating glaciers, using their classification in the RGI 6.0. Annual modeled SMB was then integrated over all the glaciers to be compared with MB estimates.

This altimetry dataset is useful in order to evaluate the SMB over large remote regions of our study, where very sparse in situ observations are available. We use the in situ SMB dataset from Machguth et al. (2016) to evaluate MAR as done in Fettweis et al. (2020) over Greenland, as the mass loss by iceberg discharge over the Greenland Ice Sheet is significant compared to smaller Arctic ice caps. This dataset contains historical SMB measurements from more than 3000 stakes over the ice sheet. It is quite different from the evaluation using the Hugonnet et al. (2021) MB product (annual spatially integrated data), so the results will not be intercomparable, but gives another estimate on the performance of MAR.

Moreover, we evaluated the annual modeled SMB on given glaciers using the World Glacier Monitoring Service (WGMS) dataset. The same method was applied than above, using RGI 6.0 glacier geometries intersected with MAR pixels to spatially integrate the Specific SMB over a given glacier. Whilst the spatial coverage of the dataset is low, it has the advantage of comparing directly SMB measurements, as opposed to the altimetry product.

3.3 Evaluation

3.3.1 Climate evaluation

Table 3.1 presents the resulting mean bias, CRMSE, and r over all regions for the near-surface temperature, pressure, and wind speed. The results are computed annually and seasonally (JJA for summer and DJF for winter) and for each MAR domain. As the dataset for Svalbard and Russian Archipelagoes are inside the same domain, we separated them for the evaluation as the observational datasets are different. The height measurement for wind speed was not always available. We then use the 2m wind speed from MAR for the comparison, potentially leading to inherent biases.

The correlation coefficient between MAR and observed 2-meters pressure (P2m) is mostly larger than 0.9 over all regions. The high negative bias over

		Annual				Summer				Winter			
		Mean obs	Bias	CRMSE	r	Mean obs	Bias	CRMSE	r	Mean obs	Bias	CRMSE	r
T2m [°C]	Canada	-10.3±11.0	-0.7	2.7	0.97	3.0±2.8	0	2	0.77	-21.0±6.2	-0.7	2.8	0.9
	Iceland	4.3±4.6	-1.3	1.3	0.96	9.1±2.0	-0.7	1.3	0.82	0.4±3.7	-1.6	1.4	0.94
	Greenland	-4.6±8.2	-1.3	2.7	0.95	4.5±2.8	-0.3	1.9	0.79	-12.7±6.0	-2	3	0.88
	Svalbard	-5.1±9.1	-2.6	2.4	0.97	4.6±2.6	-3.1	1.3	0.87	-12.4±8.1	-2.1	3	0.93
	Russia	-11.7±12.2	-0.7	3	0.97	1.7±3.3	-0.9	1.7	0.85	-23.3±8.5	-0.6	3.7	0.9
P2m [hPa]	Canada	1011.6±11.2	-17.3	2.1	0.98	1010.9±7.7	-16.3	1.5	0.98	1009.1±13.3	-17.9	2.3	0.99
	Iceland	1006.3±13.8	-7	1.1	0.99	1010.6±8.4	-7	0.7	0.99	1000.8±16.7	-7	1.2	0.99
	Greenland	1012.5±11.8	-36.7	3.4	0.93	1013.8±7.8	-38.1	2.4	0.93	1009.0±14.0	-39	3.7	0.94
	Svalbard	1007.6±11.6	-34.8	1.4	0.99	1010.2±7.7	-33.7	0.8	1	1003.4±13.7	-35.4	1.6	0.99
	Russia	1011.4±11.9	-8.1	1.8	0.99	1011.2±8.5	-7.8	1.4	0.99	1011.0±14.4	-8.1	2	0.99
WS $[m\,s^{-1}]$	Canada	3.7±2.6	0.3	2.3	0.66	3.2±2.4	0.1	2	0.74	4.0±2.7	0.4	2.4	0.61
	Iceland	5.1±3.0	-0.4	2.2	0.75	4.1±2.3	-0.4	1.8	0.72	5.9±3.4	-0.3	2.5	0.72
	Greenland	4.4±2.9	-0.4	2.3	0.64	3.5±2.0	-0.5	1.8	0.59	5.1±3.3	-0.3	2.6	0.65
	Svalbard	4.5±2.9	0.3	2.2	0.71	3.9±2.1	-0.2	1.9	0.6	5.3±3.4	0.5	2.4	0.73
	Russia	6.3±3.7	-1.5	2.5	0.75	5.5±2.8	-1.1	2	0.71	7.0±4.3	-1.6	2.7	0.78

Table 3.1: Evaluation results (Bias, Centered Root Mean Squared Error (CRMSE) and Correlation coefficient (r)) over all regions, annually and seasonally. Standard deviation is provided as a +/- value. (19 AWSs in Canada, 6 in Iceland, 69 in Greenland , 4 in Svalbard and 7 in Russian Arctic.)

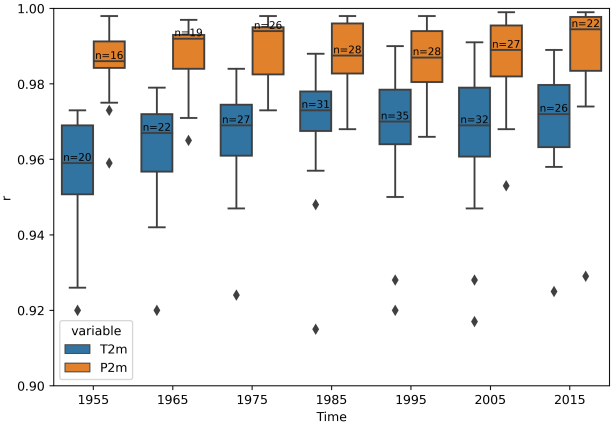

Figure 3.2: Time evolution of the near-surface Pressure (P2m) and Temperature (T2m) 10-years correlation coefficient distribution among AWSs between daily observed and modelled values. Boxes show median & quartiles of the correlation distribution amongst stations, whiskers extent to show the rest of the distribution outside of outliers (diamonds).

Svalbard and Greenland is imputable to an often high altitude difference between AWSs and MAR pixel. (See Table S1 for a comparison of altitude and temperature correction over Svalbard). This difference does not influence the correlation which is the only relevant statistical value concerning pressure. The 2m temperature is also reproduced very well in each domain (the annual correlation coefficient is artificially driven up because of the seasonal cycle). There is however a general negative bias compared to observations. Moreover, the temperature is better reproduced in winter than in summer (r = 0.91 vs 0.81), because temperature variability is lower as the near-surface temperature is close of 0°C most of the time and less driven by the general circulation dynamics than in winter. Finally, the modeled 2m wind speed has a bias lower than $1.5 m\,s^{-1}$ and the performances of the MAR reconstruction are homogeneous over all domains. However, wind speed observations are particularly sensitive to local site effects, which are not resolved at a resolution of 6km (as seen by the correlation values lower than 0.7, Lambin et al. (2022)). Moreover, we do not have the information of the height of the measurement which can also influence the comparison. The quality of the reanalysis products (ERA-5) depends largely on the number of observations that were assimilated. Because our study goes up to 1950, it is worth evaluating the precision as a function of time: the further we go back, the fewer observations available. For example, ERA-5 has been shown to be less performing prior to 1979 above the Antarctic, because of the scarcity of satellite observations over the continent (Marshall et al., 2022).

While we could expect a better agreement after 1979 in our ERA5 forced

MAR simulation due to the assimilation of satellite data in the reanalysis, there is not a significant evolution of the correlation coefficient as a function of time for the P2m (Fig.2). The latter is constant at approximately r = 0.99 from 1950 to the present day. The analysis nevertheless reveals a slight increase of the correlation coefficient in the 2m temperature, from 0.96 in 1955 to 0.97 in 1985 as a results of satellite datasets assimilation (in particular sea ice cover (SIC) and sea surface temperature (SST)) after 1979: this strongly influences the reconstructions elsewhere, mostly where observational data was scarce (Marshall et al., 2022). However, the good amount of older observations in the Arctic (compared to the Southern Hemisphere) explains the good performance of MAR forced by ERA-5 before 1979 (Hersbach et al., 2020a); and even before 1957 the International Geophysical Year (see Table S2).

3.3.2 SMB

Figure 3.3 shows the statistical distribution of annual modeled SMB values (mod) and MB satellite observation (obs) estimates over land-terminating glaciers in all sub-regions, for the period 2000–2020. There are some biases in the annual mean values, positive over Svalbard, Greenland periphery and Ellesmere Island, negative over Baffin, Devon and Iceland. The main difference is in the variability of the values, where modeled interannual variability is systematically higher than the observed one. This could be related to the lower interannual variability of altimetry products because of snowpack densification and ice dynamics (Li et al., 2023).

Land-terminating glaciers represent only a small fraction (10% when accounting for the Greenland Ice Sheet, 43% without) of all the ice areas studied here. The main bias of this evaluation comes with the integration of the 6-km MAR pixels over small glaciers (especially with small ice tongues) with a strong spatial SMB gradient, or very sensitive to site effects. Finally, while the RGI is generally precise in the classification of land/marine-terminating glaciers, it is sometimes less accurate (as in northern Svalbard for example), which could explain a slight positive bias of the simulated SMB values as some ice discharge would be included in the observation dataset.

Over the Greenland Ice Sheet, the evaluation using the PROMICE dataset yields a correlation of 0.93 between the model and the observations. The average bias is $+0.03\ m\,w.e\,yr^{-1}$(for an average observational value of -0.86 $m\,w.e\,yr^{-1}$)

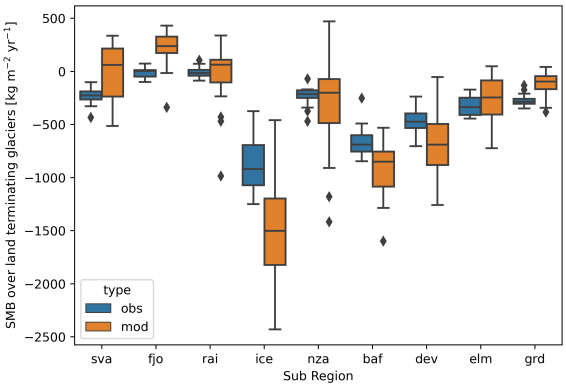

Figure 3.3: Statistical distribution of average yearly SMB values over land terminating glaciers according to the RGI 6.0, between 2000 and 2020, for modeled values (in orange) and observed (MB estimates from Hugonnet et al. 2021, in blue). (Note that Greenland (grd) only includes peripheral glaciers). Boxes show median & quartiles of the distribution amongst years, whiskers extent to show the rest of the distribution outside of outliers (diamonds).

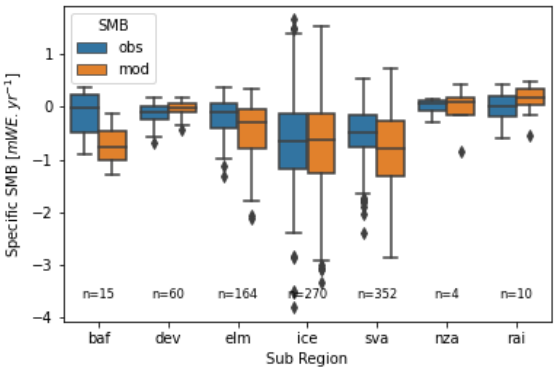

Figure 3.4: Modelled and observed annual mean specific mass balance over different glaciers of a given region using the WGMS dataset, with n the number of observations (Greenland periphery and Franz Joseph land are not included because of no observations).

and the RMSE is 0.43 $m\,w.e\,yr^{-1}$.

Figure 3.4 shows the statistical distribution of modelled and WGMS SMB observations amongst measurments for evey sub-region where data was available. The variability of the observations are closer to modelled variabilities than in the case of the altimetry product, in line with their lower interannual-variability. The main bias of this comparison (added to the 6-km MAR resolution as mentionned above) comes from the low spatial extent of the WGMS dataset for some sub-regions. As such, detailed list of all measuments can be found in supplement (Figure S2). Finally, a more refined comparison between point-stake measuments and altitudinaly downscaled modelled SMB over Svalbard is also available in

supplement (Figure S3). The values of RMSE in this study for this point-stake evaluation (0.73 m w.e. yr-1) are a bit larger than Østby et al. (2017) (0.59 $m\,w.e.\,yr^{-}1$) and Van Pelt et al. (2019) (0.43 $m\,w.e.\,yr^{-1}$) previously found, though the latter two studies calibrated their models to reduce discrepancies with the stake data.

3.4 Results

Our simulations show that the Arctic experiences an overall yearly SMB anomaly of –96.4 Gt yr-1 over 2000—2020 compared to the reference period of 1950–1970. This value becomes even more negative when considering the recent past evolution, with an anomaly of -154 Gt yr-1 between (1975–1995) and (2000–2020). This total SMB decrease is mainly driven by Greenland (as being by far the largest ice area). However, Greenland runoff has increased by 35% between (1975–1995) and (2000–2020), but has on average increased by 45% over the other regions. This difference implies that there is a clear interest in analyzing the different Arctic sub-regions independently to better identify the driving process involved.

3.4.1 Integrated SMB changes

Baffin Island, Devon and Ellesmere Island ice caps and glaciers have been losing mass since 1950. Over Baffin Island, it is accelerating in recent years with the SMB going from -22.1 $Gt\,yr^{-1}$ between 1950 and 1970 to -33 $Gt\,yr^{-1}$ from 2000 to 2020 (comparable to results from Noël et al. (2022)). The snowfall has remained stable across the whole period, while the runoff has increased significantly (from 39.6 $Gt\,yr^{-1}$ to 52.8 $Gt\,yr^{-1}$). Further north, the Devon ice cap has seen roughly the same evolution as Baffin Island. The SMB has decreased from -4 $Gt\,yr^{-1}$ over 1950–1970 to -6.5 $Gt\,yr^{-1}$ over 2000—2020 as a consequence of higher runoff (+2.4 $Gt\,yr^{-1}$) but stable snowfall. The same evolution also occurred over the Ellesmere Island where the 30% increase in runoff leads to a decrease in SMB from -9.3 to -16.8 $Gt\,yr^{-1}$ over 2000–2020 compared to 1950–1970.

Similarly, the SMB has decreased over Greenland, Iceland and Svalbard over 2000–2020 compared to the period before 1970. The strong increase in runoff (anomaly of +119.1 $Gt\,yr^{-1}$) over the Greenland Ice Sheet despite higher snowfall (+42.5 $Gt\,yr^{-1}$) has resulted in a lower SMB (from 343.7 to 267 $Gt\,yr^{-1}$.). Over

Region	Period	SMB	SF	RU
Baffin	1950–1970	-22.1 ±11.8	13.6 ±1.7	39.6 ±11.2
	1975–1995	-18.9 ±10.6	13.9 ±1.2	36.8 ±11.2
	2000–2020	-33.6 ±10.8	13.8 ±1.3	52.8 ±10.9
Devon	1950–1970	-4.7 ±3.5	3.5 ±0.6	8.9 ±3.3
	1975–1995	-3.1 ±2.1	3.7 ±0.4	7.3 ±2.2
	2000–2020	-6.5 ±3.8	3.8 ±0.6	11.3 ±3.6
Ellesmere	1950–1970	-9.3 ±15.3	18.9 ±2.6	31.1 ±14.7
	1975–1995	0.4 ±8.5	21.6 ±2.8	23.5 ±7.3
	2000–2020	-16.8 ±16.9	20.4 ±3.3	41.2 ±16.6
Greenland	1950–1970	343.7 ±110.0	677.8 ±59.2	341.9 ±74.9
	1975–1995	375.3 ±93.0	682.7 ±55.6	312.5 ±64.0
	2000–2020	267.9 ±119.6	710.3 ±52.5	461.1 ±106.2
Iceland	1950–1970	-2.7 ±3.2	12.2 ±1.8	25.2 ±4.1
	1975–1995	0.4 ±4.4	13.5 ±1.5	21.6 ±4.3
	2000–2020	-4.1 ±4.8	12.9 ±1.7	27.6 ±4.5
Svalbard	1950–1970	1.7 ±7.6	15.8 ±2.5	18.9 ±8.7
	1975–1995	1.5 ±6.3	17 ±2.0	20.4 ±7.2
	2000–2020	-0.8 ±9.1	19.7 ±3.1	27.2 ±9.7
Franz Joseph	1950–1970	1.9 ±1.2	3.8 ±0.5	3.3 ±1.3
	1975–1995	3.1 ±1.4	4.3 ±0.4	2.5 ±1.4
	2000–2020	2.6 ±2.5	4.7 ±0.8	3.7 ±2.7
Novaya Zemlya	1950–1970	-5.2 ±5.7	11 ±1.4	19.9 ±6.2
	1975–1995	-0.9 ±5.2	12.6 ±1.3	17.4 ±5.2
	2000–2020	-4.2 ±9.3	14.4 ±1.9	23.9 ±10.1
Russian High Arctic Islands	1950–1970	-1.8 ±3.5	5.1 ±0.8	8.5 ±3.6
	1975–1995	2 ±3.6	5.9 ±0.8	5.7 ±3.4
	2000–2020	0.6 ±4.1	6.5 ±0.8	8 ±4.9

Table 3.2: Regional averages and variability of the SMB, runoff (RU) and snowfall (SF) integrated over permanent ice areas for different time periods, in $Gt\,yr^{-1}$.

Figure 3.5: Annual (thin line) and 20 years running mean (thick line) of the annual integrated SMB (blue), runoff (RU) (orange) and snowfall (SF) (green), over (a) Greenland, (b) Iceland, (c) Svalbard, (d) Franz Joseph land, (e) Novaya Zemlya, (f) Russian High Arctic Islands, (g) Baffin, (h) Devon and (i) Ellesmere.

Iceland, the increase in runoff is not compensated at all by snowfall that remained stable leading to a SMB decrease of 1.4 $Gt\,yr^{-1}$. Over Svalbard, the net SMB was on average positive (1.7 $Gt\,yr^{-1}$) before 1970 but negative (-0.8 $Gt\,yr^{-1}$) after 2000 as a result of an increase in runoff (+8.3 $Gt\,yr^{-1}$).

On the other side of the Arctic, the SMB has increased over the Franz Joseph Land archipelago, Novaya Zemlya and the Russian High Arctic Island over 2000–2020 compared to 1950–1970. As a result of higher snowfall (+ 0.9 $Gt\,yr^{-1}$) and a stable RU, the SMB is now higher over the Franz Joseph Land archipelago. It is also higher over Novaya Zemlya (-5.2 to -4.2 $Gt\,yr^{-1}$) for the same reasons. Finally, over the Russian High Arctic Island, the SMB has increased steadily from -1.8 to 0.6 $Gt\,yr^{-1}$ because of both an increase in SF (5.1 to 6.5 $Gt\,yr^{-1}$) and a decrease in RU (8.5 to 8 $Gt\,yr^{-1}$). It is the only region where the RU has decreased overall in the simulation period.

The previous paragraphs suggest similar temporal evolution for different SMB components and/or regions. We then present normalized values of the 20-years running mean SMB, snowfall, and runoff over all regions for a better intercomparison regardless of the size of the different regions (Fig 3.6.).

Snowfall has increased everywhere from 1950. The Russian Archipelagos (Franz Joseph, Novaya Zemlya and Russian High Arctic archipelagos) have seen

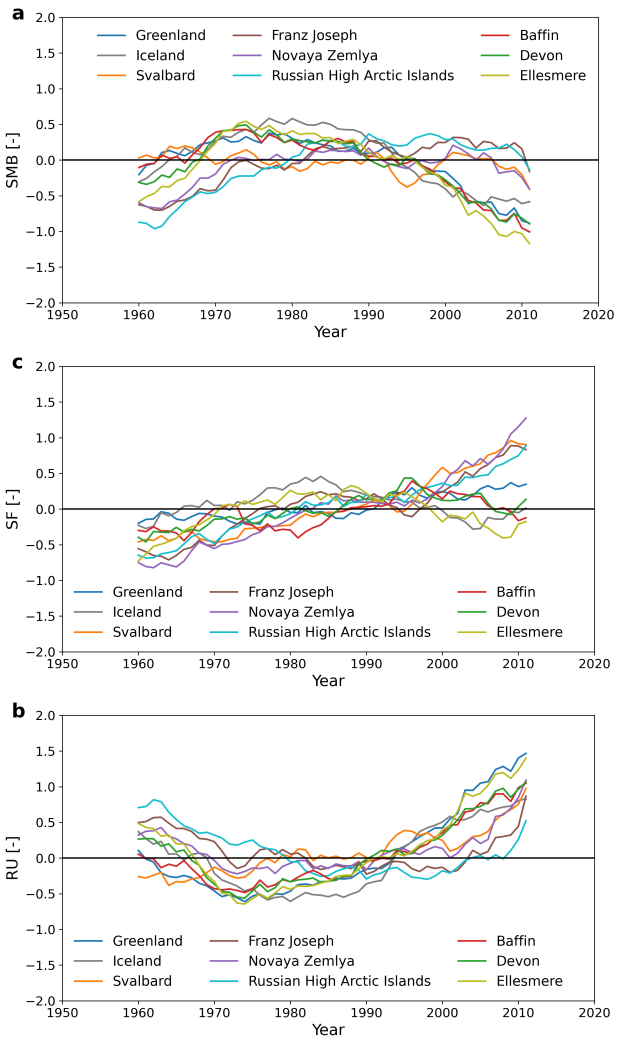

Figure 3.6: 20 years running mean of the normalized timeseries (mean-subtracted and divided by standard deviation) of (a) SMB, (b) RU and (c) SF over all regions.

the largest relative increase of snowfall with an acceleration since 1995. To a lesser extent, this can also be observed for Svalbard and Greenland. However, our results suggest that it reached a peak around 1985 over Iceland and around 1995 for the Canadian regions (Ellesmere, Devon and Baffin islands).

Svalbard excepted, all the regions experienced a large decrease in runoff before a significant increase. Runoff has decreased until 1975 over Greenland and the Canadian Arctic, and until 1985 for the Russian archipelagos. On the contrary, the runoff is steadily increasing throughout the whole period over Svalbard. While Iceland, Greenland, and the Canadian Arctic have experienced an increase in the runoff since 1975, it is clear that the climatological average runoff increase is accelerating unequivocally in all regions since 2000.

	r (SMB/SF)	r (SMB/RU)
Baffin	0.38	-0.99
Devon	0.43	-0.98
Ellesmere	0.51	-0.97
Greenland	0.63	-0.85
Iceland	0.67	-0.78
Svalbard	0.21	-0.89
Franz Joseph	0.5	-0.9
Novaya Zemlya	0.24	-0.92
Russian High Arctic Islands	0.36	-0.94

Table 3.3: Correlation coefficient between annual values of SMB, RU and SF over all sub-regions

Finally, the SMB evolution can be divided into three main periods over all regions. A first period where it increased as runoff decreased, then a second period with a stabilization (increase in both runoff and snowfall) and then a third where the strong increase in runoff has led to a large decrease in SMB. It is important to mention that Svalbard excepted, all regions had a higher SMB over 1975–1995 than over 1950–1970 or 2000–2020 (Table 3.2).

The SMB evolution is relatively associated with the runoff evolution, only of the opposite sign (see Table 3.3). This indicates that though snowfall has increased, melt and runoff variations are the main drivers of the recent SMB over the whole Arctic. Greenland, Iceland and the Canadian Arctic are following the same pattern, with a slight increase from 1960 to 1975, followed by a decrease from 1975 to 2000 that accelerates afterward. The Russian archipelagos on the other side have experienced a large increase from 1960 up to 1980, followed by a stabilization between 1980 to 2000, and a slight decrease afterward. Only Svalbard stands out as having a relatively stable SMB (increase in both runoff and snowfall compensating each other) throughout the whole simulation period, though we still find a SMB linear trend of -0.04 $Gt\,yr^{-2}$ (this is in line with some previous results (e.g., Lang et al., 2015), although there remain significant discrepancies between studies over Svalbard (see Table 3.4)).

Comparing our results to previous studies in Table 3.4, we found close integrated annual SMB values to what Noël et al. (2018) and Lenaerts et al. (2013) found over the Canadian Arctic. Our results are also comparable to what Fettweis et al. (2020) and Noël et al. (2022) found over Greenland and Iceland respectively. One main discrepancy concerns Svalbard, where our results suggest a significantly

Study	Region	Period	Average SMB [Gt.yr-1]	This study [Gt.yr-1]
Noël et al. 2018	Canada	1958-1995	-20.2	-24.4
Noël et al. 2018	Canada	1996-2015	-46.6	-49.8
Fettweis et al. 2020	Greenland	1980-2012	338	325
Lenaerts et al. 2013	Canada	2004-2013	-64	-60
Noel et al. 2022	Iceland	1958-1994	-1.4	-4.7
Noel et al. 2022	Iceland	1995-2010	-10.3	-13.7
Noel et al. 2020	Svalbard	2013-2018	-19.4	-3.9
Noel et al. 2020	Svalbard	1958-1985	6.3	2.25
Radic and Hock, 2011	Svalbard	1961-2000	-1.36	1.8
Van Pelt et al.2019	Svalbard	1957-2018	3	1.4
Aas et al. 2016	Svalbard	2003-2013	-8.7	2.3
Lang et al. 2015	Svalbard	1979-2013	-1.6	1.3

Table 3.4: Regionally integrated SMB comparisons between this study and past studies. No past estimates were found for the Russian Arctic.

higher integrated SMB compared to Radić and Hock (2011) and Aas et al. (2016). Our results are also higher than Noël et al. (2020) during the 2013-2018 period but lower during the 1958-1985 period. As said above, uncertainties are still large over Svalbard and all studies do not agree, though some progress has been made to identify a clear tendancy (Schuler et al., 2020).

3.4.2 Spatial tendencies

Generally, glaciers, ice caps and ice sheets tend to see their equilibrium lines (annual SMB equals to zero) rise because of global warming. This tendency is often driven by the increase in surface melt at lower altitudes. This phenomenon can be seen in Greenland where the ablation zone has experienced a SMB decrease of up to -350 $kg\,m^{-2}\,yr^{-1}$ on average between 1960 and 2000 (Fig 3.7,a). At the same time, the North East interior of the Greenland Ice Sheet has experienced a SMB increase of $+50\ kg\,m^{-2}\,yr^{-1}$ as a result of more snowfall (see Fig.S4).

This tendency is not present over the south Canadian ice caps (Devon, Baffin), where the SMB has decreased nearly everywhere by at least 100 $kg\,m^{-2}\,yr^{-1}$. In Iceland, the Vatnajökull ice cap has seen an overall decrease in SMB, except on its southern part. Looking at Svalbard, there is a difference between the southern part of the region where SMB has decreased significantly in the ablation zone and the northern, higher, and colder part of the region where SMB has increased more than 200 $kg\,m^{-2}\,yr^{-1}$ due to larger snowfall (see Fig.S4). Finally, the Russian archipelagos (Franz Joseph, Novaya Zemlya and Russian High Arctic) have experienced a general increase of SMB over nearly their whole surface, being ablation or accumulation area.

Overall, there is a difference in the SMB evolution between the western part of the Arctic (Canada & Greenland) where the SMB has decreased and the eastern part of the Arctic (Svalbard & Russian Archipelagoes) where the SMB has increased after 2000 compared to the period before 1970. This difference in tendency is very clear between 1950 and 1979, and remains during the recent period, though less pronounced.

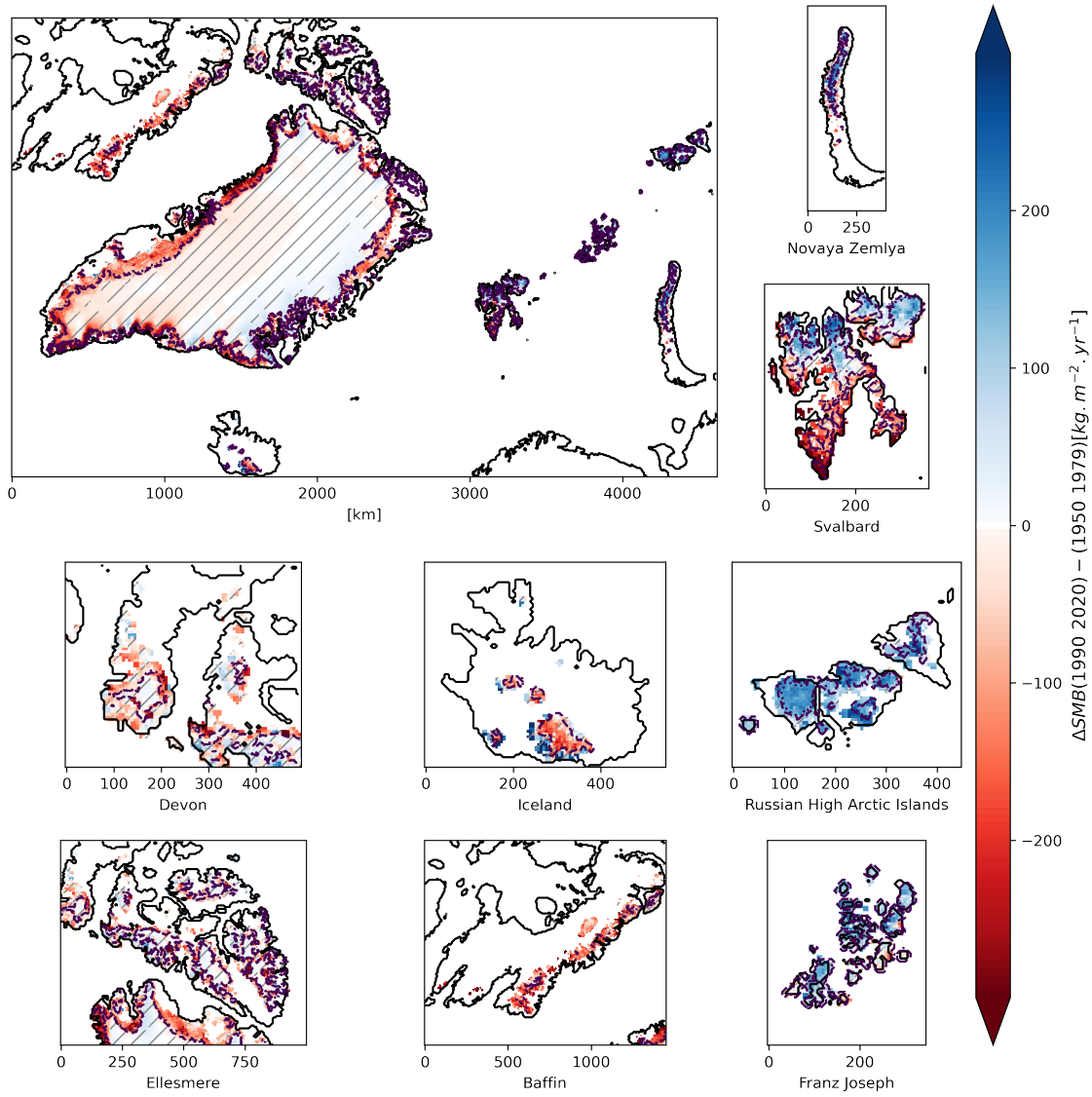

Figure 3.7: Annual SMB anomalies between the (1990-2020) and (1950-1979) periods over (a) the whole Arctic, (b) Novaya Zemlya, (c) Svalbard, (d) Devon, (e) Iceland, (f) Russian High Arctic Islands, (g) Ellesmere, (h) Baffin and (i) Franz Joseph land. Hashed areas denote where the anomaly has a low significance value regarding its variance (using Student's t-test with 90% p-value). The equilibrium line between ablation and accumulation areas for the 1990–2020 period is shown with a dashed purple line.

3.5 Discussion

3.5.1 Correlation to large scale indices

Between the dry center of Greenland to the marine Russian archipelagos, the wide variety of climates across the Arctic cryosphere may mean that its response to climate change is not homogeneous spatially. This can be already shown by comparing the climate of the recent past in Greenland (Fettweis et al., 2017) and for example, Iceland (Noël et al., 2022). In the latter region, it has been shown that the North-Atlantic cooling has contributed to stabilizing the SMB of Iceland since 2010, while over Greenland melt rates were increased by the recurring atmospheric blocking situation gauged by negative NAO conditions.

With the same idea of linking SMB variations to large-scale changes, we selected a wide variety of atmospheric indices, averaged over the whole year, to compare with the annual time series of SMB variables for every Arctic region. Fig 7 shows the correlation of annually-averaged atmospheric indices to summer (JJA) melt (a) and snowfall (b), the main drivers of SMB over the different regions. Two more oceanic indices were also added, the annual average sea surface temperature over 70°N (SST) and the annual average sea ice concentration (SIC) over 70°N. Overall, a lot of indices do not correlate with the melt rates or snowfall rates.

We see, however, a strong correlation between the melt rates in the Western part of the Arctic (Greenland and Canada) and the GBI and AMO indices. This has already been observed in the recent past (e.g., Fettweis et al., 2013) for Greenland. It implies that the blocking situation, which increases melt over Greenland, also strongly impacts the Canadian Arctic. We can also observe the anticorrelation between the GBI index and snowfall in Iceland. This might be related to the northerly flow induced by the anticyclonic conditions over Greenland when the GBI is high (with an often low NAO), as it has already been suggested by past studies (Matthews et al., 2015; Fettweis et al., 2013; Rajewicz and Marshall, 2014).

On the other side of the Arctic, no such significant correlation to atmospheric indices is found. We see however a common correlation (resp. anticorrelation) between Svalbard & Russian Archipelagos snowfall and average Arctic SST (resp. Arctic SIC). This suggests that a warmer ocean and less ice-covered ocean has likely resulted in higher evaporation and then more snowfall. We found a strong correlation between snowfall and the temperature of the atmosphere around this

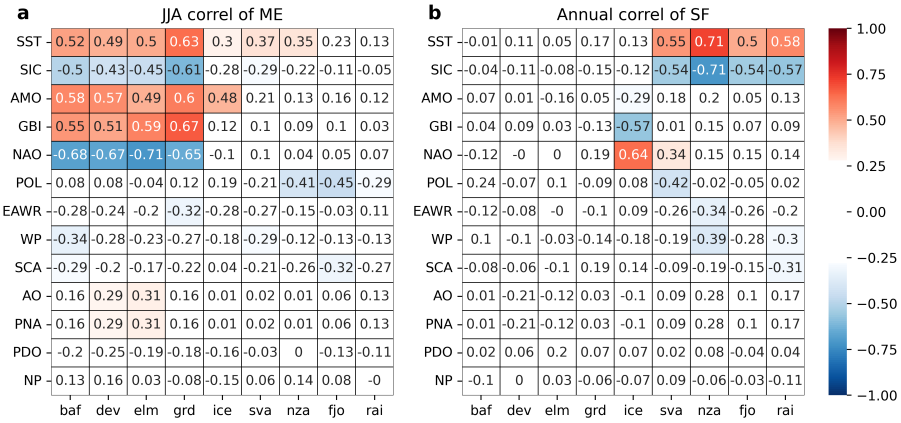

Figure 3.8: Correlation over 1950–2020 of integrated summer (JJA) ME (a) and annual SF (b) over all sub-regions and annual large scale atmospheric/oceanic indices. AMO: Atlantic Multi-decadal Oscillation, GBI: Greenland Blocking Index, NAO: North Atlantic Oscillation, POL: Polar/Eurasian pattern, EAWR: East Atlantic/Western Russia index, SCA: Scandinavian pattern, WP: West Pacific pattern, AO: Arctic oscillation, PNA: Pacific North American index, PDO: Pacific Decadal Oscillation, NP: North Pacific index, SST: Annual average Sea Surface Temperature over 70°N, SIC: Annual average Sea Ice Concentration over 70°N.

region (not shown) that also implies higher saturation water vapour pressure and further more precipitation. However, our results do not enable to state if the additional humidity mainly comes from the neighboring ocean or from more remote areas, or a combination of both sources.

Correlating annual values of SMB between all sub-regions (see Fig.3.9a) confirms the existence of two distinct sub-regions groups of similar evolutions: Greenland along with the Canadian Arctic on one side, and all of the Eastern Arctic from Svalbard to the Russian High Arctic Islands on the other. We see

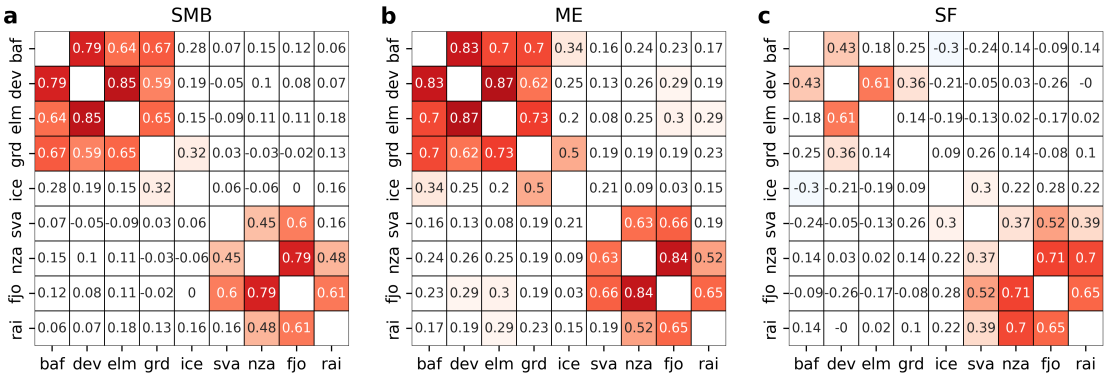

Figure 3.9: Inter-regional correlation of 1950–2020 annual SMB (a), ME (b) and SF (c)

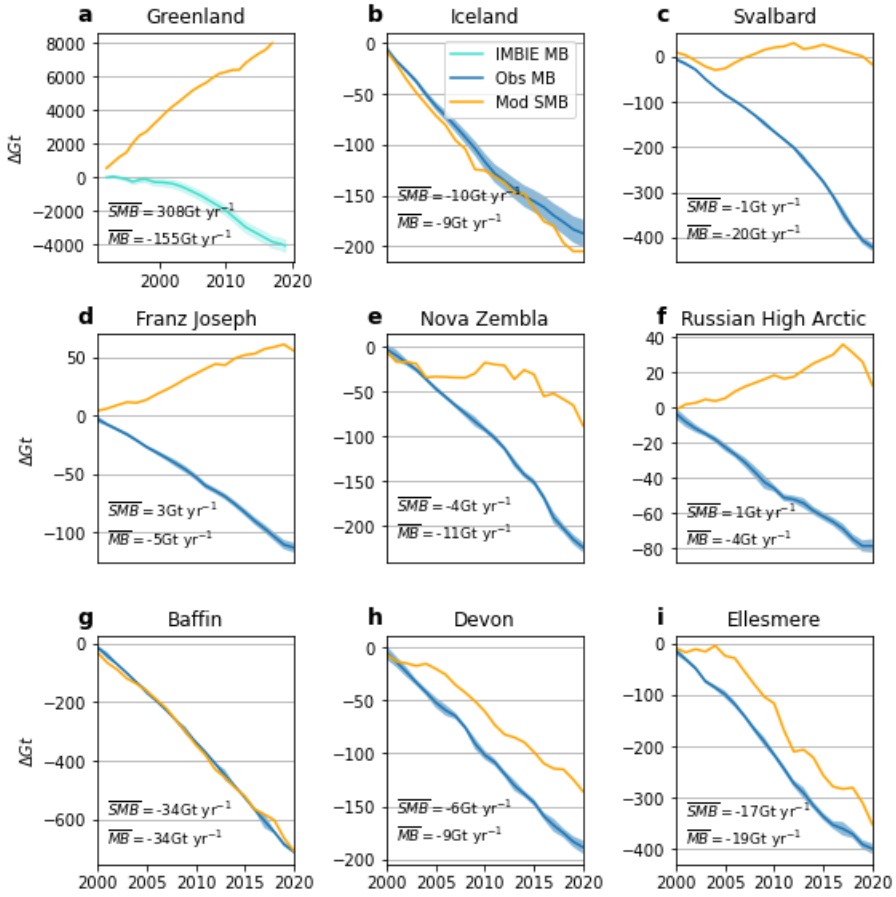

Figure 3.10: Cumulative modeled SMB and observed MB from 1990 to 2020 for (a) Greenland (using IMBIE dataset) and from 2000 to 2020 for (b) Iceland, (c) Svalbard, (d) Franz Joseph land, (e) Novaya Zemlya, (f) Russian High Arctic islands, (g) Baffin, (h) Devon and (i) Ellesmere.

again that the SMB correlation is mainly driven by ME. We also see that SF correlate more between the regions of the Eastern Arctic then the Western Arctic, noticeably between Novaya Zemlya, Franz Joseph Land and the Russian Arctic High Islands.

3.5.2 Mass balance comparison & calving rates

As we studied processes taking place at the surface of permanent ice areas, integrating the SMB spatially does not reflect the total ice Mass Balance (MB). More specifically, the increase in SMB does not imply an increase in ice mass as altimetry and gravimetry measurements demonstrated that all the regions studied here are still loosing mass. Though the scale is much smaller than in the Antarctic, ice calving can make up large proportions of the total ice loss (sometimes called

dynamic ice loss) in some Arctic subregions. For example, ice discharge was roughly equal to melting in Greenland between 2008 and 2012 (Enderlin et al., 2014). To assess the importance of calving against SMB over the different regions, we compare our SMB estimates to integrated MB products. Over the Greenland Ice Sheet, we used the IMBIE Mass Balance dataset (IMBIE, 2020). It consists of mass change measurements from satellite gravimetry and satellite altimetry from 1997 up to 2012. For the other regions, we used the altimetry dataset of (Hugonnet et al., 2021) mentioned previously.

By comparing the cumulative MB and the cumulative SMB (Fig.3.10), we can estimate the calved volume over all the sub-regions of the study. Over the Canadian Arctic (Devon, Ellesmere and Baffin), the dynamic ice loss is relatively low (even close to zero in the case of Baffin), thus the ice mass loss can be considered as mainly driven by the surface mass balance and then the atmospherics conditions. This low dynamical ice loss can be explained because only a few glaciers are marine terminating in Baffin Island. It is however not the case over Ellesmere and Devon Islands, where the surface ratio of marine terminating glaciers is close to 50%. There, the low dynamical ice loss could be explained by the SST of the waters surrounding the North Arctic Canada that has not significantly warmed yet, compared to atmosphere temperature over the glaciers. Contrarily in the eastern Arctic, while the SMB continues to be positive over Franz Joseph or Russian High Arctic Islands and has overall increased since 1950 (see Fig.3.7), the ice mass is still decreasing rapidly (up to a MB of -5 $Gt\,yr^{-1}$ over Franz Joseph land). It is also the case over Svalbard and Novaya Zemlya, where a relatively constant SMB since the beginning of the 21st century goes along with a steady decrease of the total ice mass. This can be explained by the rapid Arctic Ocean warming that increases the calving rates rapidly, particularly near Svalbard and Novaya Zemlya, where its warming is the most pronounced with more than 0.8°C per decade (Li et al., 2022). Note that while the Greenland Ice Sheet SMB is positive, lower recent values have resulted in stronger mass loss as highlighted by Fig. 3.10,a. Greenland aside, the average Arctic ice MB has been of -111 $Gt\,yr^{-1}$ since 2020, while the average SMB has been -62 $Gt\,yr^{-1}$.

3.6 Conclusions

Considering all the land ice over the Arctic, our simulations reveal that the annual surface mass balance has decreased by 120 $Gt\,yr^{-1}$ between the period

of 1950-1979 and 2000-2020. This overall mass loss has been accelerating by -4 $Gt\,yr^{-2}$ from 2000. It is mainly driven by melt, which has on average increased by 21% since 1950. This melt increase is however heterogeneous spatially, with an increase of 41% for Greenland, but only 9% on average over the Russian sub-regions where snowfall accumulation has increased by 28%. Along with Svalbard, those regions have experienced a general increase of their SMB when looking over the whole simulation period. However, record low SMB have been observed everywhere during the last decade, such as in 2020 for all of the Eastern Arctic, Devon and Ellesmere, or 2019 for Greenland and Devon.

We have also identified two distinctive sub-regions groups (Baffin, Devon, Ellesmere, Greenland; and Svalbard, Franz Joseph, Novaya Zemlya & Russian High Arctic) that seem to have the same links to climatological drivers and that went under a comparable SMB evolution. We have shown that melt is correlated to GBI over Greenland and North Canada. Snowfall over the latter group seems to be correlated to the average Arctic ocean temperatures, while it is not the case elsewhere. No atmospheric large-scale indices seem correlated to its evolution. While these links have been established for the annual mean SF and ME time series, more work remains to be done to understand what is driving the surface mass balance over those two groups. This is especially the case over the Russian Arctic, where only a few studies have been carried out.

Finally, our results suggest rapid changes in the Arctic land ice. While some regions in the Arctic have gained mass at their surface (but still losing mass taking into account the ice dynamics), these conclusions could be totally different in the years to come. For instance, most recent years were marked by several negative records over the Russian sub-regions. A repeat year of such extreme melting could quickly reverse the trend in these regions and lead to a general loss of surface mass throughout the Arctic. It will therefore be important to continue to study the Arctic land ice and to update these results regularly.

CHAPTER 4

Mitigation of sea level rise in the XXth century by increased snowfalls over Antarctica

Following: **Maure, D.**, Kittel, C., Lambin, C., Fettweis, X.: Mitigation of sea level rise in the XXth century by increased snowfalls over Antarctica, submitted, 2025

The latter Chapter was solely focused on the high latitudes of the Northern Hemisphere. Although geographically remote, the Arctic was comparatively more accessible to nineteenth-century expeditions than the Antarctic. As a result, organized exploration and early scientific activities in the Arctic preceded those conducted in Antarctica by several decades. At the beginning of the XXth century, Antarctica started to be a playground for adventurers and pioneers to discover and explore, such as Charcot, Scott and Amundsen. Countries participated in a race to reach the South Pole, that was won by the Amundsen Norwegian expedition. Once completed, the race gave way to a more scientific exploration of the continent and its surroundings, that soon transformed in a geopolitical competition at the dawn of of World War II. Eventually, the first permanent bases were established in the 1950s by the major powers during the Cold War. Antarctica then marked the resumption of scientific exchanges between East and West through the International Geophysical Year, which saw the creation of several bases and weather stations.

As such, only few observations, from expeditions, or AWSs were already available as of the IGY in the Antarctic. It was monitored later than the Arctic because of this geographic remoteness, and the scientific community reasonably tend to "trust" hindcast products in pre-satellite era more in the Northern hemisphere than in the Southern hemisphere.

No clear consensus is yet found in the extent at which we should use hindcasts dynamical downscalling over Antarctica before 1979 - especially for SMB reconstruction. The upcoming Chapter is a glimpse of answer to a highly debated - though crucial - question: What is the SMB of Antarctica before 1979 ?

Abstract Antarctica's surface mass balance (SMB) plays a central role in the global sea-level budget, yet its evolution during the pre-satellite era remains debated. Using the regional climate model MAR forced by multiple atmospheric reanalyses, we reconstruct Antarctic SMB from 1958 to 2016 to assess its contribution to sea-level changes during the twentieth century. Our simulations reveal a continent-wide SMB increase of 13% (+315 Gt yr^{-1}) between 1958–1979 and 1980–2016, equivalent to a mitigation of 31 mm of global sea-level rise. This signal is consistent with ice-core observations and robust across reanalyses with and without satellite assimilation. We attribute this increase primarily to circulation changes driven by stratospheric ozone depletion, which presumably intensified the Southern Annular Mode, deepened the Amundsen Sea Low, and enhanced moisture advection toward the Antarctic Ice Sheet. Formal causality analyses confirm a direct dynamical link between springtime ozone concentration and annual SMB, with ozone exerting a stronger control than sea-ice or oceanic conditions. These findings demonstrate that the Antarctic Ice Sheet acted as a transient buffer of sea-level rise in the late twentieth century, with stratospheric ozone depletion—a hallmark of anthropogenic forcing—emerging as a paradoxical driver of enhanced snowfall.

4.1 Introduction

Antarctica is a latent giant, whose vast snowfall shapes its potential to influence sea level. Although it is not yet the main contributor to recent anthropogenic sea-level rise (Bamber et al., 2018), it contains the planet's largest ice mass, equivalent to 57.9 m of sea-level rise (Fretwell et al., 2013a), and receives more than four times Greenland's annual snowfall (Mottram et al., 2021; Fettweis et al., 2013). Even small changes in precipitation could therefore turn it into a significant contributor.

Whilst recent studies link a recent increase in Antarctica's Surface Mass Balance (SMB) to anthropogenic climate change (Wang et al., 2025, 2023; Kromer and Trusel, 2023; Velicogna et al., 2020), some uncertainty remains about the recent past SMB estimate state of Antarctica (van Dalum et al., 2025). In particular, while regional climate models agrees on the total surface mass budget after the introduction of satellite datasets in atmospheric reanalysis products (Mottram et al., 2021; Hersbach et al., 2020b), there is still considerable skepticism before 1979. It has been noted that some heterogeneities appear at the introduction of the satellite assimilation in various products, accompanied with less accuracy before 1979 (Huai et al., 2019).

In parallel, some studies already suggest a significant change in the circulation regimes and climate in Antarctica in the 1970s (Marshall et al., 2022; Favier et al., 2017) with respect to the present climate, strongly linked with the Southern Annular Mode (SAM) intensification. Ice core reconstructions point towards a strong SMB increase over the Antarctica Ice Sheet during the second half of the XX$^{\text{th}}$ century (Chemke et al., 2020; Thomas et al., 2008, 2017), while part of the modeling community remains skeptical about a potential SMB increase in the 1970s (van Dalum et al., 2025).

We dynamically reconstruct the SMB of Antarctica since the International Geophysical Year (IGY) using a polar-oriented Regional Climate Model forced by multiple bias-corrected atmospheric reanalysis to unravel its evolution during the second half of the 20$^{\text{th}}$ century, linking it to physical processes and circulation change. We show that the AIS has experienced a 13% SMB increase over the second half of the 20$^{\text{th}}$ century, in relationship with a circulation change induced partly by the depletion of stratospheric ozone in the 1970s.

4.2 Results

4.2.1 Increased SMB over the recent past

The general evolution of the AIS SMB follows a clear positive trend throughout the century (Fig.4.1d). A non-parametric break-point detection test (Pettitt, 1979) of the SMB evolution yield a significant change in 1980, partitioning the

Table 4.1: Spatially integrated annual SMB, before and after 1980

Annual SMB ($Gt.yr^{-1}$)	East AIS	West AIS	Peninsula	All AIS
1958-1979	1193±123	768±67	268±38	2334±162
1980-2016	1380±97	835±74	361±39	2649±132
Difference	186±29	67±19	47±10	315±41

Table 4.2: Average annual SMB, before and after 1980 for all regions delimited in Fig.4.1. All differences computed are student-t test significant with a p-value < 0.001.

time series in two periods. Over the whole continent, the increase of SMB is of +13% (315 $Gt.yr^{-1}$) between 1958-1979 and 1980-2016 (Table 4.2). Those two period exhibit a relatively stable SMB compared to the period around the 1980 break-point (See Supp Table S1) Notably, the relative increase is more pronounced over the peninsulae, with +17 % (47 $Gt.yr^{-1}$). This is inline with a previously documented pronounced increase of the peninsula Surface Mass Balance (Thomas et al., 2008). By far the strongest contributor to this increase is East Antarctica - 186 $Gt.yr^{-1}$ (15%) -, with up to 200 $mmWE.yr^{-1}$ increase in the coast near Adélie, Wilkes and Princess Elizabeth land. Most of the increase is located on the Eastern sides of ridges that are perpendicular to the coast, where precipitation rates are higher because of orographic effects. Similar increase is found in ice-core measurements (Ekaykin et al., 2024). West Antarctica also experiences an increase in SMB of 67 $Gt.yr^{-1}$ (8%), though a strong disparity exists between Amundsen sea / Bellinghausen sea coastal regions, that exhibits a strong increase; and the region near Siple coast and the Ross ice shelf that experience a net decrease in annual SMB. This latter is the only region of the AIS experiencing a net decrease. This dipole-like pattern has also been documented in the study by Man et al. (2025). It is linked with a deepening of the Amundsen Sea Low (ASL) inline with the SAM intensification (See following section). Overall, the patterns described here over the AIS are well captured by ice-cores measurements albeit a few outliers, as in Fig.4.1a (More measurements locations are shown in Supp Fig.B.6).

Nearly all variations in the SMB are driven by changes in snowfall, with sublimation, evaporation, and runoff remaining roughly constant (see Supp. Fig. B.1). Overall, the increase seen throughout the timeseries has cumulatively led to a total of 31mm SLR equivalent mitigation from the AIS from 1980 to 2016 with respect to 1958-1979, inline with the findings of Medley and Thomas (2019b).

4.2.2 Circulation Change

Throughout the second half of the 20^{th} century, this general SMB increase can be explained by various synoptic circulation changes. Antarctica has experienced a strong annual sea level pressure (SLP) decrease of 2hPa between 1958 and 2016, mostly related to the SAM evolution and deepening of the polar vortex (Langematz and Kunze, 2006). This evolution is relatively well captured by atmospheric reanalyses assimilating observed SLP, as pointed out in Fig.4.2, and

Figure 4.1: Diagnosis of Antarctica SMB increase

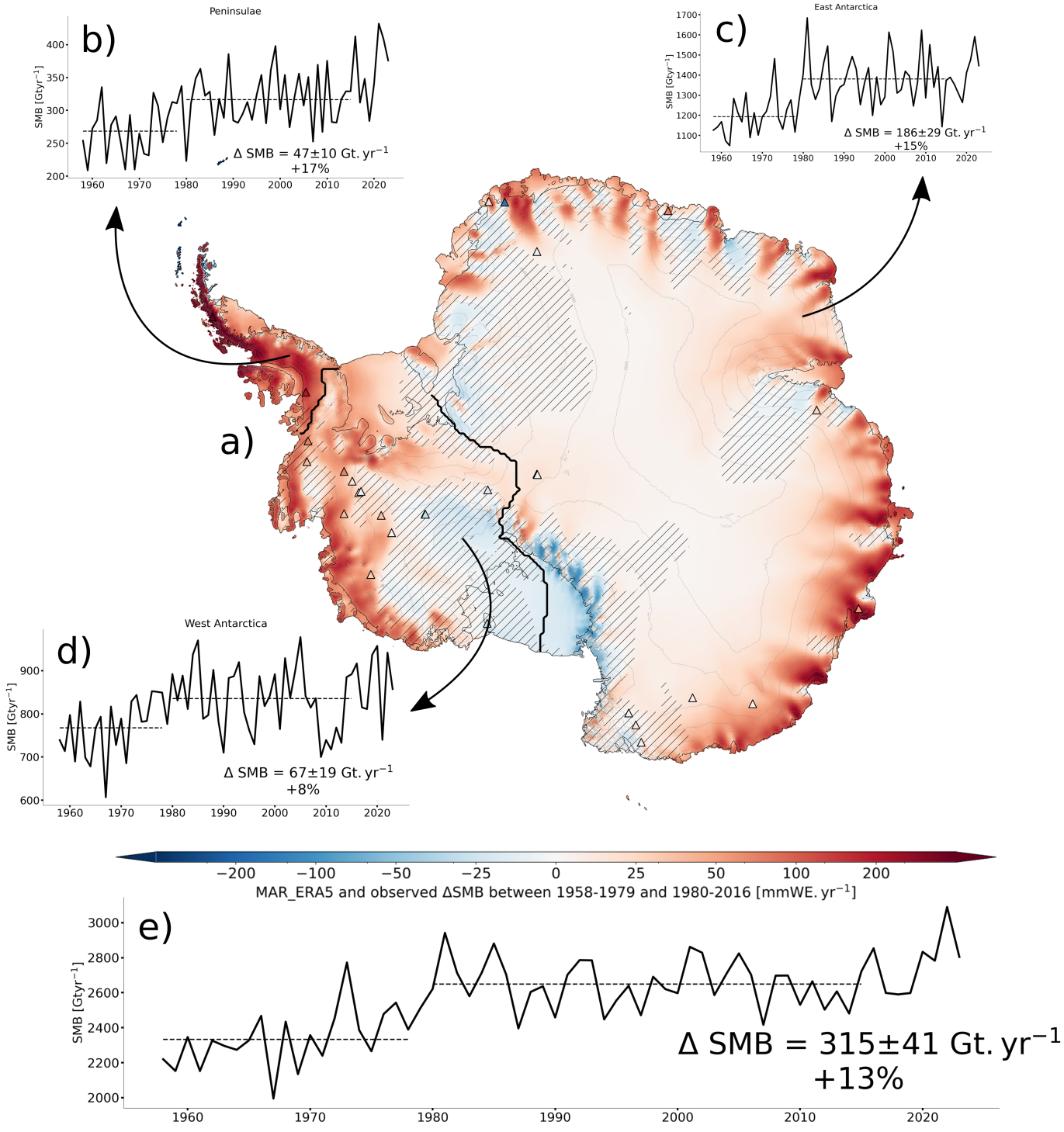

Difference between 1980-2016 and 1958-1979 annual modeled MAR_ERA5 SMB. Observed difference between the two period in ice-core measurements are shown as triangles when data is available at least until 2000. Hatches show where student t-test p-value is superior to 0.05 between the two periods (a). Integrated SMB evolution over Peninsula (b), East Antarctica (c), West Antarctica (d) and all AIS (e).

Figure 4.2: Surface Pressure evolutions from 1958 to 2016

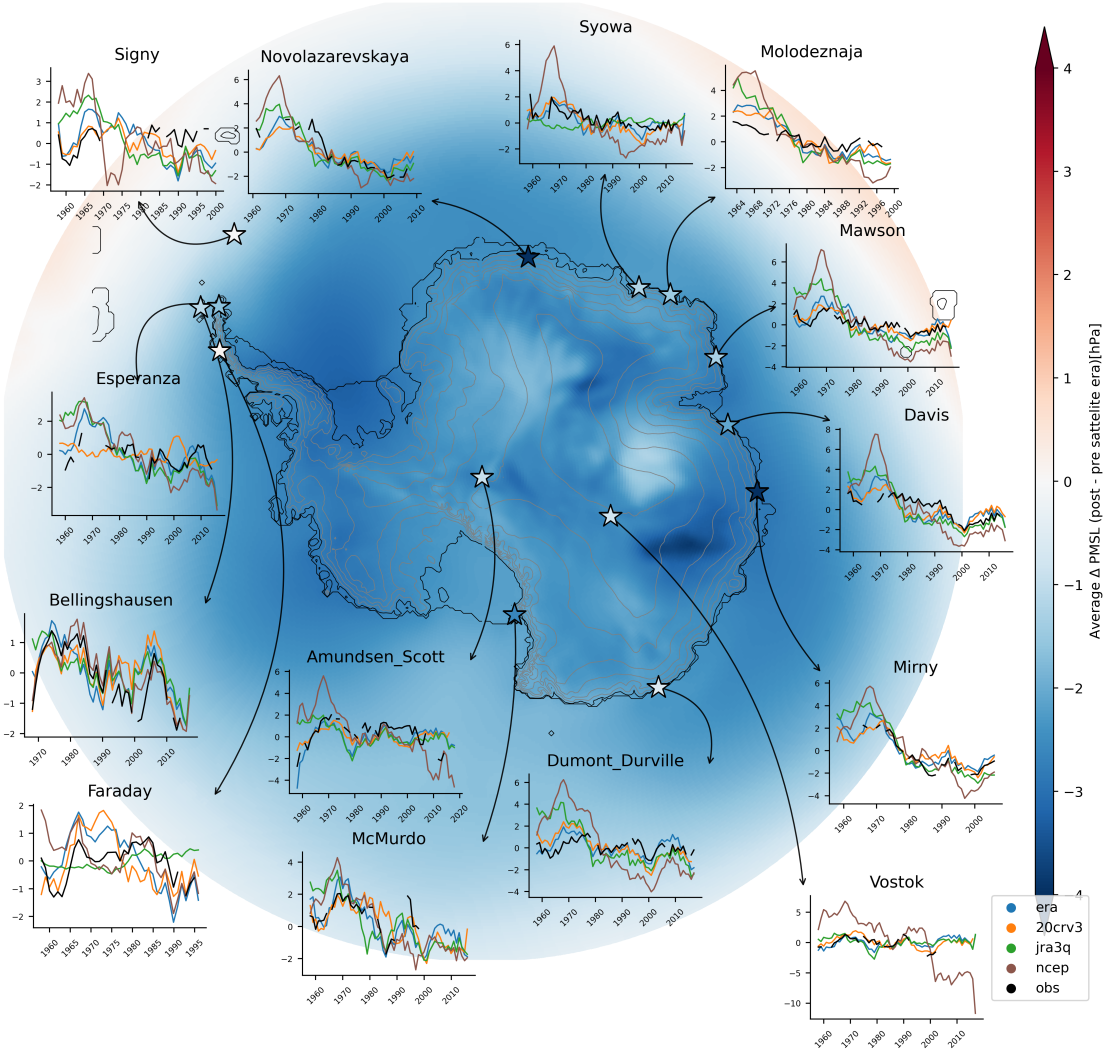

Difference between 1980-2016 and 1958-1979 annual MLSP, averaged over NCEP, 20CRv3, ERA5 and JRA3q. Stars show the location of AWSs and the observed MSLP average difference between 1980-2016 and 1958-1979. Inline plots show annual observed deviations of MSLP at each AWS compared to the reanalyses.

Figure 4.3: Annual SMB against surface temperature

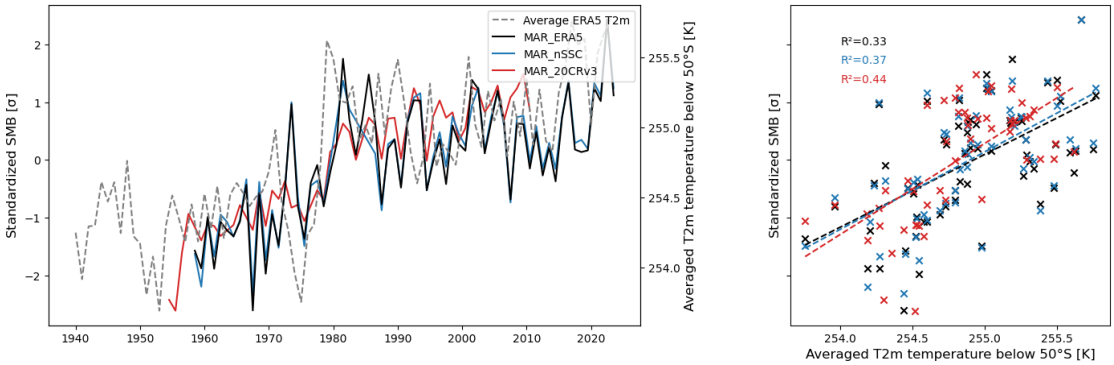

Standardized annual AIS SMB evolution in MAR_ERA5, MAR_nSSC and MAR_20CRv3, alongside averaged ERA5 T2m annual temperature evolution below 50°S (a). Annual T2m average below 50°S against standardized SMB for all simulations (b).

in Marshall et al. (2022) for older products.

This deepening of the polar vortex is accompanied throughout the period with a general temperature increase below 50°S. It closely follows the annual SMB evolution, with determination coefficients ranging from 0.33 in MAR_ERA5 to 0.44 in MAR_20CRv3. Marshall et al. (2022) documented a clear circulation change, with a close link between polar vortex strength and surface temperatures recorded by AWSs, and well captured by reanalyses: After the 1970s, a positive SAM is associated with more frequent warm northerly winds along the coast. This explains the overall increase of snowfall rates, as more moisture (from warmer air) is advected south. Most of the reanalysis used here are able to capture this evolution (Fig.4.2, Fig.4.4), even the ones that do not assimilate satellite data - NCEP and 20CRv3.

4.2.3 Ozone depletion influence on synoptic circulation

Ozone Depleting Substances (ODS) have been a major issue in the 1980s, cooling the stratosphere and driving changes in surface circulation. Even after the decrease of their production worldwide following Montreal protocol, ODS have continue to reach the polar stratosphere where a cold and insulated air favors their activation. Though the ozone hole - most pronounced in spring each year - shows some signs of recovery today (Kuttippurath and Nair, 2017), it has been present throughout the 1970-2016 period (see Fig.4.5). Ozone depletion, by decreasing UV absorption in the polar stratosphere, effectively cools it by 6 to 10 K (Danilin et al., 1998). It in turn increases the thermal gradient between sub-tropical and polar stratosphere, enhancing the polar vortex, then decreasing sea level pressure (Fig.4.2).

A strong correlation exists between austral spring total column ozone above the Amundsen–Scott station—at the center of the ozone hole—and annual SMB evolution (Fig. 4.5). The determination coefficients between annual SMB

Figure 4.4: Surface Temperature evolutions from 1958 to 2016

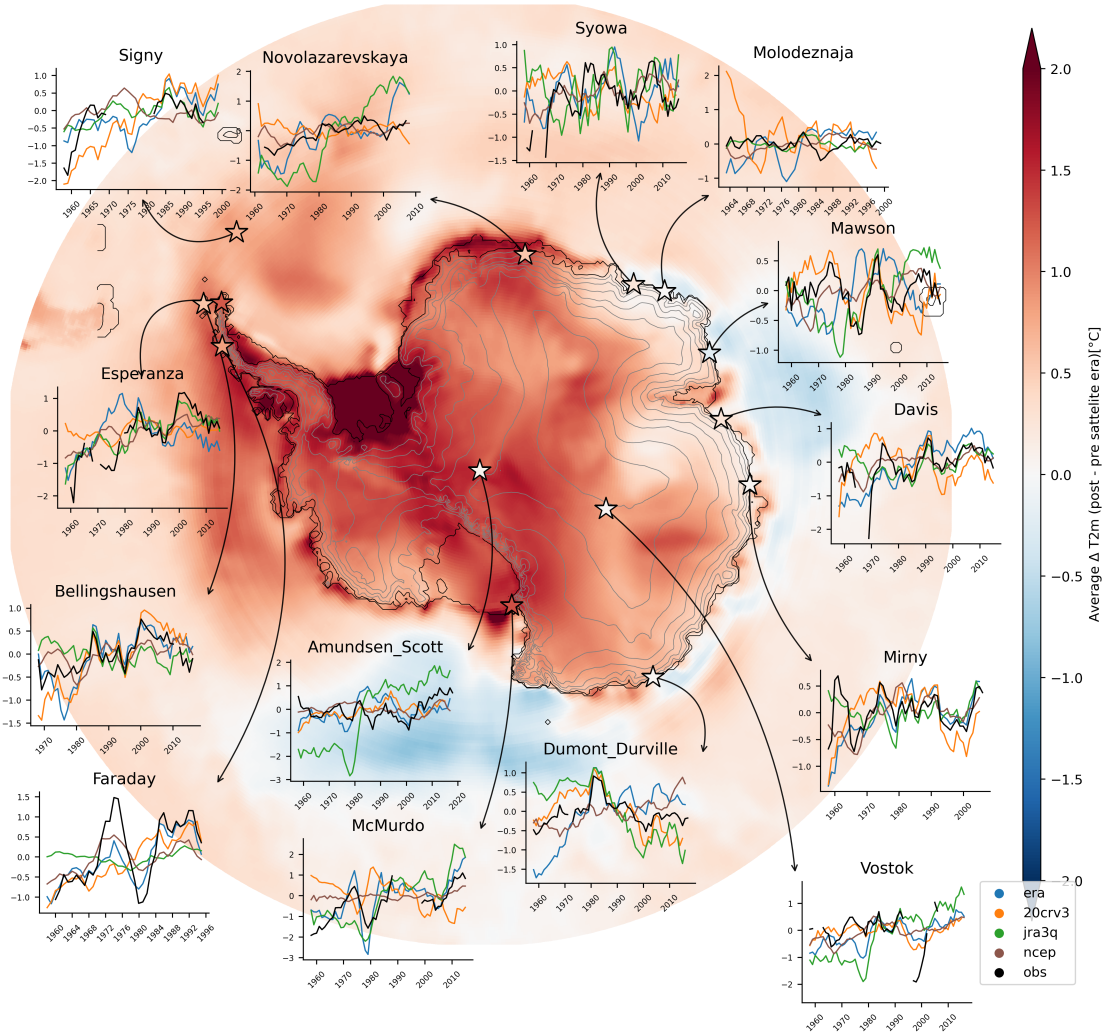

Difference between 1980-2016 and 1958-1979 annual T2m, averaged over NCEP, 20CRv3,ERA5 and JRA3q. Stars show the location of AWSs and the observed T2m average difference between 1980-2016 and 1958-1979. Inline plots show annual observed deviations of T2m at each AWS compared to the reanalyses.

Figure 4.5: Annual SMB against ozone measurements

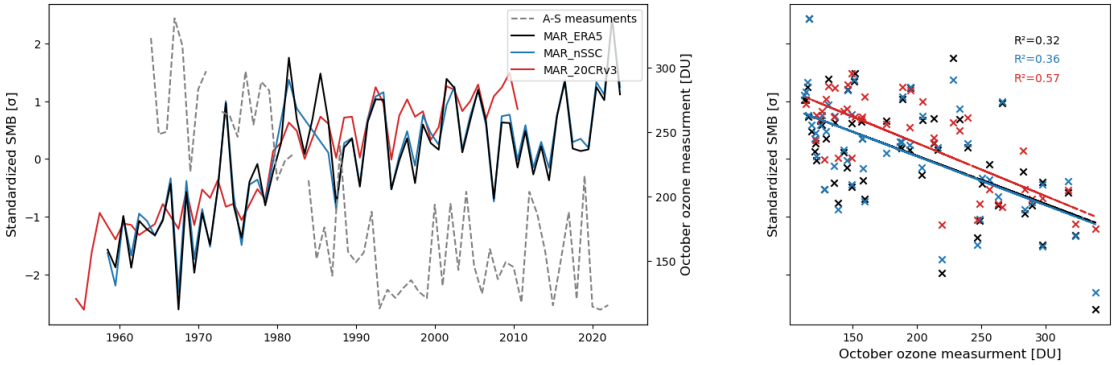

Standardized annual AIS SMB evolution in MAR_ERA5, MAR_nSSC and MAR_20CRv3, alongside October ozone measurements at Amundsen-Scott base (a). Observed October ozone against standardized SMB for all simulations (b).

Figure 4.6: Ozone concentration and SMB causal link

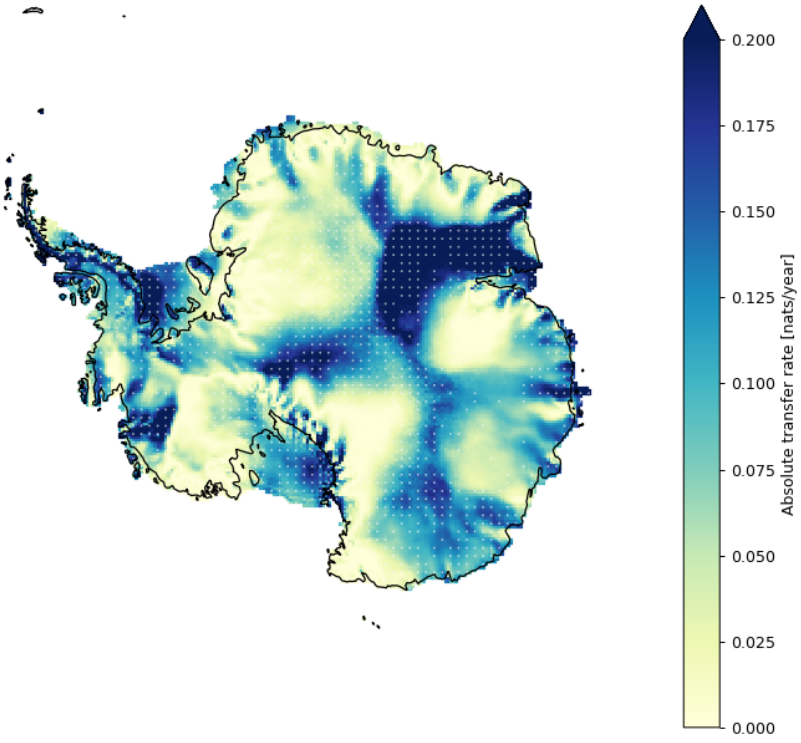

Absolute transfer rate (in bits of information per year) from spring minimal ozone concentration observed at Amundsen-Scott to annual SMB. White dots indicate 95% significance under 1000 block-bootstrap realizations of the Liang (2014) method.

Figure 4.7: Multi-variables correlation and causation matrices

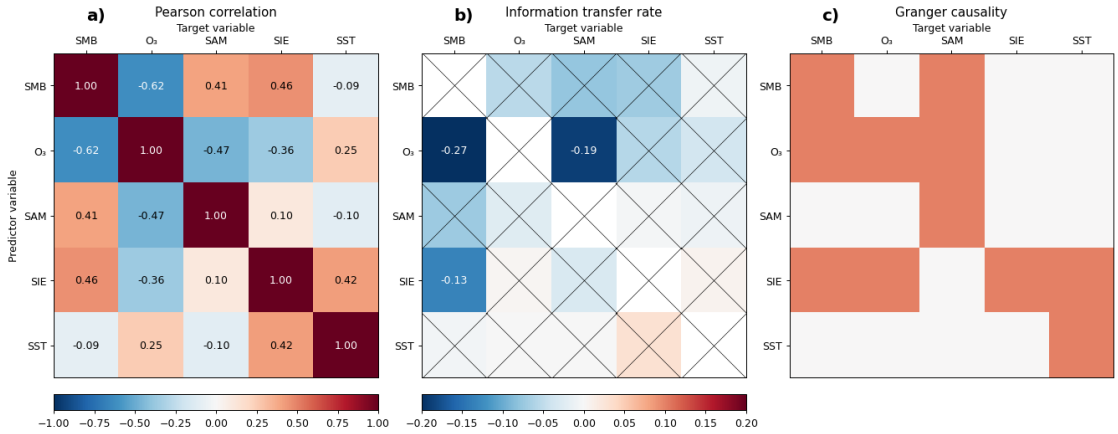

Pearson correlation coefficients between SMB, October ozone concentration measurements at Amundsen-Scott, annual SAM index, SIE annual average and annual average open ocean SST in the MAR domains (a). Information transfer rate between the variables, crosses indicate unsignificance (in nats/year)(b). Granger causality correlation between the variables, red indicates p-value lower than 0.05 (c).

and observed ozone concentration range from 0.32 for MAR_ERA5 to 0.57 in MAR_20CRv3. By using a recent formal formulation of information transfer rate between two climate variables (Liang, 2014) that has already been applied to SMB in Vannitsem et al. (2019), we reveal a dynamical dependence of total annual SMB to spring ozone concentration (Fig.4.6). This suggests that the observed correlation largely reflects a direct causal link from ozone concentration to annual SMB. Spatially, this causation is significant over the peninsula, the Amundsen-Sea coast, Eastern Ross ice shelf and Mac Robertson land. The same pattern is found when applying a Granger-causality method with a 1-year lag over the continent (See supp. Fig.B.5). Computing for multiple variables - SMB, October ozone concentration, annual SAM index, annual average SIE and annual average SST of the ice-free ocean below 55°S - yields multiple high correlations (Fig.4.7a). However, only the predictor–target pairs $O_3 \rightarrow SMB$, $O_3 \rightarrow SAM$, and $SIE \rightarrow SMB$ exhibit a significant information transfer. Using this approach, we find that over the entire period, information flow from ozone to SMB is twice that from SIE to SMB (Fig. 4.7b).To confirm the link, we performed a 1-year lag Granger-causality analysis (4.7c). All predictor/target pairs that have a significant information transfer flow are Granger-causal and all variables exhibit self-causality.

Although the 20CRv3 reanalysis does not assimilate ozone measurements and therefore does not reproduce the stratospheric ozone depletion observed after the 1970s (Supp. Fig. B.2), it still captures the observed SMB increase. This is because 20CRv3 is constrained by synoptic surface pressure through assimilation of AWS data. As a result, it can represent circulation changes and the associated increase in precipitation in the 1970s by compensating for the missing stratospheric thermal gradient—effectively "artificially" deepening the polar vortex (see Supp. Fig. B.3, where the deepening is stronger in 20CRv3 than in ERA5).

4.2.4 Homogeneity before and after satellites

Evidence for this SMB increase in the 1970s has previously emerged from downscaling atmospheric hindcasts (ERA5) with RCMs (van Dalum et al., 2025). This apparent change coincides with the introduction of satellite data into hindcast assimilation, inherently increasing their accuracy—particularly in AWS-sparse regions like the AIS (Sterl, 2004; Huai et al., 2019). Notably, a jump in the sea ice extent and sea surface temperature evolution is present in hindcasts (Goosse et al., 2024, e.g. ERA5,) in 1979. Caution is therefore warranted regarding the pre-1979 signal, as early reconstructed SMB may be underestimated. To assess its influence, we (1) forced MAR with ERA5 using bias-corrected SSCs throughout the entire period (MAR_nSSC; see Goosse et al. (2024)), and (2) forced MAR with 20CRv3, a reanalysis that does not assimilate satellite data after 1979 except for sea-ice concentration. Yearly integration over the AIS reveals little change in total SMB when SSTs and SSCs are varied (see Fig. 4.5 for standardized values and Suppl. Fig. B.1 for absolute values). This is inline with Kittel et al. (2018), where realistic changes in SSCs (considering the 20th century) have limited impact on total SMB. In MAR_20CRv3 the reconstructed SMB is substantially different than with MAR_ERA5, mostly because the product suggests a clear unrealistic positive trend in daily surface pressure variability throughout the simulation. As 20CRv3 is an ensemble mean, less AWSs means more spread amongst the ensemble members, and thus more smoothed pressure fields in the ensemble mean used to force MAR here. By progressively strengthening the synoptic pressure variability from 1958 to present day, it artificially increases the amount of precipitation throughout the simulation through more humidity advection (See Supp. Fig.B.4a). This property of 20CRv3 and its influence on reconstructed SMB has been documented in Fettweis et al. (2017), albeit for the Greenland Ice Sheet. However, it still reproduces a strong gap in SMB during the 1970s, where it could not originate from a heterogeneity in the assimilation.

The bias-corrected 20CRv3 MAR simulation (see Methods, section 4.4.1.2) still exhibits a pronounced difference between the pre-1980 and post-1980 periods. Therefore, we conclude that the poor SSCs conditions in hindcasts prior to the satellite-era are not likely influencing the changes described in this study. Moreover, the general introduction of satellite assimilation is most likely not responsible for this increasing SMB over the second half of the 20th century as this increase is also suggested by MAR_20CRv3 not assimilating satellite data apart from SIC and SST measurements after 1980.

4.3 Conclusions

We provide a new 4 km-resolution SMB reconstruction for Antarctica from 1958 onward, revealing a 13% increase (+315 Gt yr^{-1}) after 1980, with East Antarctica contributing most (+186 Gt yr^{-1}). This estimate is consistent with ice-core reconstructions reporting strong 20th-century SMB growth (Thomas et al.,

2008, 2017; Ekaykin et al., 2024). It is also supported by modeling reconstructions using GCMs (Previdi and Polvani, 2017; Chemke et al., 2020) that document an SMB increase (of +375 Gt yr^{-1} in the case of Previdi and Polvani, 2017) and link part of this SMB increase to ODS.

This increase might have mitigated global sea-level rise by $\sim$ 30 mm SLR equivalent between 1980 and 2016. This compensation is smaller than the MB total loss resulting from ice-shelves melting and grounding line retreat over the same period. However, the total SLR from Antarctica MB loss between 1979 and 2017, estimated at $\sim$16mm by Otosaka et al. (2023), could have been three times higher without SMB compensation. It also shows that post-1980 SMB conditions differ sharply from earlier decades, challenging the assumption of stability and suggesting that reference SMB pre-anthropogenic change may lie in the pre-1980 climate.

Looking ahead, the recovery of the ozone layer could weaken the circulation patterns that drove this past increase. On the other hand, global warming is expected to enhance precipitation, while stronger warming will also intensify surface melt. The competition between these three opposing influences—ozone-driven circulation changes, warming-enhanced precipitation, and warming-driven melt—will ultimately determine whether Antarctic SMB continues to offset sea-level rise or becomes a major contributor in the coming decades.

4.4 Methods

4.4.1 Atmospheric reanalysis

For this study, 4 atmospheric reanalysis were considered to reconstruct the SMB by forcing MAR from 1958 to 2020, namely, ERA5, 20CRv3, NCEP2 and JRA3q. The two latter were discarded because of poor performance against AWSs observations (surface pressure and and temperature, see Suppl Table S2), but also discrepancies in the high atmosphere (see Suppl Fig.B.3). Moreover, Marshall et al. (2022) has already documented the good performance of ERA5 and 20CRv3 in reproducing the SAT-SAM relationship.

4.4.1.1 ERA5

ERA5 is the atmospheric reanalysis produced by ECMWF, described in Hersbach et al. (2020b). It has been used in numerous SMB studies to drive MAR (Agosta et al., 2019a; Kittel et al., 2018). It assimilates surface observations from AWSs, but also a considerable amount of satellite data (including SSCs or stratospheric ozone). It has been shown to perform very well in the post-satellite era, but some concern has been made before 1979, and possible heterogeneities from the inclusion of such satellite datasets - and as such has never been used to reconstruct SMB before that period. In particular, SSCs are known to be poorly

resolved prior to 1979 (Goosse et al., 2024). This issue is addressed in our study by comparing MAR_ERA5 to MAR_nSSC in Fig.4.3, where we show little influence of the SSCs correction on SMB prior to 1979.

4.4.1.2 20CRv3

20CRv3 is NOAA latest atmospheric reanalysis for the 19th and 20th century (described in Slivinski et al. (2019a, 2021)). Compared to ERA5, it does not include satellite datasets - except for the sea ice extent and SST - after 1979, thereby having limited heterogeneity between pre and post-satellite era. It is however less accurate in representing surface pressure and temperature, as it only assimilates AWSs observations (see Supp Table S2). As noted in Sect. 4.2.3, it does not reproduce recent stratospheric ozone depletion because no ozone data are assimilated (Supp. Fig. B.2) This is leveraged by a deepened polar vortex that compensates for the lack of stronger thermal gradient after the 1970s, forced by AWSs SLP assimilation.

4.4.2 MAR

MAR is a polar-oriented regional climate model (RCM), initially developed by Gallée and Schayes (1994). It has been used over Antarctica for SMB reconstructions in numerous studies, locally (eg. Adélie Land (Amory et al., 2020)) or over the whole continent (Agosta et al., 2019b; Kittel et al., 2021b).

It is a hydrostatic model that uses sigma vertical coordinate system. Its polar-orientation comes from its complex 1D snowpack and surface module SISVAT (Soil Ice Snow Vegetation Atmosphere Transfer) that enables for an accurate representation of the snow properties and evolution (Gallée et al., 2001).

We use here MAR version 3.14 (hereafter MARv3.14). It has been fully rewritten in Fortran 90 from the version used in Maure et al. (2023), and also includes a new radiative scheme from ECMWF ecRad, detailed in Grailet et al. (2025). The latter is not supposed to have a large influence on the simulations. Moreover, our atmosphere evaluation and SMB integration for the satellite-era yields similar results than previous studies using older MAR versions (Agosta et al., 2019b; Kittel et al., 2021b).

MAR is 6-hourly driven at its lateral boundaries (pressure, wind speed, temperature, specific humidity), at the top of the troposphere (temperature, wind speed) and at the ocean surface (sea ice concentration, sea surface temperature) by atmospheric reanalysis (described in Section 4.4.1). The atmosphere is described with 24 vertical sigma layers, 8 of which are below 200m. Our model topography is derived from Fretwell et al. (2013a) BedMachinev3 product.

We used here a 326x326 grid with a 25km resolution, that extends far over the southern oceans. It enables MAR to capture the influence of sea surface conditions (SSCs) in the boundary layer. Following previously documented

statistical downscalling techniques (Franco et al., 2012), the output SMB fields are statistically downscalled to a 4km grid by a bilinear interpolation from the 4 closest pixels. A height influence correction is then applied by computing an altitudinal SMB gradient from the 8 closest neighboring pixels.

The SMB, locally ($mmWE.m^2$) or integrated over space ($Gt.yr^{-1}$) is computed as

$$SMB = PR - RU - SU \tag{4.1}$$

where PR is the total solid and liquid precipitation, RU is the total meltwater runoff (in itself melting plus liquid precipitation minus refreezing) and SU is the total sublimation of the snowpack. Note that this corresponds to the definition of 'climatic mass balance' by Cogley et al. (2010).

As mentioned earlier, we have performed 3 simulations using different forcings for this study:

- MAR_ERA5 is a standard simulation using MAR forced by the ERA5 reanalysis from ECMWF (Hersbach et al., 2020a). It uses defaults ERA5 SIC and SST over the southern oceans, from HadISST. The latter SSC are made of satellite observations after 1979 and model values before 1979 - known to be poorly accurate (Goosse et al., 2024).
- MAR_nSSC has the same forcings as MAR_ERA5 except for the SST and SIC that are replaced by the reconstruction from Goosse et al. (2024). It is made using NEMO-SI^3 forced by a regional particle-filtering hindcast from different climate models, that tends to reduce the inaccuracy from HadISST before 1979. Only the boundary layer interactions from sea-ice and ocean are changed, while the synoptic circulation remains similar to MAR_ERA5.
- MAR_20CRv3 is a standard simulation using MAR forced by the 20CRv3 reanalysis from NOAA (Slivinski et al., 2019b). It is made by assimilating only AWSs surface pressure observations - apart from SIC and SST satellite observations after 1979 (HadISST.2). No other data is assimilated in the free atmosphere, limiting the heterogeneity between the two periods.

In this study, we compare periods before and after 1980, with a respectively lower and higher SMB. We chose to compute means up to 2016 because of a clear drop in SIE after 2016 (Goosse et al., 2024) that might affect annual SMB and could indicate a continent-wide shift in climate regimes.

4.5 Evaluation

4.5.1 Atmosphere evaluation

The different MAR simulations were evaluated against AWSs observations using daily anomalies of SP and T2m - to avoid spurious correlation from seasonal

Table 4.3: Surface pressure evaluation

SP	Period	r	Bias	CRMSE
MAR_ERA5	1958-1979	0.80	-13.5	6.17
	1980-2023	0.94	-1.67	3.23
MAR_nSSC	1958-1979	0.81	-13.63	6.10
	1980-2023	0.94	-1.88	3.25
MAR_20CRv3	1958-1979	0.85	-11.07	5.41
	1980-2023	0.91	-3.19	4.08

Surface pressure evaluation of the 3 simulations used in this study, before and after the satellite inclusion in hindcasts.

Table 4.4: Surface temperature evaluation

T2m	Period	r	Bias	CRMSE
MAR_ERA5	1958-1979	0.84	-0.99	4.73
	1980-2023	0.93	1.10	3.57
MAR_nSSC	1958-1979	0.84	-1.07	4.82
	1980-2023	0.93	1.06	3.61
MAR_20CRv3	1958-1979	0.85	-2.49	4.74
	1980-2023	0.89	-0.06	4.42

Near-surface temperature evaluation of the 3 simulations used in this study, before and after the satellite inclusion in hindcasts.

variability. The model values are bilinearly interpolated from the 4 pixels closest to the AWS. The statistics are shown in Table 4.3 and 4.4. At the beginning of the simulation, a dozen of measurements are available (the AWSs installed during the IGY - see Fig.4.2). The number of observation available then steadily increases until 2023. The evaluation of the raw hindcast products is available in Suppl. Table S2. Inherently, the simulations are less accurate in the pre-satellite era - though still realistic. This is also the case in reanalysis or downscalled reanalysis that do not assimilate satellite datasets, because of an overall increase of observations - through more AWSs - throughout the continent in between the two periods.

4.5.2 Ice-cores evaluation

To asses the accuracy of our SMB reconstruction, we have used the compiled dataset from Wang et al. (2021) after our statistical downscalling to 4km resolution. Model values were interpolated from the 4 nearest pixels of the ice-cores location. The evaluation for the 3 simulations is presented in Fig.4.8.

The Pearson correlation coefficient is a bit smaller in all 3 simulations before 1979 than all time, tough on the same order of magnitude. The average bias is higher before 1979, again understandably because of the lower accuracy of the

Figure 4.8: Model SMB evaluation

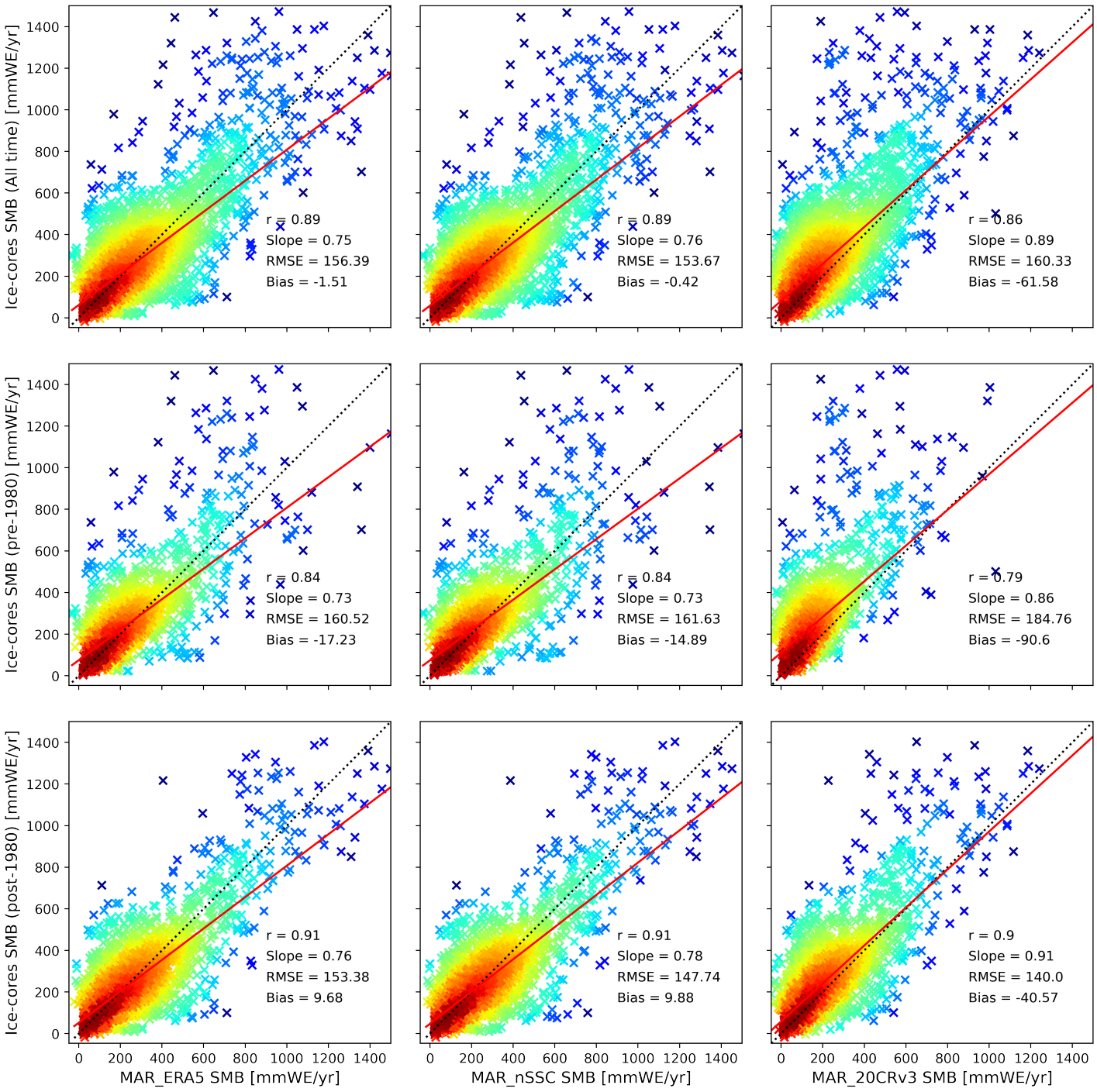

Modeled against observed annual SMB at a given pixel. Modeled values are billienarly interpolated from the 4 closest grid pixels from the core location.

atmospheric reanalysis. However, the pre-1979 bias tends to slightly underestimate SMB, while the post-1980 bias is positive. This is caused by a spatial heterogeneity of the ice-cores depending on the time period, as the cores spanning both periods are in agreement with model values (Fig. 4.1). MAR_20CRv3 underestimates the SMB in both periods, as it has an overall less dynamic atmosphere (As explained in section 4.4.1.2). Integrated values over Antarctica were corrected in Fig.B.4.

4.5.3 Causality analysis

To infer causality between stratospheric ozone and SMB and quantify its strength, we apply the information transfer method of Liang (2014), further detailed in Liang (2015, 2016), which is grounded in Shannon's entropy theory (Shannon, 1948).

The transfer rate between two variables is defined as

$$T_{2\to1} = \frac{C_{11}C_{12}C_{2,d1} - C_{12}^2 C_{1,d1}}{C_{11}^2 C_{22} - C_{11}C_{12}^2} \tag{4.2}$$

where $C_{i,j}$ are the covariances between X_i and X_j, and $C_{i,dj}$ are the covariances between the variable X_i and $\frac{dX_j}{dt}$. In this formulation, the magnitude of $T_{j\to i}$ gives an estimation of the strength of the causality link, while the sign indicates the influence of the variable j on variable i. A positive (negative) value indicates that j influences i by making it more (less) uncertain. It has to be noted that our timeseries is relatively short for such a methodology (as mentioned in Vannitsem et al., 2019). Thus, we use a block-bootstrapping method to assess the reliability of the information computed flow. After 1000 bootstrap realizations, the causal link between predictor-target variables is considered significant if 95% of the bootstrapping iterations yields information transfer of the same sign.

We also use a Granger-causality test (Granger, 1969) to validate the methodology of information transfer on our data. The Granger-causality method, while used more frequently, lacks a quantitative measure of the causality link between the variables, acting only as a yes-no question. It is however useful to discriminate between simple correlation and causation. As such, all the pairs of variable that exhibit a significant information transfer in Fig.4.7 are also Granger-causal, while the opposite is not true.

Part III

Better constraining the climate processes controlling SMB in polar regions

CHAPTER 5

Fully coupled system

Part of this chapter was written for *D5.8 – Synthetizing new understandings and interactions in the fully coupled climate model* (PolarRES consortium, 2025)

Abstract

This chapter presents the development and evaluation of a fully coupled ocean–sea ice–atmosphere regional modeling framework for Antarctica, with a parallel effort for the Arctic. The coupling integrates the MAR regional climate model with the NEMO–SI^3 ocean–sea ice system through the OASIS3-MCT coupler, enabling inline exchanges of fluxes and state variables at a pan-Antarctic scale. Standalone NEMO simulations show realistic sea ice extent and dynamics when compared with satellite observations, providing a reliable basis for coupling experiments. However, the coupled configuration reveals significant challenges: an energy imbalance in downward fluxes from MAR leads to excessive ocean warming, reduced sea ice extent, and disrupted dense water formation. Sensitivity experiments identify biases in MAR radiative fluxes and surface energy exchanges as the main drivers of this drift, amplified by the long residence times of polar water masses. While Antarctic simulations remain unstable, the analogous Arctic configuration displays no significant drift, suggesting a domain-dependent response. Despite technical limitations—particularly related to MAR parallelization—the coupling framework successfully establishes a scalable methodology for studying polar climate feedbacks. The work highlights both the potential and the challenges of regional fully-coupled modeling for advancing process-level understanding of ocean–atmosphere–ice interactions in polar regions.

5.1 Introduction

Water has a volumetric heat capacity of more than 3000 times that of dry air at sea level pressure - it is in fact one of the materials with the highest heat capacity on Earth. This single property makes the word oceans a huge modulator of the global climate, by inducing large scale energy redistribution, transport, and acting as a long term modular of the climate. One famous illustration of this is the El Niño-Southern Oscillation (ENSO) phenomenon, where a thermal anomaly from Pacific equatorial surface water has implications in a large portion of the tropics and subtropics, by changing the general Walker circulation and wind/precipitations patterns substantially over the Americas.

In the polar regions, the ocean is a major driver of seasonal variability. In winter - austral or boreal - the free ocean makes way for the Sea Ice, effectively shutting down the warming from the ocean to the atmosphere. It is a crucial phenomenon that tends to isolate the poles from warm air intrusions, but it also has a substantial impact for the coastal precipitations, as air masses are not recharged in humidity over sea ice. For example, Kittel et al. (2018) has extensively downtracked and quantified the direct influence of a change in SIE or SST around Antarctica on its SMB.

The last years over Antarctica have been marked with record low maximal SIE, and the Arctic is paving the way to a new record minimum in 2025. The combined action of sea ice retreat and temperature increase has and will have a major influence on polar climates in the near future.

Of interest to the polar land ice regions, we have already encountered in this thesis the direct past influence of ocean waters on SMB: In Chapter 3, we have seen how the Arctic Ocean SSC have a direct impact on SMB, most importantly in the eastern sector. As such, the SIE and SST evolution are largely correlated to the annual SF rate, from Iceland to the Russian High Arctic Islands; but also the annual melt rates of Greenland. In Chapter 4, we have highlighted a direct causality between the annual SIE and the annual SMB of the AIS.

While not at the heart of the prvious parts of this manuscript, the atmospheric circulation also has in return a strong influence on the ocean. For example in Antarctica, the strong persistent katabatic winds create coastal polynyas by pushing the sea-ice offshore. This creates areas of permanent sea-ice formation, that eventually form denser waters by brine rejection. This dense water is at the heart of the global thermohaline circulation that 1) helps to mitigate anthropogenic warming by capturing CO2 at ocean depth and 2) participates to redistribute the global heat contents around Earth.

Processes such as these, that lie at the Sea-Ice - Ocean - Atmosphere interface, are poorly represented in regional modeling. A standalone model (oceanic or atmospheric) cannot reproduce on its own the feedbacks at play. While GCMs have such coupled components, they lack in physics accuracy (e.g. for snow dynamics representation), resolution, or flexibility in their usage.

In the upcoming Chapter, we will be developing a fully coupled Sea-Ice - Ocean - Atmosphere regional model, with the aim to accurately represent the feedbacks at play in the polar regions. We will be tackling the case of Antarctica, while the Arctic will be co-developed in the thesis of Clara Lambin. The upcoming coupling framework section does not include a detailed MAR description of the Antarctic configuration as it has been already done in Chapter 2 and Chapter 4.

5.2 NEMO-SI^3 model

The Nucleus for European Modelling of the Ocean (NEMO) is a primitive equation model adapted to simulate regional and global ocean circulation up to kilometric scales. It uses the hydrostatic and Boussinesq approximations. Along equations similar to MAR for momentum balance, it accounts for heat and salinity conservation. The equation of state used by NEMO is the standard TEOS-10 formulation, described in McDougall and Barker (2011).

NEMO includes a built-in coupling with the sea ice model SI^3 (Sea Ice modelling Integrated Initiative). The latter is based on 3 former sea-ice models

(CICE,LIM and GELATO) and includes a plastic visco-elastic rehology, momentum, energy and salinity conservation in an ice thickness distribution framework.

For Antarctica specifically, a configuration has been developed to include open-cavities beneath the ice shelves. It is used to explicitly compute heat and freshwater fluxes from exchanges between the ice and the underlying ocean. The geometry is fixed by assuming that the ice shelf is at equilibrium, the melting ice being replenished by the flow of the ice shelf. We use a specific configuration of this open cavities developed for ISOMIP+ and detailed in Asay-Davis et al. (2016).

5.3 Coupling interface

5.3.1 Coupling general description

NEMO and MAR coupling interface has been developed by Nicolas Jourdain[1] during his PhD thesis and has been thoroughly detailed in Jourdain et al. (2011). It has been improved since with an update of the model components, as well as the revision of the fluxes formulation by Pierre-Vincent Huot[2] and Christoph Kittel[3] in Huot et al. (2022). The novelty of the configuration in this present section lies in the pan-Antarctic scale domain, enabling studies over the whole sea ice extent.

From a technical standpoint, the coupling is managed by the 3rd party coupled OASIS3-MCT. It is used to spatially interpolate all of the fields (conservatively or not) from one model grid to another. The coupling is done inline, meaning the field exchange is achieved while the two models are running in parallel - compared to offline coupling where the two models would stop, exchange fields, and restart. While the latter method is technically easier to setup, even more so in a computationally intensive framework, it does not allow for high frequency fields exchange (Because often models would need to save their current state by writing consequent amounts of data at every coupling timestep, which takes much longer than reading them directly from the RAM). So, while it is often used in atmosphere-ice sheet coupling because of the very low response time of the ice sheet (annual at the very most), inline coupling is needed for ocean-ice-atmosphere coupling, where atmospheric and oceanic surface properties can change in the order of hours to days.

[1]Univ. Grenoble Alpes/CNRS/IRD/G-INP, Institut des Géosciences de l'Environnement, Grenoble, France

[2]Department of Earth and Environmental Sciences, KU Leuven, Leuven, Belgium

[3]Laboratoire de Climatologie et Topoclimatologie, Département de Géographie, UR SPHERES, ULiège, Liège, Belgium

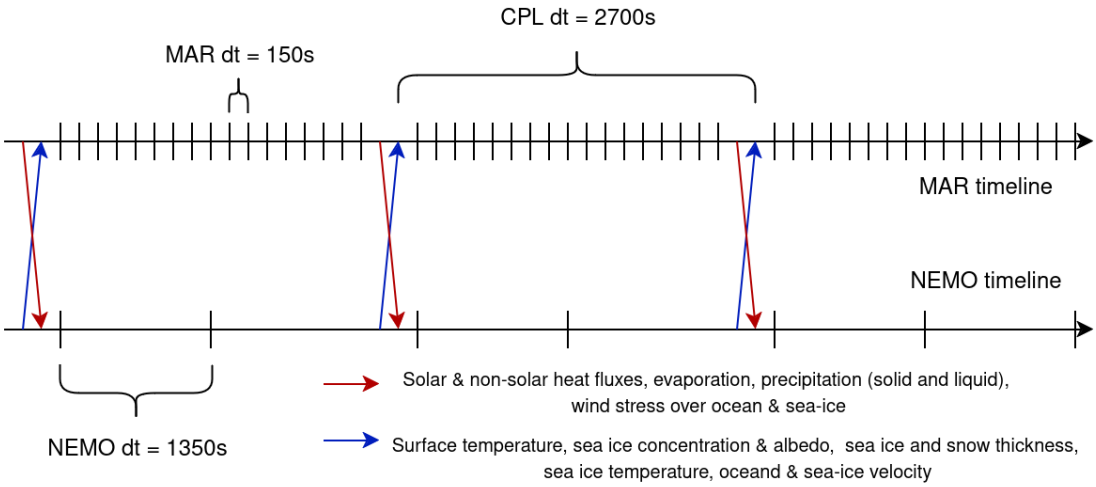

Figure 5.1: Coupling interface diagram after spinup. The fist field exchange happens before the launch of both models using after-spinup status.

5.3.2 Fields exchanged and domains

The first idea that comes to mind when tackling ocean-atmosphere coupling is of course related to momentum and energy exchanges. The mixed layer currents and temperature is strongly dependent on the atmosphere dynamics above. The atmosphere is also strongly influenced by the temperature of the ocean below it. To ensure energy conservation, the information is exchanged as energy and momentum fluxes (respectively sensible and latent heat, and wind stress over the surface). We are exchanging instantaneous fields (TANGO-A version in Jourdain et al. (2011)).

One of the main advantages of using a coupled system is that we can also make use of the strengths of both models regarding snow and sea-ice. While MAR has a good snow representation with a discretized snowpack, metamorphism, refreezing, densification of the layers and a complex albedo scheme, its sea ice module lacks interactions with the ocean surface and is prescribed from forcings. On the opposite side, NEMO-SI^3 has a good representation of the sea ice processes, allowing for growth/melt, ocean-sea ice interaction and advection, while it is lacking a good snow representation above the sea ice.

The 3rd party coupler OASIS3-MCT at the interface of the two models is used to exchange multiple fields while the models run in parallel. Every 1h30 in simulated time, MAR sends to NEMO-SI^3 solar & non-solar energy fluxes, liquid and solid precipitation and wind stress over ocean & sea-ice. NEMO-SI^3 sends back ocean & sea-ice surface temperature, sea ice concentration, sea ice and snow thicknesses & albedo and ocean & sea-ice velocities. The use of a 3rd party coupler enables for an interpolation on-the-fly of all the fields exchanged from one grid to another (See Fig.5.1).

Such a framework was already existing between those two models (Jourdain et al., 2011; Huot et al., 2022), but over small integration domains, disallowing the

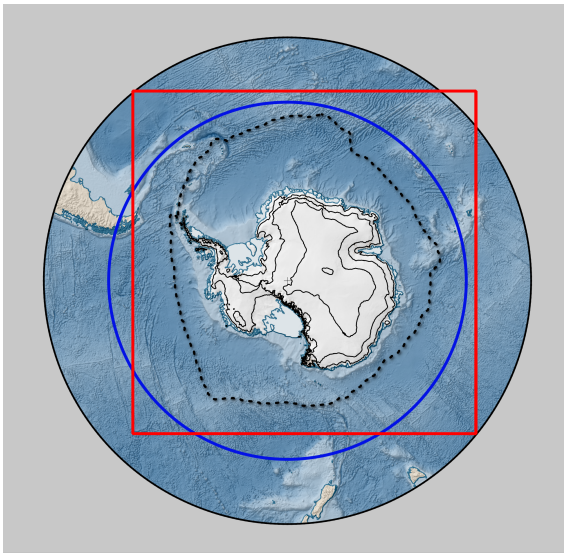

Figure 5.2: Map of the two domains used for the coupling. The red (blue) boundary delimitates the MAR (NEMO-SI^3) domain. Some parts of the NEMO-SI^3 domains are not covered by the MAR domain and vice-versa. The black dotted line, fully encompassed in the two domains, indicates the median September SIE between 1980 and 2020 (data from .

models to drift due to the lateral boundaries forcing (atmospheric/oceanic general circulation) and constraining a lot the models. So, the novelty of this effort lies in the pan-Antarctic domain we developed. Coupling at such a scale, with long residential times of the water and air masses, represents a major challenge in balancing the two, particularly in terms of energy fluxes. The two domains that were used are shown in Fig.5.2. The NEMO-SI^3 domain extends up to 55°S with a 1/4° resolution (439x1440 pixels). It has up to 121 vertical levels in the deepest parts and open ice-shelf cavities. The MAR domain covers the entire continent and Drake passage with a 326x326 grid at a 25km resolution in a polar-stereographic projection.

The grids of the two domains do not overlap completely. For the corners of the MAR domain, where there is no ocean simulated by NEMO-SI^3 below, MAR is forced by ERA5 sea surface conditions. Likewise, where the atmosphere is not simulated by MAR, NEMO-SI^3 is forced by ERA5. A linear interpolation is applied in a transition zone between coupling and forcing fields at the boundaries, for the 7-outermost ocean pixels or atmosphere pixels.

Because MAR is only parallelized using OpenMP, the coupled simulations are relatively slow, since the scalability of the atmosphere model is limited by the number of CPUs per node. This makes it unpractical to do a proper spin-up period of the coupled model, especially since the oceanic spin-up time is longer than atmospheric spin-up time. Instead, each model is initialized in standalone mode. MAR has a 9-month spin-up, and NEMO-SI^3 a 40 years spin-up, the latter ensuring that general circulation and water masses are properly represented (Fig. 5.3). During the spin-up, MAR is forced with ERA5 sea surface conditions, and NEMO-SI^3 is forced with near-surface ERA5 based fields from 1980 to 2020.

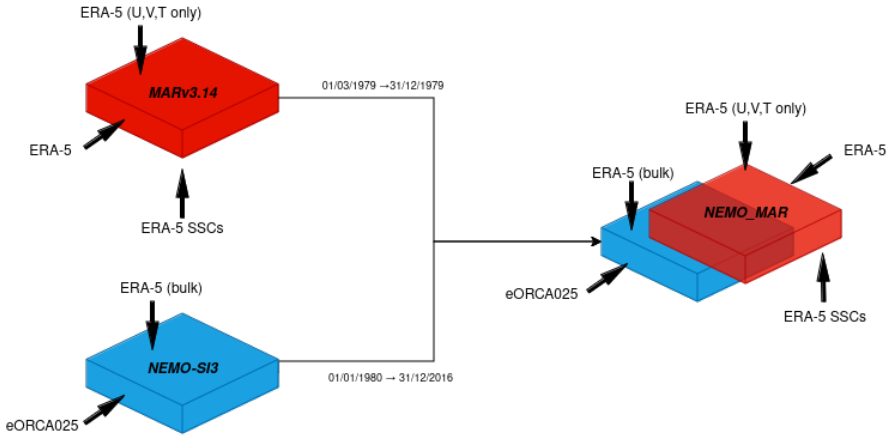

Figure 5.3: Diagram of the coupled system, adapted from Jourdain et al. (2011)

5.4 Standalone NEMO-SI^3 domain sea ice evaluation

The regional NEMO-SI^3 domain described above is a sub-grid from the reference ORCA025 global NEMO-SI^3 configuration, that is used by some high-resolution GCMs. The stability and accuracy of the regional domain simulation; in salinity, currents and temperature, was thoroughly tested and tuned by C. Kittel and described in Olive Abello et al. (2025). Some of the validation is shown in Suppl. Fig.C.1.

Using OSISAF sea-ice concentration satellite product (Tonboe et al., 2016), we have compared observational records to an after-spinup (as described in Fig.5.3) standalone NEMO-SI^3 simulation forced by ERA5. Overall, the simulation reproduces well the seasonal variability (Fig.5.4), but overestimates slightly the winter maximal extent by ∼3%. The inter-annual spread is lower than in OSISAF in winter but slightly higher in summer - especially in March.

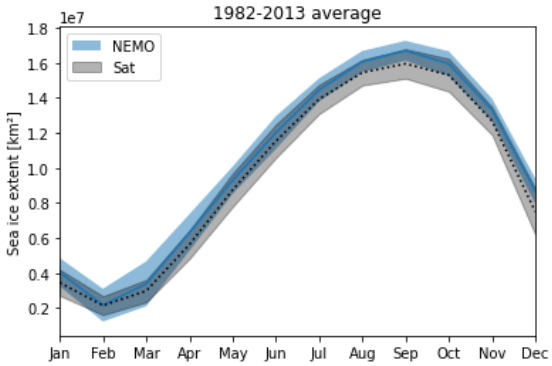

Figure 5.4: Monthly SIE average over the 1982-2013 period in NEMO-SI3_ERA5 (blue) and in OSISAF (black, dotted). Shaded areas are between the 5 and 95 percentile of the distribution among years.

While it is difficult to follow the accuracy of the modeled SIE when looking at integrated values, comparing monthly regional anomalies yields a very conclusive result (Fig.5.5). While the SIE is slightly overestimated in the Ross sea and in the Weddell Sea in the 1980s, the model anomalies follow closely the observed anomalies.

Looking at spatial averages, we find again that the SIC is slightly overestimated in all seasons (Fig.5.6, middle). However, we identify an underestimation by NEMO-SI^3 of the summer coastal sea-ice, as well as an underestimation in the Weddell Sea.

Using NSIDC sea-ice motion dataset (Tschudi et al., 2020), we have also tracked down potential biases in the sea-ice advection in NEMO-SI^3 compared to satellite measurements (Fig.5.7). We identify overall a drifting velocity overestimation in NEMO-SI^3_ERA5 in winter and spring. This can be because of a poor representation of the land-fast ice in NEMO-SI^3 simulations (Pirlet et al., 2025). This can indeed be further confirmed when looking at spatial differences: a strong positive bias is found near the coastline (Supp. Fig.C.2).

The sea-ice being at the interface of the two coupled atmosphere and ocean models, it is crucial to verify that its representation is fair before coupling. We here confirm that standalone NEM-SI^3_ERA5 sea-ice concentration and motion evolutions is 1) stable across the simulation period and 2) realistic enough to be considered as a reference to evaluate coupling experiments.

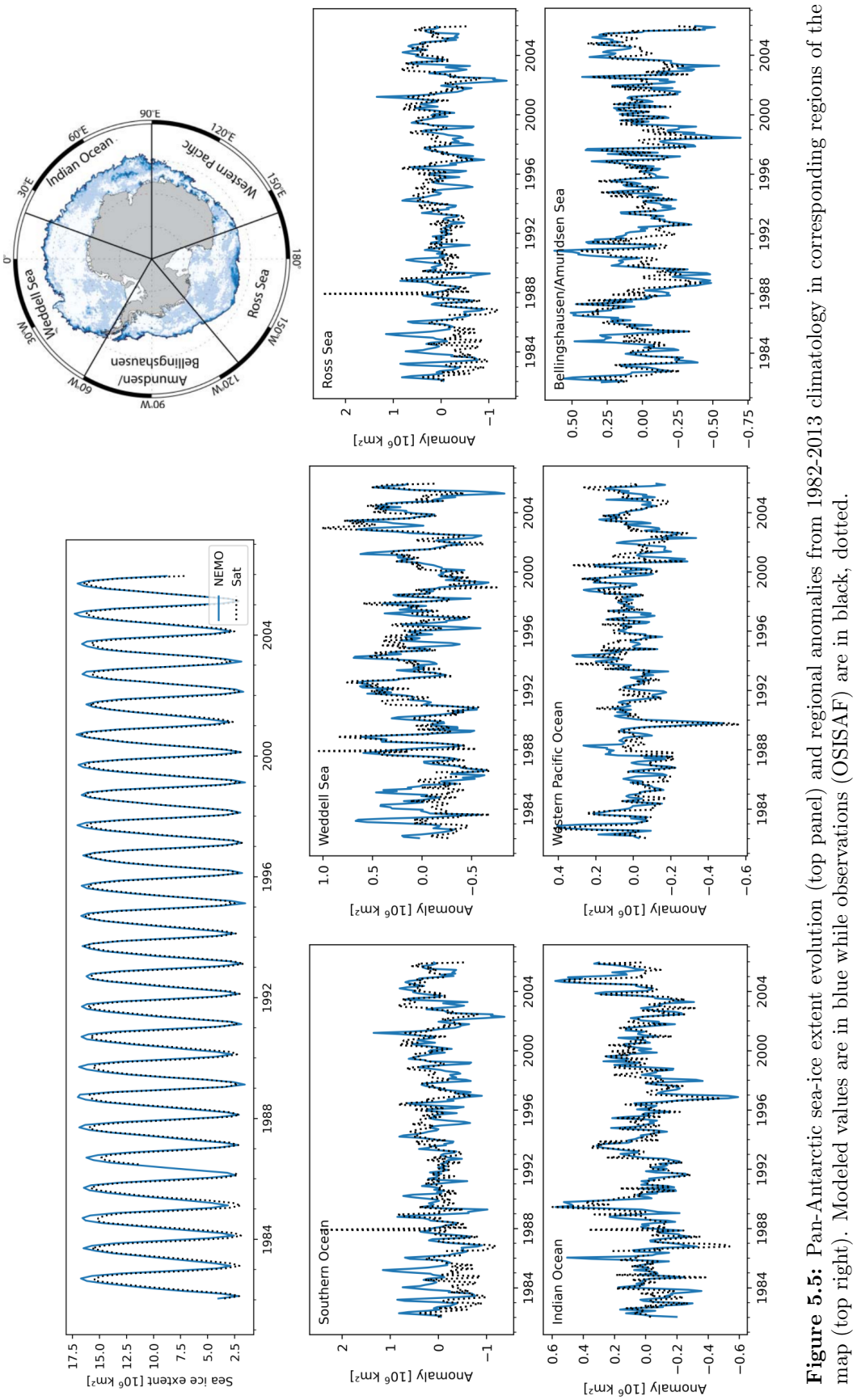

Figure 5.5: Pan-Antarctic sea-ice extent evolution (top panel) and regional anomalies from 1982-2013 climatology in corresponding regions of the map (top right). Modeled values are in blue while observations (OSISAF) are in black, dotted.

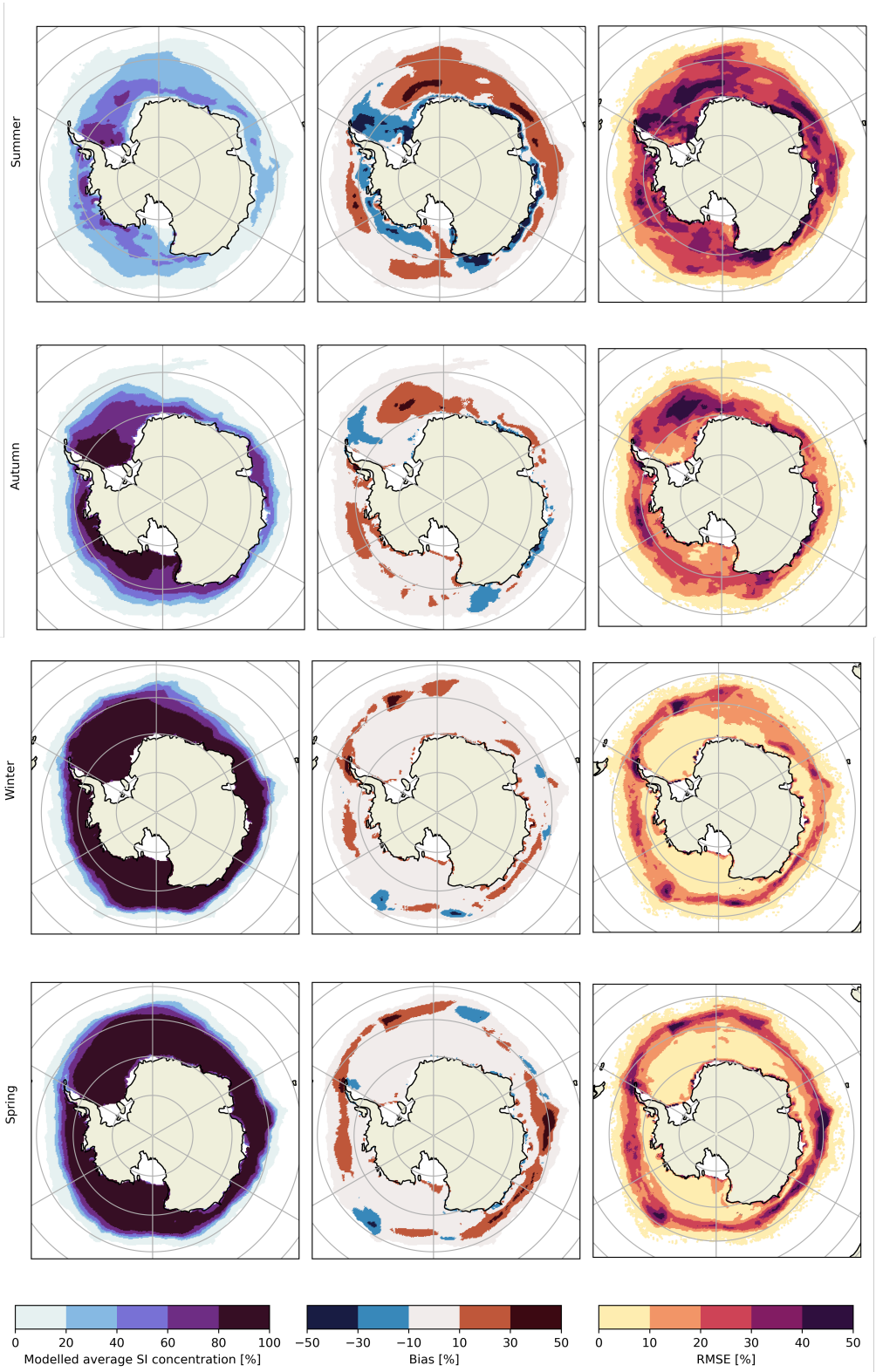

Figure 5.6: Modeled average SIC (left), bias (middle) and RMSE (right) compared to OSISAF observations for all 4 seasons.

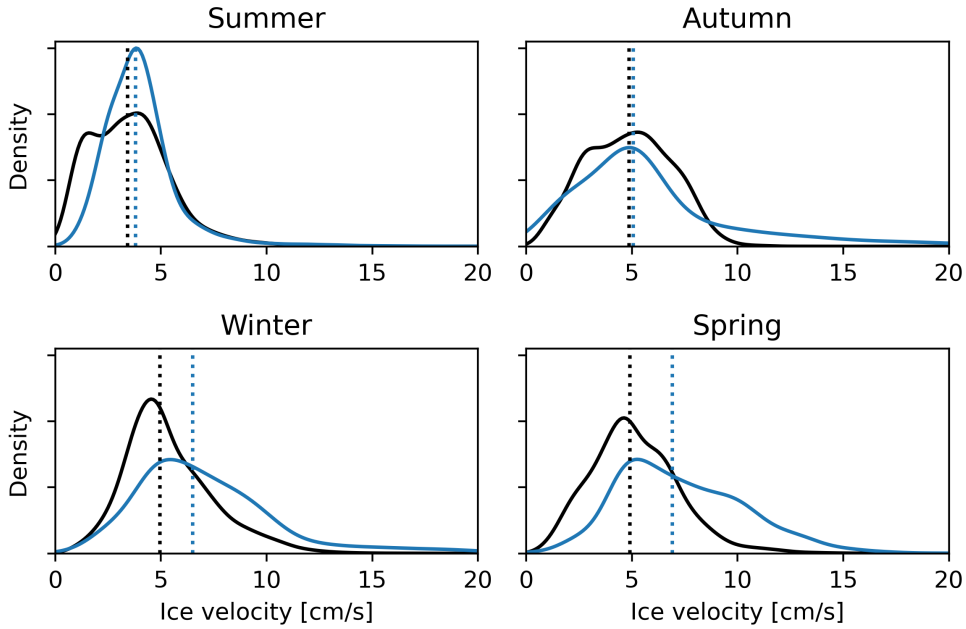

Figure 5.7: Pixel-wise (25kmx25km) sea-ice velocity distribution for NEMO simulation (blue) and observations (black) in all 4 seasons for the period 1982-2013. Vertical lines indicates median values.

5.5 Simulations carried out

After a 1-year atmospheric standalone spin-up of MAR and a 40-years oceanic spin-up of NEM-SI^3, the exchange interface between MAR and NEMO-SI^3 is activated in place of the regular forcing fields (Fig.5.1, with simulations starting from the 1rst January 1980. The different experiments carried out, focused mainly on changing energy fluxes into NEMO, are described in Table 5.1.

Focusing on the reference simulation (Fig.5.8), we see that the evolution of the modeled sea ice extent in the coupled simulation (blue line) follows the reference stand-alone simulation (black line) during the first year of the experiment, with a (likely) positive bias in winter and a negative bias in summer. However, while the yearly minimal sea ice extent remains stable, we see a clear negative drift of the maximal sea ice extent in the coupled simulation, indicating that the energy exchanges between the two models might not be well balanced. This is related to a gradual warming of the ocean mixed layer (Fig. 5.9), more pronounced in summer, presumably because the ice retreat enables more energy into the ocean.

The deep ocean in the coupled model also experiences a slight temperature decrease compared to the standalone one. This is explained by a decrease of the dense water production and export everywhere around the continent. From the first month of the coupled simulation, a strong salinity decrease is observed at the top of the mixed layer (Fig. 5.9), indicating a stronger sea-ice melting from the first simulated summer. This excessive melting seen from the first simulation

Experiment name	Coupled	Description
NEMO_ERA5	No	Reference NEMO-SI^3 simulation where the atmospheric forcings come from the ERA5 reanalysis.
NEMO_MARcpl	Yes	Reference coupling simulation with original codes from both MAR and NEMO
NEMO_MARstandalone	No	Standalone NEMO simulation with forcing from MAR (1 way coupling using original bulk formulations)
NEMO_MAR60standalone	No	Standalone NEMO simulation with forcing from MAR, with MAR forced himself by ERA5 but with a fixed sea ice extent all year thouhout up to 60°S.
NEMO_MARstandalonecplform	No	Standalone NEMO simulation with forcing from MAR (1 way coupling using coupled fluxes formulations)
NEMO_MARcorrv1cpl	Yes	Coupling simulation with MAR code modified to decrease energy fluxes into the ocean.

Table 5.1: Coupled and oceanic standalone simulations carried out.

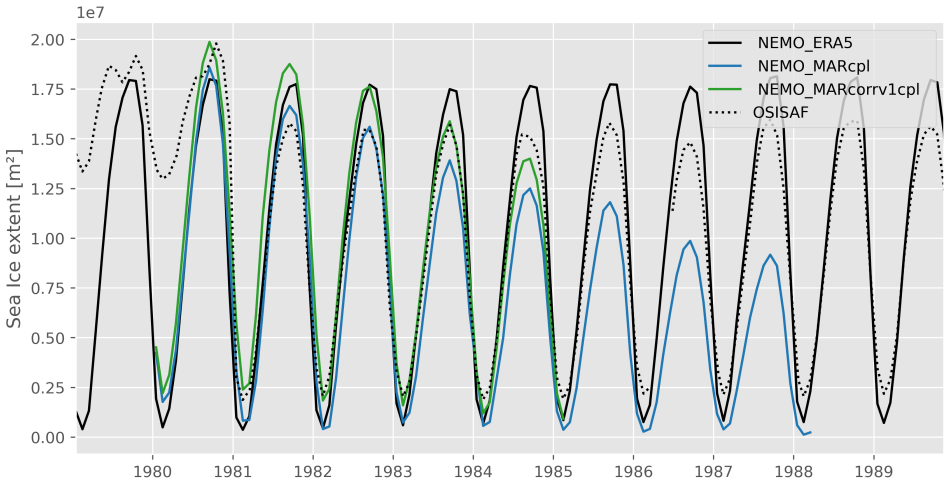

Figure 5.8: Modelled (solid lines) and observed (dotted line) sea ice extent evolution in different experiments. Observations before 1981 are likely not accurate.

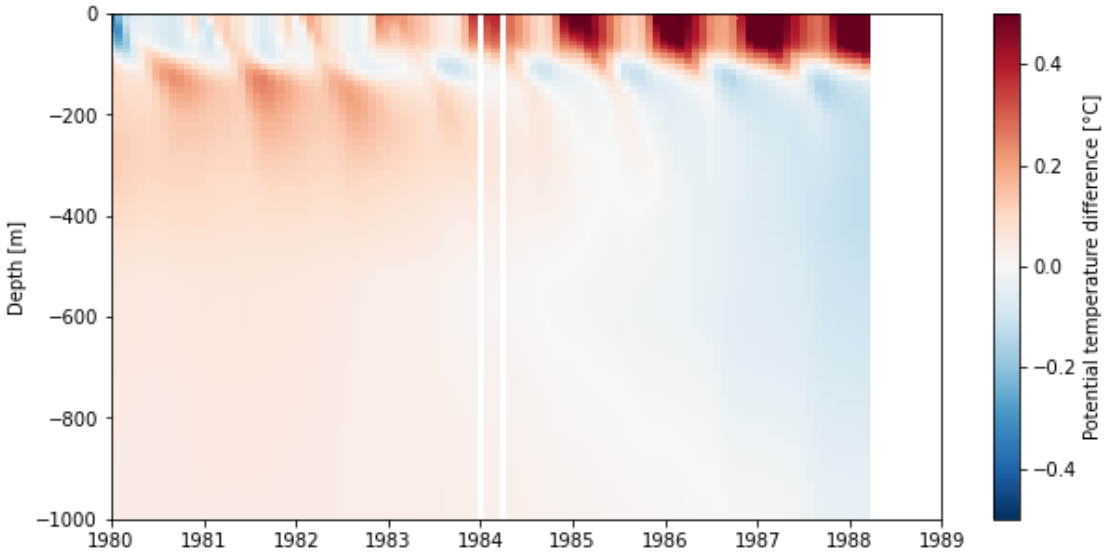

Figure 5.9: Horizontally averaged (all domain) difference between NEMO_MAR (coupled), and NEMO_ERA (standalone) potential temperature evolution across the water column.

month in the coupled system leads to pervasive changes in the entire domain, with a subsequent warming of the atmosphere above the ocean, decrease of dense water production via an ocean destratification, and a very strong decrease of sea ice production over the whole domain. It was decided to stop the simulation after 1988 because it was not usable.

To prevent the unrealistic warming seen of the ocean, the MAR code was changed by retuning parameters of the radiative scheme. These changes include an increased ocean albedo, snow albedo, and decreased conversion of hydrometeors from liquid to solid particles to decrease the SWD with an increased reflectivity. These adjusted were tested with a new simulation that was continued until the long-term trend in summer sea ice had emerged. All those chose changes combined led to an overall colder atmosphere, leading to a higher sea ice maximum in the first simulated year (Fig. 3, green line). However, the drift seen in the original coupled formulation still occurs at a similar speed.

To understand the drift seen in the coupled system, multiple sensibility studies were conducted by forcing NEMO with different products (Table 5.1 & Fig. 5.10). As both models are stable when running in standalone mode, the focus was placed on determining whether the coupling interface could be faulty. First, when NEMO is forced by MAR outputs (Fig.5, red line, NEMO_MARstandalone), the sea ice extent follows a realistic signal - close to the one when NEMO is forced by ERA5. No drift can be seen in the sea ice extent evolution.

Next, it was tested if the added degrees of freedom in the coupled model could explain this drift. In standalone mode, NEMO is forced by an atmospheric product that already has a signal of the sea ice extent evolution as the observed ERA5 based SST and sea ice cover is prescribed into MAR in this case. These prescribed sea state conditions come from other models, or, in the case of using

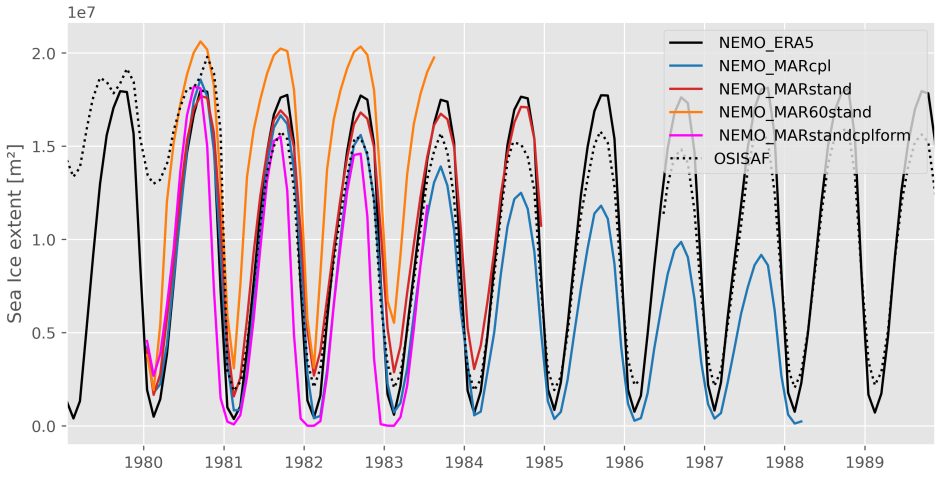

Figure 5.10: Same as Fig.5.8 with other forcings. NEMO_ERA5 (black line) and NEMO_MAR (blue line) are shown as reference.

ERA5/MAR, from satellite data. This test was carried out to inquire much this "forcing of the atmospheric forcing" did constrain NEMO in its sea ice evolution, and, conversely, if this lack of constrain could lead to a drift in the coupled model. To test this hypothesis, a simulation was carried out in which MAR was forced by ERA5 with a fixed sea ice extent up to 60°S, all year round (NEMO_MAR60standalone).

The NEMO sea-ice extent evolution when forced the MAR outputs from this experiment are shown in Fig. 5.10 (orange line). Though the atmospheric forcing has a fixed sea ice extent, NEMO is still able to recreate a seasonal variability - though inherently with a higher sea ice extent because of the overall colder forcing. This shows that NEMO has its own liberty in terms of sea ice extent, even in standalone mode, so it is likely not the reason for the drift observed. The next sensitivity test involved testing the updated coupling method, which replaced the original bulk method. Usually, NEMO is forced using bulk methods for sensible, latent and momentum fluxes by recomputing these fluxes using u,v, t2m and q2m from forcing. When coupling to an atmospheric model, this method leads to a non-conservative energy interface as the way to compute the energy near surface fluxes is different in both models. This is likely to be a problem when dealing with long residential time of the water masses, because an energy imbalance is not evacuated at the lateral boundaries (Jourdain et al., 2011). This bulk method was also used in the preceding sensitivity simulation NEMO_MARstandalone, as for stand-alone tests energy conservation by the coupler is not required as energy is, by construction, not conserved in stand-alone simulations.

The results of a stand-alone simulation of NEMO, forced by MAR, in turn driven by ERA5, using the update coupling method of the coupled simulations, are shown in Fig.5.10 (magenta line, NEMO_MARstandalonecplform). In contrast to the stable bulk method simulation, this simulation has an underestimation of

the minimal and maximal sea ice extent, with a total disappearance of sea ice in the first summer. This is an indication that the problem lies in the downward surface energy fluxes provided by MAR. Moreover, the sensible and latent heat flux simulated by MAR over open ocean has never been evaluated as the sea surface temperature is usually prescribed into MAR and biases in these fluxes do not impact MAR result. Such an issue was not seen in the previous studies using the MAR- NEMO coupling because of smaller integration domain, with shorter water residential times, disallowing to NEMO (and MAR) to drift.

5.6 MAR fluxes analysis

To see where the problem could lie, the NEMO_MARcpl and NEMO_ERA5 solar and non-solar fluxes are compared. Integrated over time (Fig.5.11), a very large difference between the ERA5 and MAR downward non solar-energy is apparent. This is more pronounced above 60°S, corresponding roughly to the ice free region, where the bias is constant during the whole simulation. It is less pronounced below 60°S, where the main difference in energy income appears after a few years of simulation, when the decrease in sea ice extent in NEMO_MARcpl becomes significant and more solar energy is absorbed by the ocean. Furthermore, the non-solar energy imbalance decreases after a few years. This might be because the strong warming of the ocean eventually increases the sensible and latent heat flux from the ocean towards the atmosphere enough to stabilize the system after a few years.

In Fig.5.12, we clearly identify a yearly +7 $W.m^{-2}$ difference between the coupled standard run and the standalone forced by ERA5. It is most pronounced in austral autumn, where the non-solar heat flux bias is of +11 $W.m^{-2}$. This is explained by the retreat of the sea-ice that enables more open-ocean to absorb excessive amounts of energy from MAR, though the non-solar heat flux bias is significant in all seasons.

Eventually, the bias seen near the MAR domain borders (confirmed when comparing non- solar fluxes of MAR and ERA-5) will be corrected in a future version of the model. They result of the ERA5 based temperature nudging in the MAR high troposphere perturbing the clouds and precipitation formation in MAR. Such perturbations were also identified over Arctic with MAR and one of the solution is to only nudge the wind from ERA5 (and significantly less the temperature) at the high vertical levels of MAR. For small integration domain, we need only a nudging in the stratosphere (above 100-200hPa) not impacting the MAR clouds formation. But, for large integration domains, MAR tends to generate its own general circulation except if the upper nudging starts at 500hPa, which impacts the clouds formation in MAR if the temperature from ERA5 is nudged.

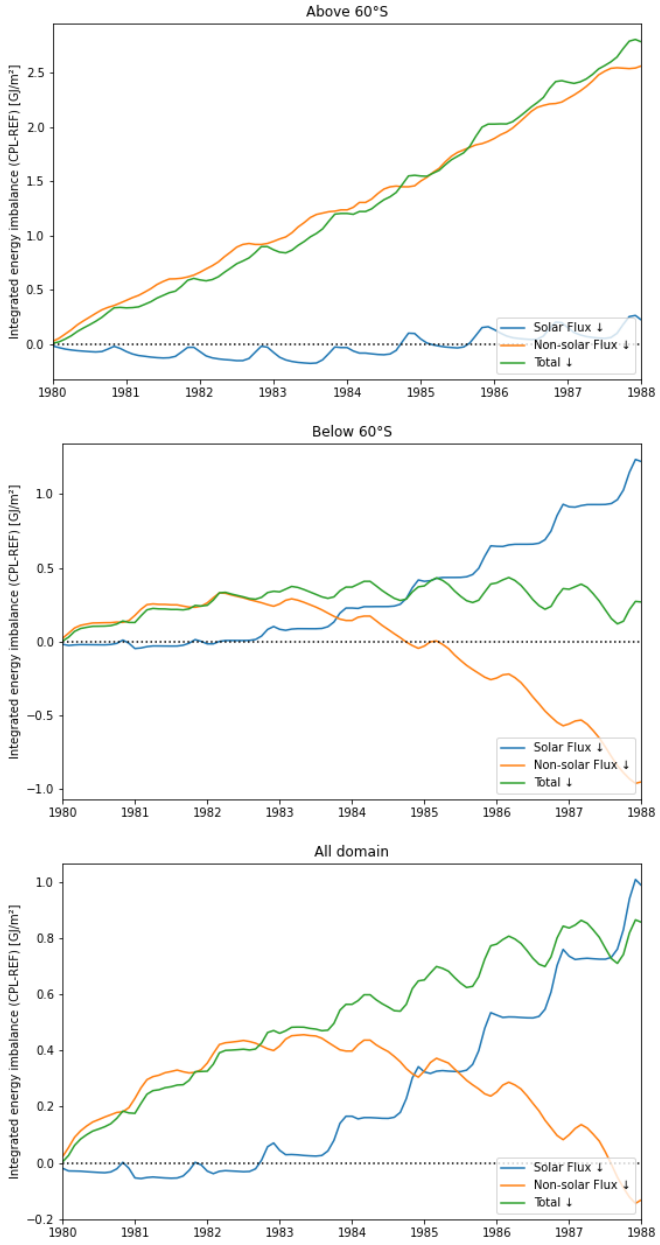

Figure 5.11: Cumulative downward radiative energy difference between coupled (NEMO_MAR) and standalone (NEMO_ERA5) simulations. Total energy (green line) is the sum of the solar (blue line) and non-solar heat fluxes (orange line).

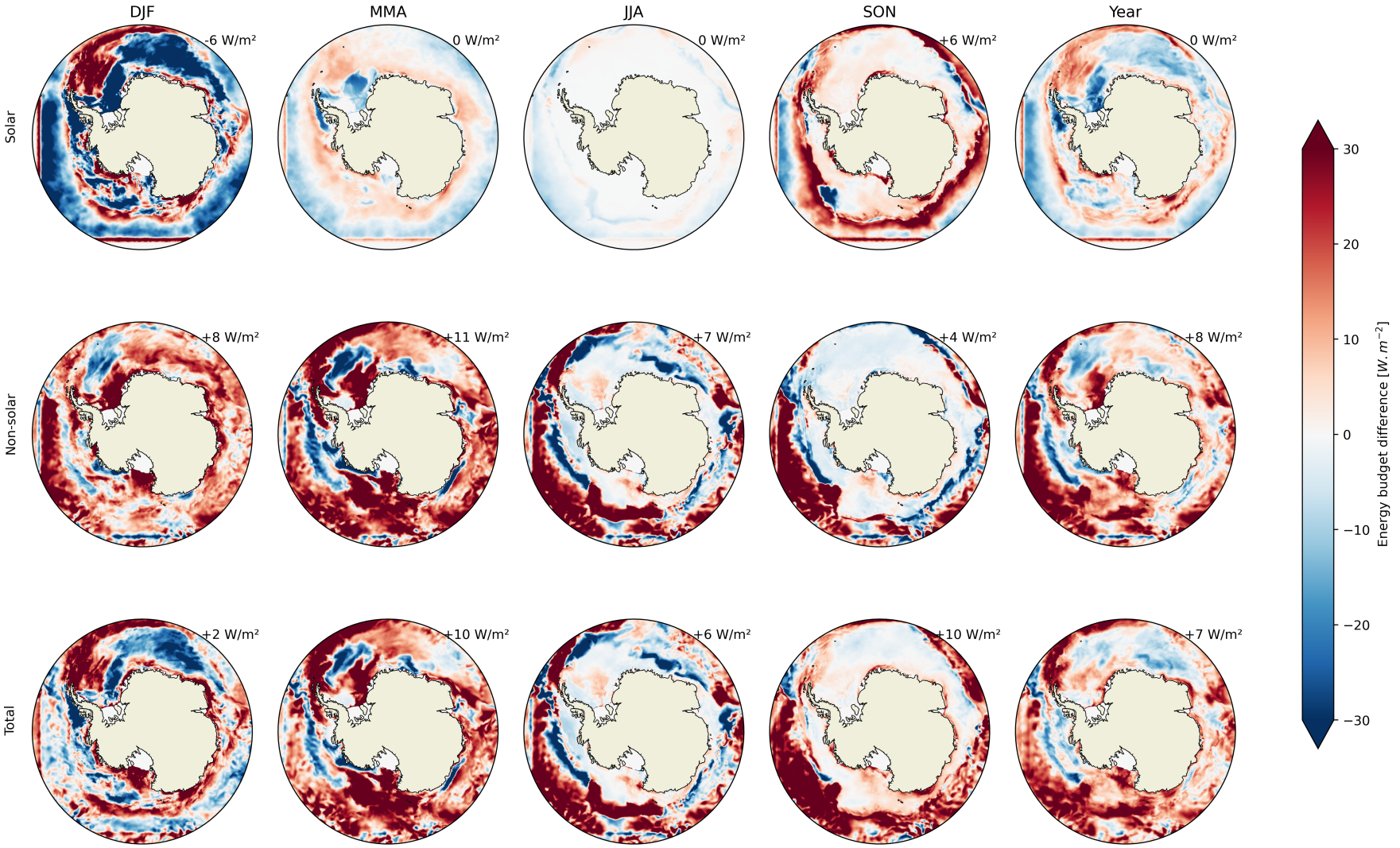

Figure 5.12: Seasonally and annually averaged energy fluxes differences between NEMO_MARcpl and NEMO_ERA5 for the first simulated year. Spatial averages are shown in the top right map corners.

5.7 Arctic counterpart

Using the same coupling interface, Clara Lambin[4] developed another Arctic configuration using novel pan-Arctic MAR and NEMO domains. While the full description will be left for Lambin's PhD manuscript, a fluxes analogy and drift comparison yields significant information in the context of an energy-diverging Antarctic configuration.

Compared to the Antarctic domain, no drift can be seen when looking at SIE evolution over the Arctic. The simulation seems stable in terms of annual mean temperatures evolution. Naturally, when integrating the energy flux entering the ocean, both solar and non-solar (as in Fig.5.12), we do not find a bias of the same order of magnitude (Fig.5.13). As the largest positive biases in incoming energy flows in the Antarctic domain were close to its edges, it is possible that this phenomenon is attenuated in the Arctic. Indeed, much of the periphery of the Arctic domain consists of land rather than ocean.

[4]Department of Geography, University of Liège, Liège, Belgium

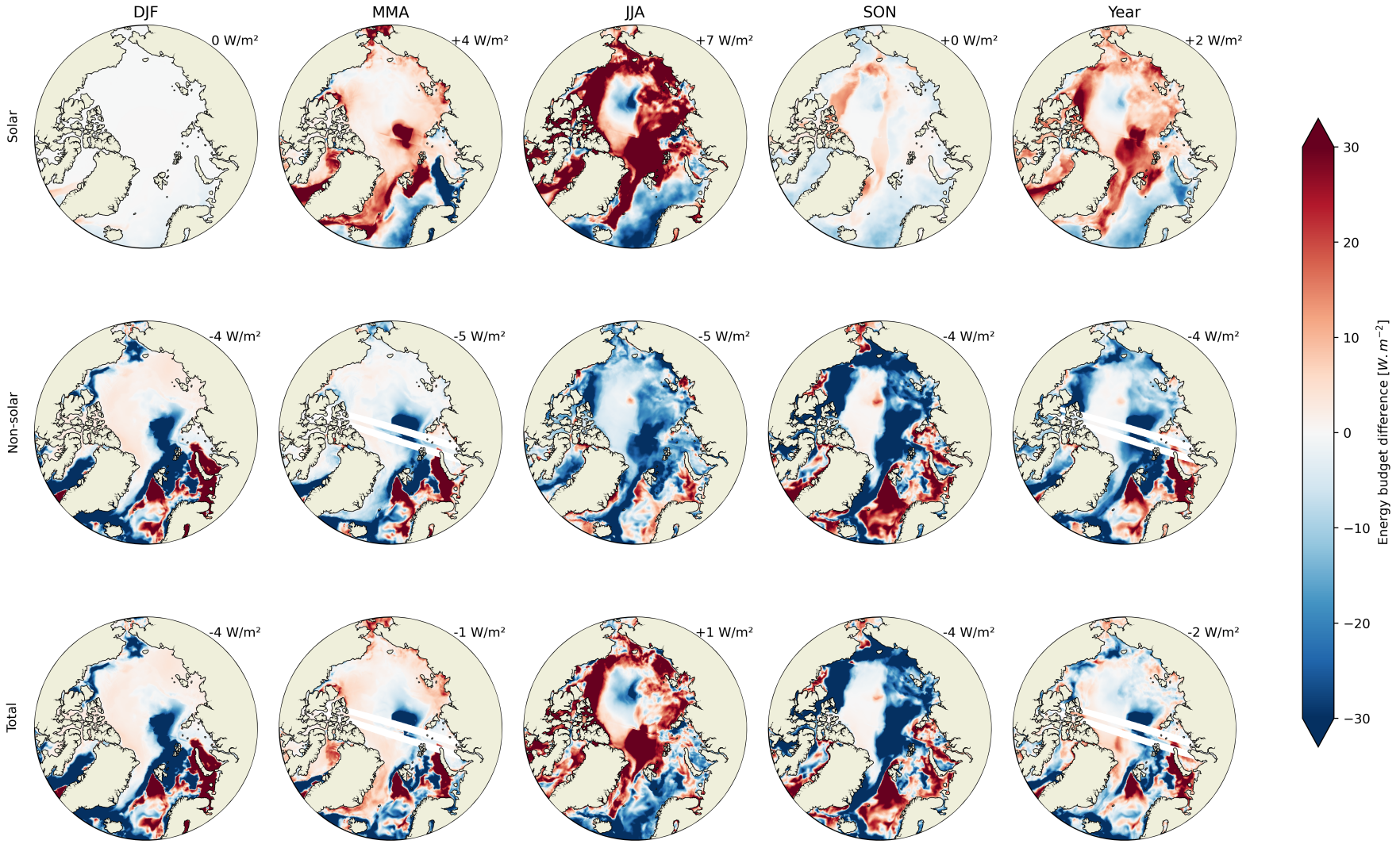

Figure 5.13: Seasonally and annually averaged energy fluxes differences over the analogous Arctic domains between NEMO_MARcpl and NEMO_ERA5 for the first simulated year. Spatial averages are shown in the top right map corners.

5.8 Technical limitations, discussion and conclusion

Apart from the internal problem of described above, the coupling setup suffers from other major issues that will need to be addressed in the future. First, we used the Tier-1 Walloon national HPC infrastructure Lucia, from Cenaero. While being very efficient and up-to-date, it is first designed for industrial and private companies. The latter have a higher priority than academics, and very often saturate the cluster. This would certainly be less of a problem, as the 300 nodes of the cluster can be emptied at night and weekends, if not for the second point that has to do with MAR computing speed. While it is - generally - not a problem in standalone, because the relatively short spinup time of the atmosphere enables multiple short simulations to be run in parallel, the coupled simulation has to be run completely inline. The parallelization of MAR is only coded in specific routines that do not need information from neighboring grid cells (using OpenMP), contrarily to other, more flexible parallelization that distribute spatially the work to the different CPUs, with a specific treatment to exchange information in between the sub-grids (as done in NEMO-SI^3 using MPI).

This makes it so that MAR cannot be parallelized with more than $\sim$24 CPUs efficiently, and is a struggle when tackling high-resolution pan Antarctic domains.

However, we have created an interface that allows any two domains, such as MAR and NEMO, to be seamlessly coupled. This meant that the Arctic domains could be coupled relatively easily once they had been defined separately. The drift observed in the Antarctic domain is not present in the Arctic, where the domain appears to be stable. The latter is therefore ready for use without modifications to MAR. Clara Lambin plans to carry out a comprehensive assessment of this domain in the future and to use it to study the mechanisms of Arctic amplification in greater detail.

CHAPTER 6

Parallel preliminary studies and additional discussion elements

This chapter contains some additional short scope studies and experiments that were done in parallel of the other chapters of this thesis. First, we explore the parameterization of blowing snow on sea ice and its influence in NEMO-SI^3. (Sect 6.1) We then describe a newly derived observational dataset made from ship expedition observations reports.

This chapter contains preliminary studies meant to be completed and expanded by coupled Atmosphere-Ocean simulations. The latter being delayed because of technical limitations (see Chapter 5), the end of those study was postponed until the coupled system is operational.

6.1 Blowing snow over sea ice representation in NEMO-SI^3

Disclaimer: This section was written with material partially lost because of a laptop theft. It is made with a limited backup of draft figures.

The effect of wind on the snowpack has been studied extensively over the Antarctic inlandsis, both in observations (Palm et al., 2011; Mann et al., 2000) and also in models - such as MAR, who explicitly represent the drifting-snow process (Amory et al., 2015, 2020). However, its impact on sea ice remains largely unknown. Although the process is sometimes included in sea ice models, it is generally tuned and rarely looked at.

In SI^3, the blowing-snow process is parameterized as

$$PR_{ice} = (1 - (1 - SIC)^{\alpha}) * PR \tag{6.1}$$

where PR_{ice} is the amount of falling precipitation staying over a pixel of sea ice, PR is the amount of precipitation on that pixel, and α is a parameter with a constant value, tuned at $\alpha = 0.66$. The equation linking precipitation and parameter is plotted in Fig. 6.1. With the value often set in NEMO-SI^3, we see that above a sea ice concentration of 20%, approximately 10% of the precipitations are transferred from the ice to the sea. The extreme values, $\alpha = 0$ and $\alpha = 1$, correspond to the case where all the snow is blown into the ocean ($PR_{ice} = 0$) and the case where none is blown ($PR_{ice} = SIC * PR$), respectively. Notably, this parametrization does not depend on actual wind speed, or any other factor than SIC or α.

To understand the influence of this parameterization on sea-ice, multiple simulations were conducted, starting from an after-spinup ocean state in 1979 (as described in Chapter 5). 4 experiments were conducted with α set at 1, 0.6 (the reference value in NEMO), 0.3 and 0, named respectively BS10, BS06, BS03 BS00.

Sea ice concentration

Looking at the SIE evolution, a small decrease in summer SIE can be observed when more snow is blown into the ocean, though of limited magnitude (Fig.6.2. Look-

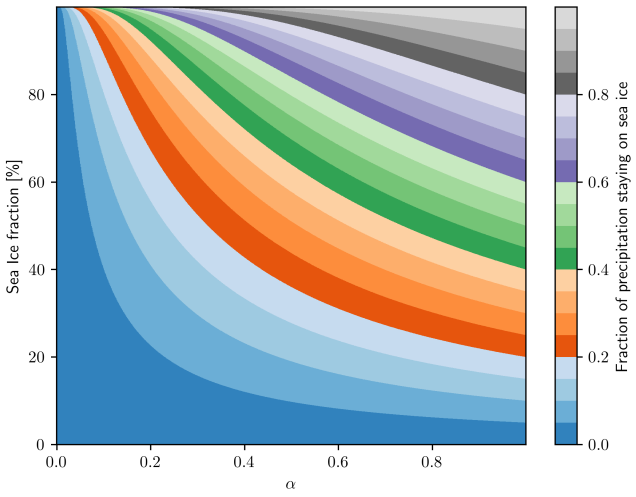

Figure 6.1: Fraction of precipitation staying over ice as a function of SIC and α

ing at spatial differences of SIC, no significant differences can be seen between the four simulations, excepted at the margins of the SIE Fig.6.3. This result is expected and reassuring, as we expected no significant influence on general SIC patterns from this NEMO parameterization (reinforced by the fact that no clear documentation could be found).

Snow Volume

We naturally see a clear difference in the snow thickness above the sea ice. Maximal α leads to a small constant thickness difference of around 5 cm on average over the sea-ice (Fig.6.4. The differences are roughly proportional to the precipitation rates and reference snow thickness, being more pronounced around the Western Antarctica and the Peninsula. In winter, more differences are seen near the coast than offshore in BS10 (Fig.6.5)., while it is not the case in BS03, where strong differences are seen in the Weddell sea.

Sea Ice Thickness

When there is less snow that deposits on the sea-ice surface, the sea-ice tends to grow thicker (Fig.6.4). The low thermal conductivity of snow decreases the heat transfer rate from the sea ice bottom to the atmosphere, reducing ocean water freezing rates at the bottom of the ice-pack (Lecomte et al., 2013; Nie et al., 2022). This phenomenon is more pronounced in winter, in areas where a strong difference of snow volume is also seen (Fig.6.7 and 6.5). There is however an inversion offshore near the sea-ice edge, where the newly formed sea-ice is thicker in BS10 and thinner in BS03 than in the reference simulation. This might be because when the sea-ice is thin, snow is able to convert in snow-ice when the freeboard is negative (i.e when there is enough snow load on ice). In that case, more snow would lead to more sea-ice, dominating the insulation effect.

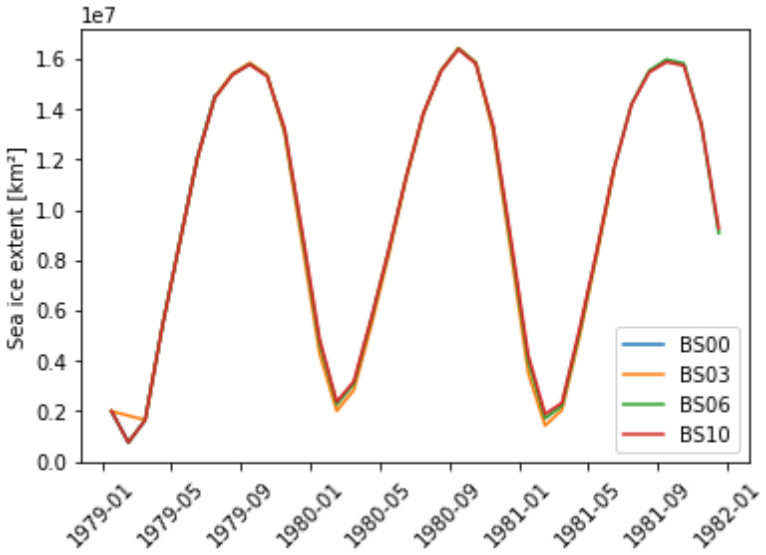

Figure 6.2: Sea Ice Extent evolution for all 4 simulations.

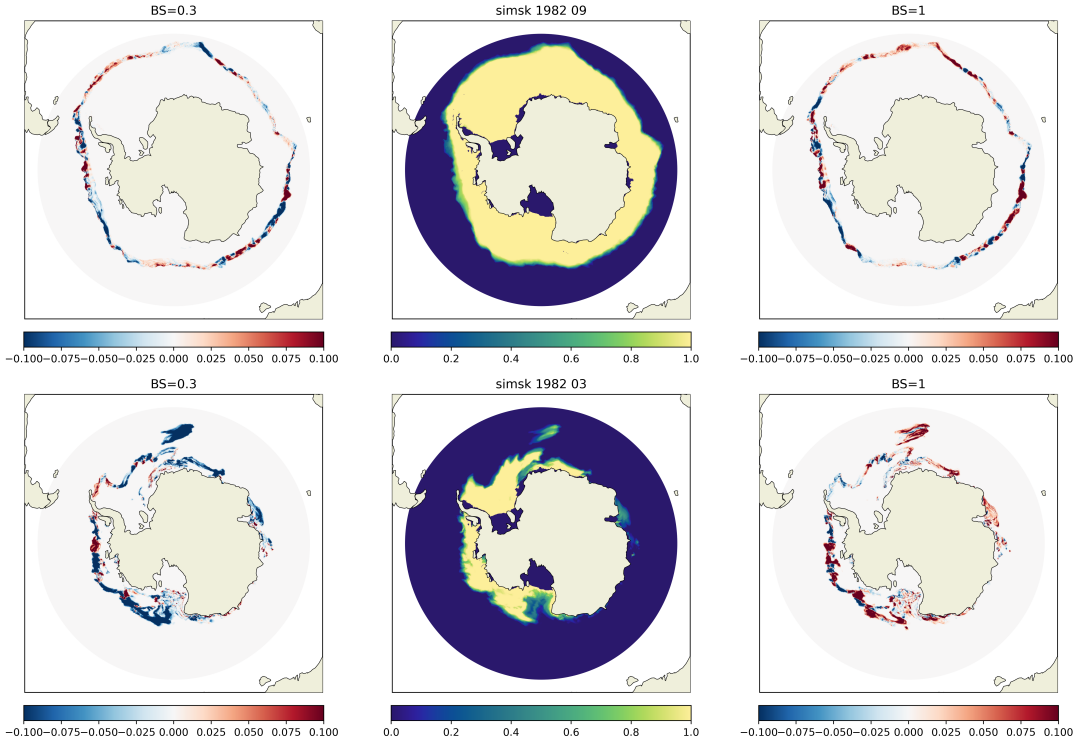

Figure 6.3: Sea Ice Concentration difference between BS03 and reference (BS06) (left), reference sea ice concentration (BS06) (middle) and difference between BS10 and BS06 (right), for september (top) and march (bottom).

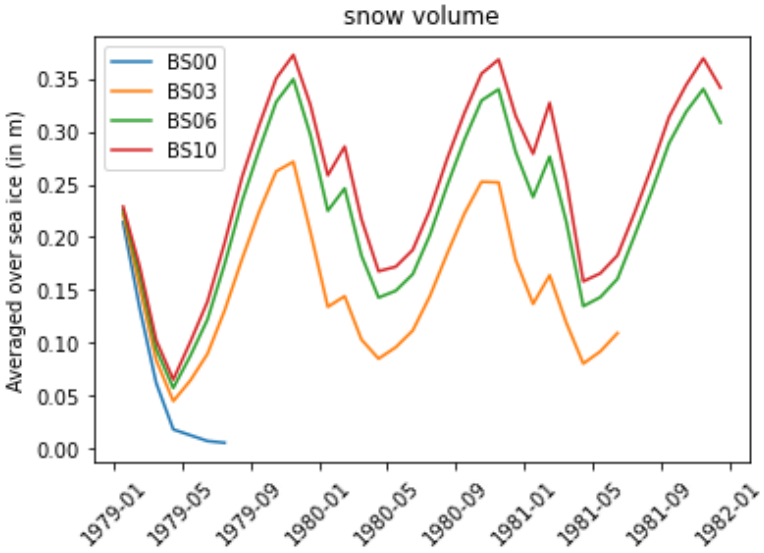

Figure 6.4: Average snow thickness over sea-ice evolution.

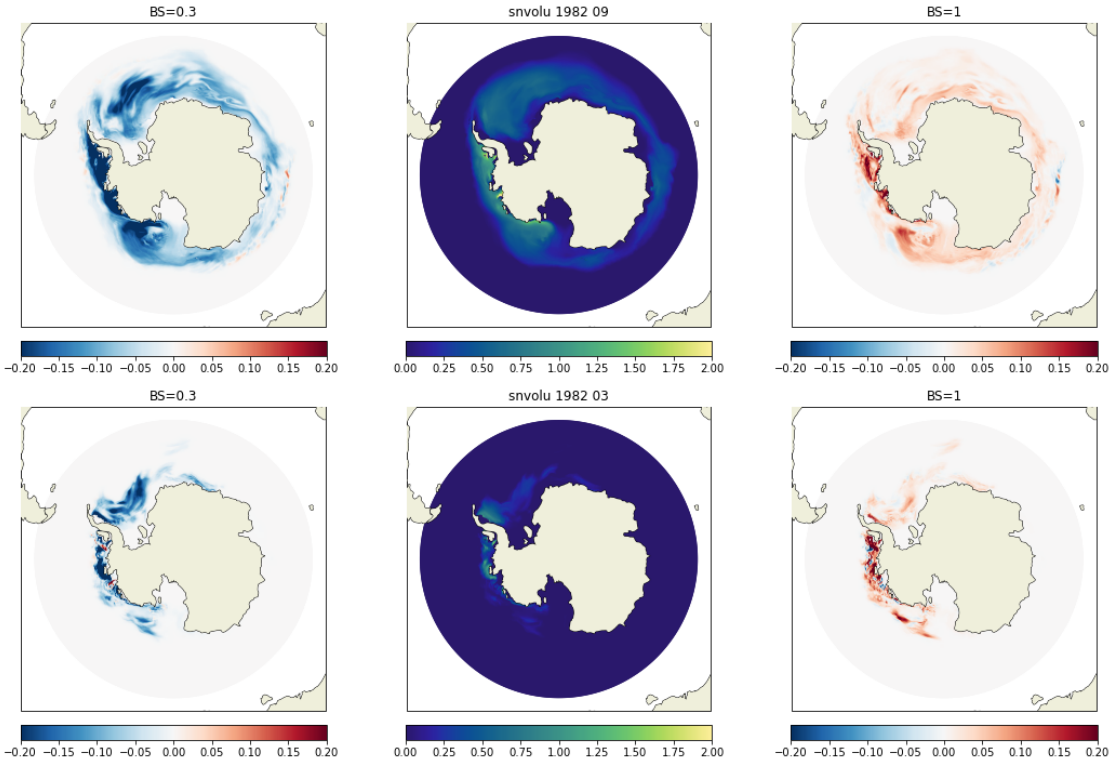

Figure 6.5: Analogous to Fig.6.2 but with snow thickness over sea-ice (in m).

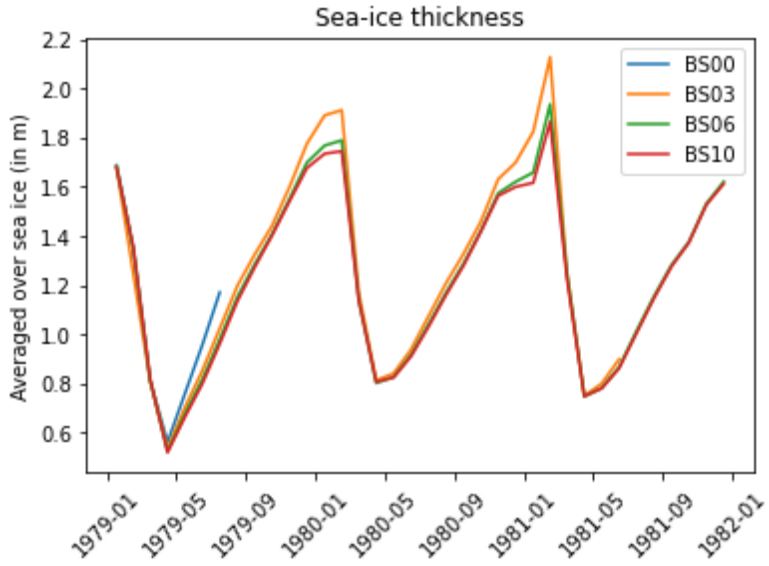

Figure 6.6: Average sea-ice thickness evolution.

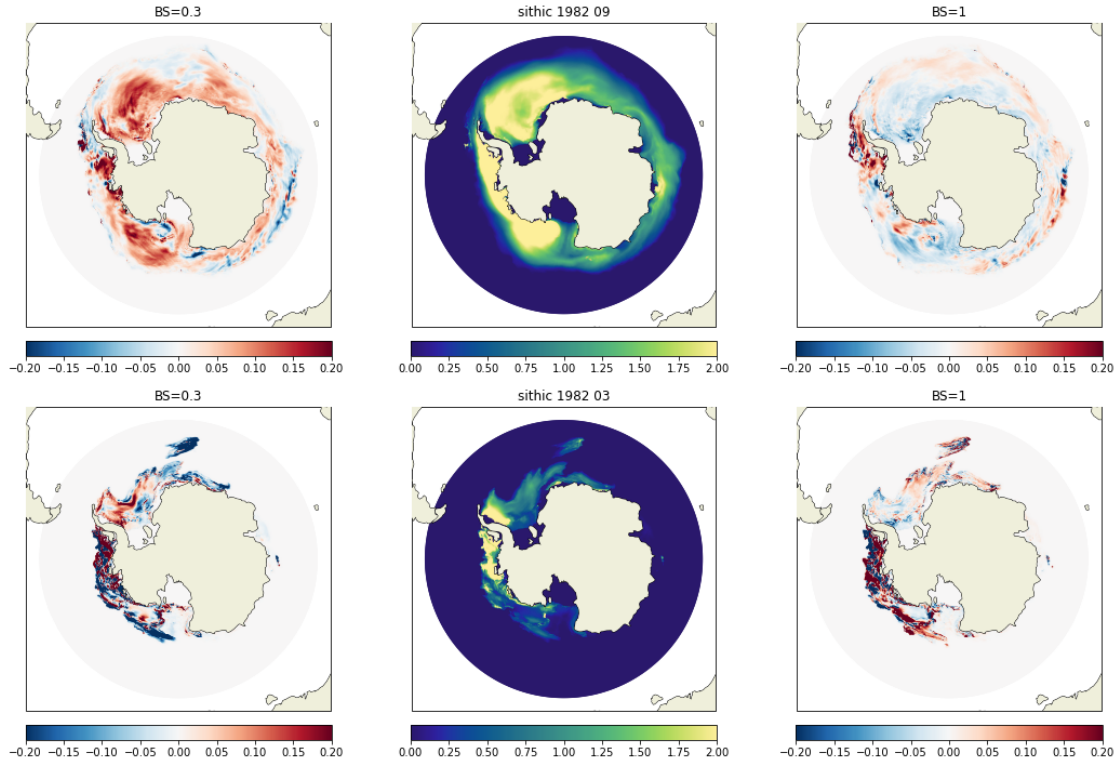

Figure 6.7: Analogous to Fig.6.2 but with sea-ice thickness (in m).

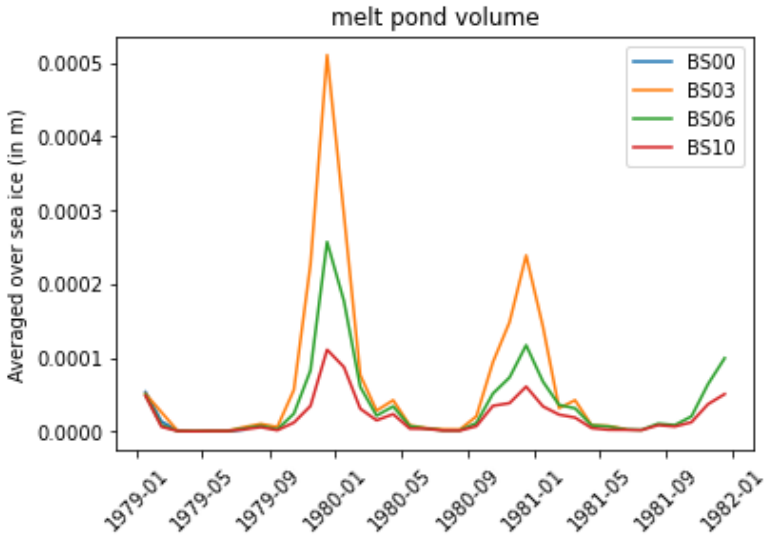

Figure 6.8: Average melt pond volume evolution.

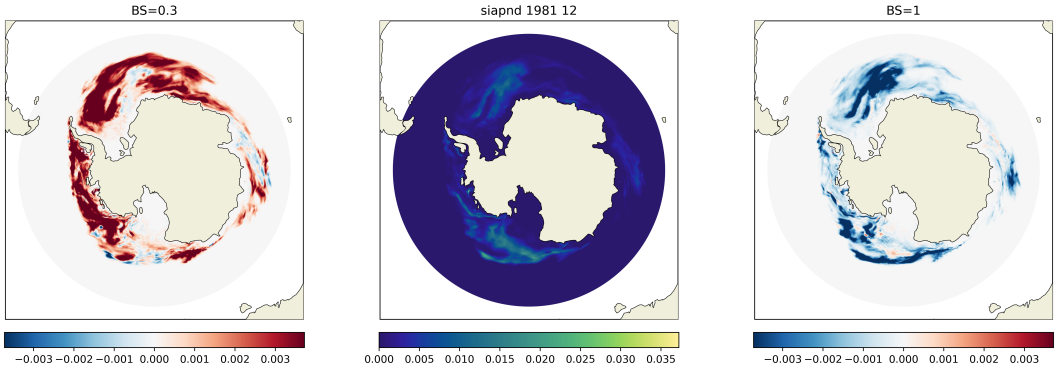

Figure 6.9: December reference melt-pond fraction in BS06 (middle), BS03 anomaly (left) and BS10 anomaly (right).

Melt ponds

Overall, the melt pond volume is twice as important in spring in BS03 than in BS06 (Fig.6.8), peaking in all simulation in December before sea-ice extends starts decreasing strongly. This result is surprising, as more snow on sea-ice would more melting available to form melt ponds. In the sensibility studies of Flocco and Feltham (2007), describing the melt-ponds scheme implemented in SI^3, they obtain a bigger volume of melt pond with thick snow than bare-ice. However, they get a much lower melt pond covered area with thick snow than with the bare-ice experiment, explaining why integrating over all of sea ice could lead to a bigger volume in BS03 in Fig.6.8. In line with this argument, we see in Fig.6.9 that the area covered by melt ponds is larger in BS03 than BS06, but their thickness can be lower in BS03 where deeper melt ponds occur in BS06 (e.g. in the Ross Sea or above the Weddell Abyssal Plain.

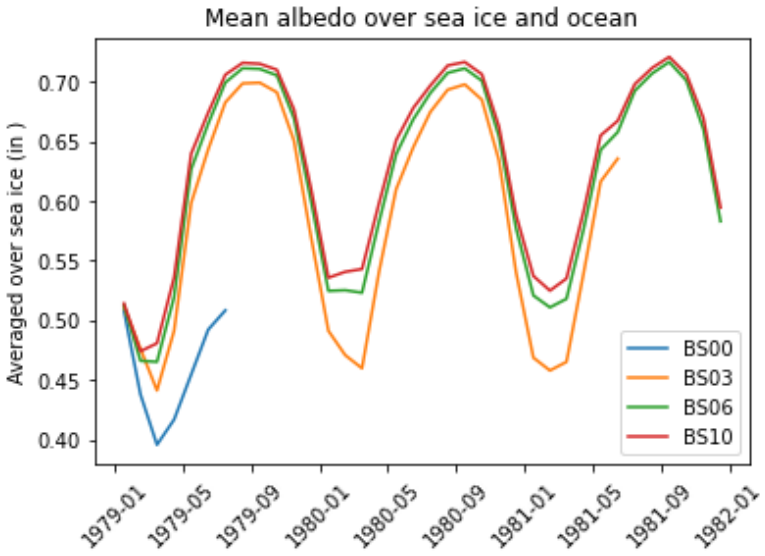

Figure 6.10: Average albedo evolution for all 4 experiments.

Albedo

Because snow tends to increase the albedo of sea ice, it is constantly lower (higher) in BS03 (BS10) than BS06 (Fig6.10.) Consequent to melt ponds influence, this difference more pronounced in spring / summer, because melt ponds drastically lower the sea-ice albedo (6.11).

Wrap-up

This parameterization of blowing snow over SI^3 sea ice is not expected to be determinant for the sea-ice evolution of Antarctica, as it remains a marginal process for sea ice formation (that mostly grows by water freezing underneath the ice than snow accumulation), and that no proper documentation exists in the SI^3 manual (NEMO-Sea-Ice-Working-Group, 2011). Fortunately, we show that no significant changes can be seen from extreme values of the tuning parameter α. However, changing the amount of snow that stays over sea ice changes the seasonal freshwater input to the ocean, with less freshwater in winter when snow is not blown in leads. This could in turn affect the surface salinity evolution, albeit more analysis is needed. These conclusions certainly do not hold for the Arctic sea ice, as multiyear-ice is not as important in the Southern-Ocean than in the Arctic-Ocean, and a build-up of snow cover difference over multiple years could change the melting dynamics of Northern sea-ice. Finally, no explanation could be found for the reference value chosen (0.6) in the NEMO code.

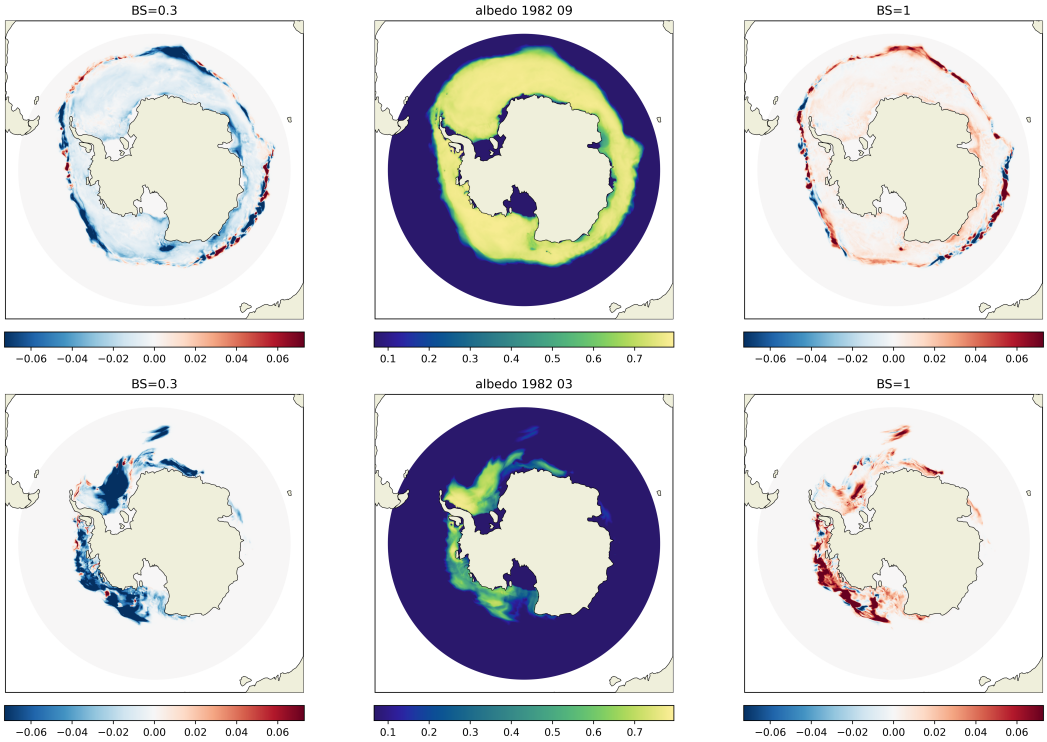

Figure 6.11: Analogous to Fig.6.2 but with sea-ice albedo.

6.2 Antarctic Slope Current future evolution

The Antarctic Slope Current (ASC) is a narrow, westward-flowing ocean current that circulates along the continental slope surrounding the Antarctic margin. It forms a key component of the Antarctic coastal oceanography, playing a vital role in the exchange of water masses between the continental shelf and the deep ocean. The ASC arises from a combination of geostrophic balance, wind forcing, and buoyancy-driven flows associated with the sharp density gradients between cold, fresh shelf waters and warmer, saltier deep waters offshore (Thompson et al., 2018).

This current acts as a dynamic barrier that modulates the onshore intrusions of Circumpolar Deep Water (CDW), a relatively warm and nutrient-rich water mass. CDW has the potential to access ice-shelf cavities and drive basal melting of ice shelves, contributing significantly to Antarctic mass loss and global sea level rise (Jacobs et al., 2011). The strength and variability of the ASC, influenced by mesoscale eddies and topographic steering, determine how much CDW is able to cross the continental slope front and reach the ice-shelf bases (Nakayama et al., 2021).

Recent studies using both in situ observations and high-resolution modeling have highlighted the ASC role in regulating heat fluxes to the shelf and controlling the extent of ocean-driven melting beneath ice shelves such as the Pine Island and Thwaites (Stewart et al., 2019; Nakayama et al., 2021). Understanding the dynamics of the ASC is therefore critical for predicting the stability of Antarctic ice shelves in a warming climate and for improving projections of future sea level rise.

Two NEMO simulations were used: one forced by ERA5, NEMO_ERA5 - from

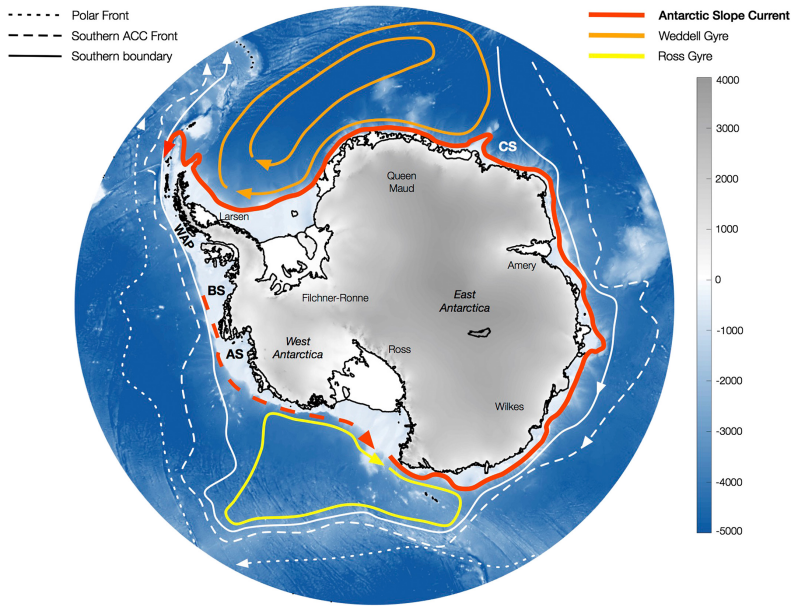

Figure 6.12: Antarctic Slope Current and major features governing Souther Oceans oceanic circulation, along with topography and bathymetry (in m) - from Thompson et al. (2018).

1980 to 2016, described in Chapter 5; and one forced by CNRM-CM6-1-ssp585, from 2014 to 2100. The latter was produced by C. Kittel and will be detailed thoroughly in a future study. The two configurations only differ by their forcings. The January 2014 state of NEMO_ERA5 is used to initialize the oceanic fields of NEMO_CNRM.

A clear increase in the strength of the ASC is found when comparing upper 500m annual mean velocity magnitude from 2014-2024 to 2090-2100 in NEMO_CNRM (Fig.6.13a). The velocity increase extends further East (along the coastline) than today's source of the ASC. Along West Antarctica, this leads to an inversion of the oceanic current along the continental slope (Gate at 130°W Fig.6.13b). The increase is non-linear across the future period of NEMO_CNRM, occuring solely from the 2070s in the gate at 130°W, and in the 2080s for the gate at 150°E. The increase is linear over the whole future period when looking at the western gate at 20°E, where the ASC is usually more built up. The inter-annual variability of the flux in the NEMO_CNRM simulation at this location is very high compared to NEMO_ERA5. This could indicate a future instability of the ASC, though detailed study of this issue is needed.

The overall strengthening of the ASC might be a consequence of stronger future easterlies. The latter could be caused by the overall contraction of the polar vortex seen in some GCMs (Williams et al., 2024).

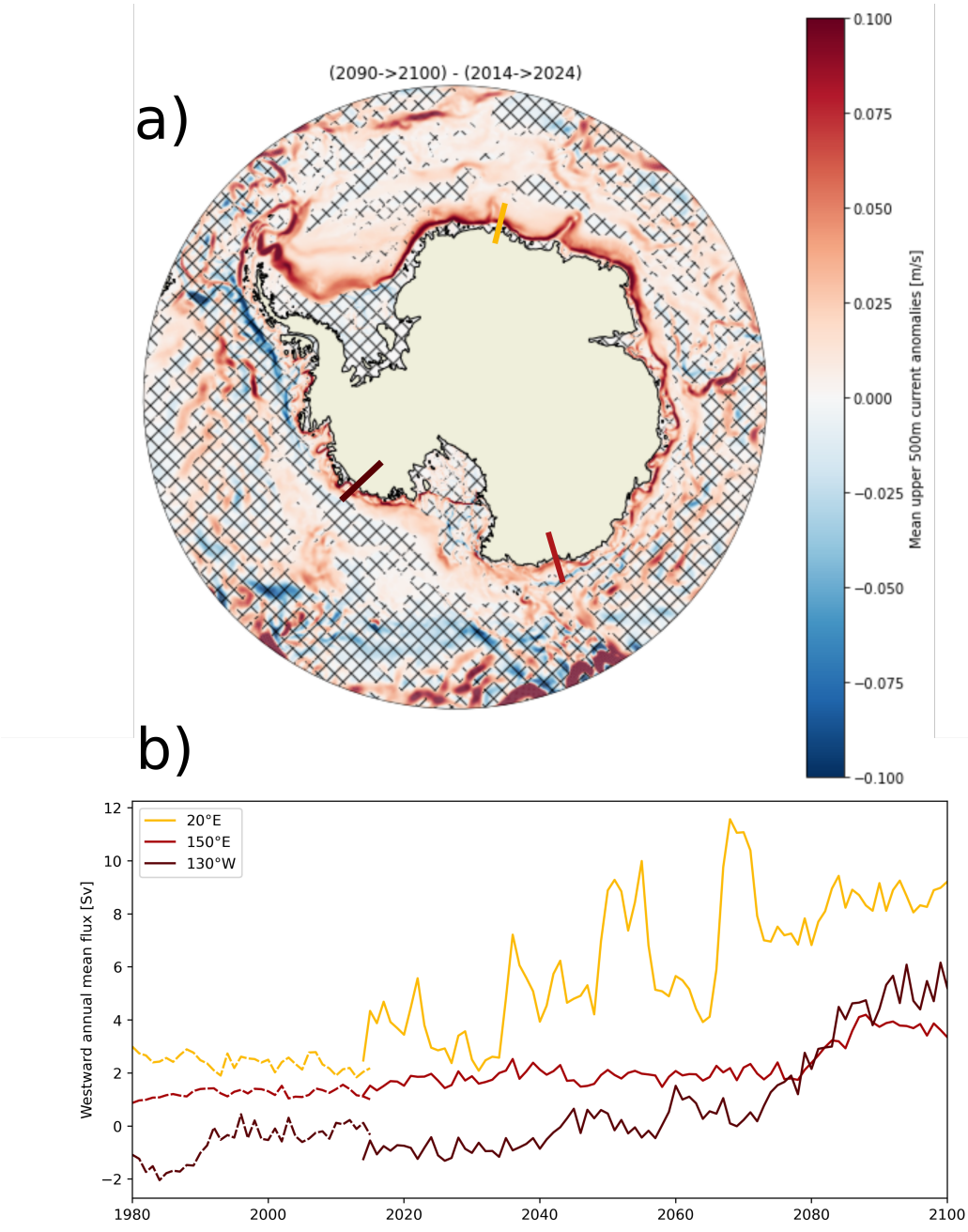

Figure 6.13: a) Difference between 2090-2100 and 2014-2024 mean upper 500m current velocity in NEMO_CNRM. Hatches indicate insignificance under student t-test. b) Annual mean integrated westward flux evolution between continent and continental slope at 3 different gates shown in (a). (Dashed lines: NEMO_ERA5 and solid lines: NEMO_CNRM.)

Part IV

Synthesis of new understandings, outcomes and challenges

CHAPTER 7

Conclusions

This thesis sets out to improve our understanding of the processes governing polar surface mass balance (SMB) and its recent past variability, along with investigating new processes through the use of a coupled O-A-I system. To achieve this, the research followed three interconnected objectives: (1) to provide reconstructions of past SMB evolution in both the Arctic and Antarctic, (2) to assess the drivers and mechanisms underlying observed variability and trends, and (3) to advance modeling capabilities through the development of a fully coupled ocean–sea ice–atmosphere regional domain.

Key Findings and Contributions

Historical SMB Variability and Drivers

The first contribution of this thesis lies in the reconstruction and analysis of SMB changes across both polar regions during the second half of the 20th century and early 21st century. In the Arctic (Chapter 3), simulations performed with the MAR regional climate model at 6 km resolution reveal a significant decrease in SMB since 1950, amounting to an integrated reduction of approximately 120 $Gt.yr^{-1}$ between the 1950–1979 and 2000–2020 periods. This decline has accelerated in recent decades, driven primarily by increased melt rates (+21% since 1950), which are themselves linked to enhanced summer blocking and persistent high-pressure systems. Yet, the response is not homogeneous: Greenland and the Canadian Arctic exhibit a strong melt-driven mass loss, while regions such as the Russian High Arctic show a more complex picture, with snowfall increases partially offsetting melt. These findings highlight the spatial heterogeneity of the Arctic SMB trends and highlight the need for regional assessments. The observed correlations with large-scale climate modes such as the Greenland Blocking Index (GBI) emphasize the role of atmospheric circulation in modulating SMB, with again heterogeneities between the western Arctic and the eastern less-studied regions like the Russian Arctic. In contrast, Antarctica (Chapter 4) displays a different signal over the same period. Reconstructions from 1958 to 2016 indicate a continent-wide SMB increase of about 13% (+315 $Gt.yr^{-1}$) after 1980, with East Antarctica contributing most to this gain. This rise in SMB could have mitigated up to $\sim$ 30 mm of global sea-level rise, acting as a transient buffer against the accelerating ice dynamic losses of the late 20th century. The analysis links this trend primarily to stratospheric ozone depletion, which enhanced the Southern Annular Mode and strengthened moisture advection toward the interior of the ice sheet. Causality tests confirm ozone as a dominant driver, outweighing the roles of sea ice. These results expose

how anthropogenic forcing can influence the climate apart from GHG emissions: while global warming accelerates ice loss in most regions, human-induced ozone depletion might have temporarily increased Antarctic snowfall. This compensation, however, is unlikely to persist under future warming and ozone recovery, with an increasing influence of warming on the balance between precipitation gains and melt losses.

Advancing Polar Regional Modeling

Beyond historical reconstructions, this thesis contributes to the representation of coupled processes that control SMB through the implementation of a fully coupled regional modeling framework (Chapter 5). By linking MAR with the NEMO–SI^3 ocean–sea ice model at a continent-wide scale, the system enables explicit flux exchanges between the atmosphere, ocean, and sea ice components. This step represents a methodological advance toward capturing key feedbacks that standalone models cannot reproduce, such as those involving sea ice dynamics, ocean heat storage, and atmospheric moisture supply. However, the coupled simulations expose significant technical and scientific challenges. Antarctic configurations exhibit strong energy imbalances, primarily driven by biases in MAR radiative fluxes, which propagate into ocean warming and sea-ice loss, ultimately destabilizing the system. The Arctic counterpart, by contrast, demonstrates stable behavior, suggesting domain-dependent sensitivities and confirming the feasibility of such an approach. While computational limitations remain a barrier to high-resolution, pan-Antarctic coupling, the framework established here provides a foundation for future process-based investigations of polar feedbacks in a changing climate.

Open questions and future research directions

From work presented here, natural questions emerge:

- In the Arctic, how will the combined influence of decreasing sea ice, changing ocean stratification, and stronger warming affect SMB and feedback loops in coming decades?
- We have identified that more than 40% of Arctic MB loss comes from other ice bodies than Greenland. While a lot of efforts has been made to project the future MB of the latter, less studies are interested in the other Arctic ice bodies. To what extent the MB of the other Arctic land ice will evolve with future Arctic amplification ?

- In Antarctica, as the ozone layer recovers, the atmospheric circulation anomalies that drove part of SMB increases in the late 20th century are expected to weaken (Previdi and Polvani, 2017). However, warming-enhanced precipitation and melt will act in opposite directions, with recent work highlighting a strong SMB increase due to atmospheric rivers in the last years (Kolbe et al., 2025). Quantifying the net effect of these competing influences under high-end warming scenarios remains a critical open question for future sea-level projections.

- Working with the Antarctic MAR-NEMO domain, we have seen how the fluxes formulations leads to a drift in the system as downward energy fluxes from MAR are biased. Does working with a bulk formulation stabilizes the models? And what implications would this have from fluxes formulations on the coupled processes ?

Furthermore, once the drift in the O-A-I coupling is resolved, this powerful tool could be used to continue the topics addressed in Chapter 6: It would enable a proper study on blowing snow over sea-ice to understand the redistribution of mass across the ice and its effect on local sea-ice albedo. The coupled system could also be used to investigate the ASC future evolution and its ability to regulate CDW entries below the ice-shelves.

Using MAR-NEMO, preliminar work has also been made to investigate the hypothetical future of the Southern oceans circulation under a world without ice-shelves. The disintegration of ice shelves as a strong influence on ice discharge by reducing the buttressing effect, but it will also change the atmospheric and oceanic circulation patterns. For example, costal polynyas, sources of AABW, might move as a consequence of shelves disappearances. How will this affect the production and export of AABW ? How does this changes general deep convection ?

To answer all of those questions, the coupled system is key to fully capture the feedbacks at play between ocean, atmosphere and sea-ice. As such, working towards a stable configuration would remain very useful for studying O-A-I interactions at a pan-Antarctic scale.

References

Aas, K. S., Dunse, T., Collier, E., Schuler, T. V., Berntsen, T. K., Kohler, J., and Luks, B.: The climatic mass balance of Svalbard glaciers: a 10-year simulation with a coupled atmosphere–glacier mass balance model, The Cryosphere, 10, 1089–1104, 2016.

Agosta, C., Amory, C., Kittel, C., Orsi, A., Favier, V., Gallée, H., van den Broeke, M. R., Lenaerts, J., van Wessem, J. M., van de Berg, W. J., et al.: Estimation of the Antarctic surface mass balance using the regional climate model MAR (1979–2015) and identification of dominant processes, The Cryosphere, 13, 281–296, 2019a.

Agosta, C., Amory, C., Kittel, C., Orsi, A., Favier, V., Gallée, H., van den Broeke, M. R., Lenaerts, J. T. M., van Wessem, J. M., van de Berg, W. J., and Fettweis, X.: Estimation of the Antarctic surface mass balance using the regional climate model MAR (1979–2015) and identification of dominant processes, The Cryosphere, 13, 281–296, doi: 10.5194/tc-13-281-2019, URL https://tc.copernicus.org/articles/13/281/2019/, publisher: Copernicus GmbH, 2019b.

Amory, C., Trouvilliez, A., Gallée, H., Favier, V., Naaim-Bouvet, F., Genthon, C., Agosta, C., Piard, L., and Bellot, H.: Comparison between observed and simulated aeolian snow mass fluxes in Adélie Land, East Antarctica, The Cryosphere, 9, 1373–1383, 2015.

Amory, C., Kittel, C., Le Toumelin, L., Agosta, C., Delhasse, A., Favier, V., and Fettweis, X.: Performance of MAR (v3. 11) in simulating the drifting-snow climate and surface mass balance of Adélie Land, East Antarctica, Geoscientific Model Development Discussions, 2020, 1–35, 2020.

Arrhenius, S.: XXXI. On the influence of carbonic acid in the air upon the temperature of the ground, The London, Edinburgh, and Dublin Philosophical Magazine and Journal of Science, 41, 237–276, 1896.

Arthern, R. J., Winebrenner, D. P., and Vaughan, D. G.: Antarctic snow accumulation mapped using polarization of 4.3-cm wavelength microwave emission, Journal of Geophysical Research: Atmospheres, 111, 2006.

Asay-Davis, X. S., Cornford, S. L., Durand, G., Galton-Fenzi, B. K., Gladstone, R. M., Gudmundsson, G. H., Hattermann, T., Holland, D. M., Holland, D., Holland, P. R., et al.: Experimental design for three interrelated marine ice sheet and ocean model intercomparison projects: MISMIP v. 3 (MISMIP+), ISOMIP v. 2 (ISOMIP+) and MISOMIP v. 1 (MISOMIP1), Geoscientific Model Development, 9, 2471–2497, 2016.

Bamber, J. L., Westaway, R. M., Marzeion, B., and Wouters, B.: The land ice contribution to sea level during the satellite era, Environmental Research Letters, 13, 063 008, 2018.

Beaumet, J., Ménégoz, M., Morin, S., Gallée, H., Fettweis, X., Six, D., Vincent, C., Wilhelm, B., and Anquetin, S.: Twentieth century temperature and snow cover changes in the French Alps, Regional Environmental Change, 21, 114, 2021.

Box, J. E., Colgan, W. T., Christensen, T. R., Schmidt, N. M., Lund, M., Parmentier, F.-J. W., Brown, R., Bhatt, U. S., Euskirchen, E. S., Romanovsky, V. E., et al.: Key indicators of Arctic climate change: 1971–2017, Environmental Research Letters, 14, 045 010, 2019.

Brun, E., Martin, E., Simon, V., Gendre, C., and Coleou, C.: An energy and mass model of snow cover suitable for operational avalanche forecasting, Journal of glaciology, 35, 333–342, 1989.

Cape, M., Vernet, M., Skvarca, P., Marinsek, S., Scambos, T., and Domack, E.: Foehn winds link climate-driven warming to ice shelf evolution in Antarctica, Journal of Geophysical Research: Atmospheres, 120, 11–037, 2015.

Chemke, R., Previdi, M., England, M. R., and Polvani, L. M.: Distinguishing the impacts of ozone and ozone-depleting substances on the recent increase in Antarctic surface mass balance, The Cryosphere, 14, 4135–4144, doi: 10.5194/tc-14-4135-2020, URL https://tc.copernicus.org/articles/14/4135/2020/, publisher: Copernicus GmbH, 2020.

Cogley, J. G., Arendt, A., Bauder, A., Braithwaite, R., Hock, R., Jansson, P., Kaser, G., Moller, M., Nicholson, L., Rasmussen, L., et al.: Glossary of glacier mass balance and related terms, 2010.

Damseaux, A., Fettweis, X., Lambert, M., and Cornet, Y.: Representation of the rain shadow effect in Patagonia using an orographic-derived regional climate model, International Journal of Climatology, 2019.

Danilin, M. Y., Sze, N.-D., Ko, M. K., Rodriguez, J. M., and Tabazadeh, A.: Stratospheric cooling and Arctic ozone recovery, Geophysical research letters, 25, 2141–2144, 1998.

De Ridder, K. and Gallée, H.: Land surface–induced regional climate change in southern Israel, Journal of applied meteorology, 37, 1470–1485, 1998.

Delhasse, A., Kittel, C., Amory, C., Hofer, S., Van As, D., S Fausto, R., and Fettweis, X.: Brief communication: Evaluation of the near-surface climate in ERA5 over the Greenland Ice Sheet, The Cryosphere, 14, 957–965, 2020.

Ekaykin, A. A., Veres, A. N., and Wang, Y.: Recent increase in the surface mass balance in central East Antarctica is unprecedented for the last 2000 years, Communications Earth & Environment, 5, 200, 2024.

Enderlin, E. M., Howat, I. M., Jeong, S., Noh, M.-J., Van Angelen, J. H., and Van Den Broeke, M. R.: An improved mass budget for the Greenland ice sheet, Geophysical Research Letters, 41, 866–872, 2014.

Favier, V., Krinner, G., Amory, C., Gallée, H., Beaumet, J., and Agosta, C.: Antarctica-Regional Climate and Surface Mass Budget, Current Climate Change Reports, 3, 303–315, doi: 10.1007/s40641-017-0072-z, URL http://link.springer.com/10.1007/s40641-017-0072-z, 2017.

Fettweis, X., Franco, B., Tedesco, M., Van Angelen, J., Lenaerts, J. T., van den Broeke, M. R., and Gallée, H.: Estimating the Greenland ice sheet surface mass balance contribution to future sea level rise using the regional atmospheric climate model MAR, The Cryosphere, 7, 469–489, 2013.

Fettweis, X., Box, J. E., Agosta, C., Amory, C., Kittel, C., Lang, C., van As, D., Machguth, H., and Gallée, H.: Reconstructions of the 1900–2015 Greenland ice sheet surface mass balance using the regional climate MAR model, The Cryosphere, 11, 1015–1033, 2017.

Fettweis, X., Hofer, S., Krebs-Kanzow, U., Amory, C., Aoki, T., Berends, C. J., Born, A., Box, J. E., Delhasse, A., Fujita, K., et al.: GrSMBMIP: intercomparison of the modelled 1980–2012 surface mass balance over the Greenland Ice Sheet, The Cryosphere, 14, 3935–3958, 2020.

Flocco, D. and Feltham, D. L.: A continuum model of melt pond evolution on Arctic sea ice, Journal of Geophysical Research: Oceans, 112, 2007.

Førland, E., Hanssen-Bauer, I., Jónsson, T., Kern-Hansen, C., Nordli, P., Tveito, O., and Laursen, E. V.: Twentieth-century variations in temperature and precipitation in the Nordic Arctic, Polar Record, 38, 203–210, 2002.

Franco, B., Fettweis, X., Lang, C., and Erpicum, M.: Impact of spatial resolution on the modelling of the Greenland ice sheet surface mass balance between 1990–2010, using the regional climate model MAR, The Cryosphere, 6, 695–711, 2012.

Fretwell, P., Pritchard, H. D., Vaughan, D. G., Bamber, J. L., Barrand, N. E., Bell, R., Bianchi, C., Bingham, R., Blankenship, D. D., Casassa, G., et al.: Bedmap2: improved ice bed, surface and thickness datasets for Antarctica, The cryosphere, 7, 375–393, 2013a.

Fretwell, P., Pritchard, H. D., Vaughan, D. G., Bamber, J. L., Barrand, N. E., Bell, R., Bianchi, C., Bingham, R. G., Blankenship, D. D., Casassa, G., Catania, G., Callens, D., Conway, H., Cook, A. J., Corr, H. F. J., Damaske, D., Damm, V., Ferraccioli, F., Forsberg, R., Fujita, S., Gim, Y., Gogineni, P., Griggs, J. A., Hindmarsh, R. C. A., Holmlund, P., Holt, J. W., Jacobel, R. W., Jenkins, A., Jokat, W., Jordan, T., King, E. C., Kohler, J., Krabill, W., Riger-Kusk, M., Langley, K. A., Leitchenkov, G., Leuschen, C., Luyendyk, B. P., Matsuoka, K., Mouginot, J., Nitsche, F. O., Nogi, Y., Nost, O. A., Popov, S. V., Rignot, E., Rippin, D. M., Rivera, A., Roberts, J., Ross, N., Siegert, M. J., Smith, A. M., Steinhage, D., Studinger, M., Sun, B., Tinto, B. K., Welch, B. C., Wilson, D., Young, D. A., Xiangbin, C., and Zirizzotti, A.: Bedmap2: improved ice bed, surface and thickness datasets for Antarctica, The Cryosphere, 7, 375–393, doi: 10.5194/tc-7-375-2013, URL https://tc.copernicus.org/articles/7/375/2013/, publisher: Copernicus GmbH, 2013b.

Fürst, J. J., Goelzer, H., and Huybrechts, P.: Ice-dynamic projections of the Greenland ice sheet in response to atmospheric and oceanic warming, The Cryosphere, 9, 1039–1062, 2015.

Gallée, H. and Duynkerke, P. G.: Air-snow interactions and the surface energy and mass balance over the melting zone of west Greenland during the Greenland Ice Margin Experiment, Journal of Geophysical Research: Atmospheres, 102, 13 813–13 824, 1997.

Gallée, H. and Schayes, G.: Development of a three-dimensional meso-γ primitive equation model: katabatic winds simulation in the area of Terra Nova Bay, Antarctica, Monthly Weather Review, 122, 671–685, 1994.

Gallée, H., Fontaine de Ghélin, O., and van den Broeke, M. R.: Simulation of atmospheric circulation during the GIMEX 91 experiment using a meso-γ primitive equations model, Journal of climate, 8, 2843–2859, 1995.

Gallée, H., Guyomarc'h, G., and Brun, E.: Impact of snow drift on the Antarctic ice sheet surface mass balance: possible sensitivity to snow-surface properties, Boundary-Layer Meteorology, 99, 1–19, 2001.

Gallée, H. and Schayes, G.: Development of a Three-Dimensional Meso- Primitive Equation Model: Katabatic Winds Simulation in the Area of Terra Nova Bay, Antarctica, Monthly Weather Review, 122, 671–685, doi: 10.1175/1520-0493(1994)122<0671:

DOATDM>2.0.CO;2, URL https://journals.ametsoc.org/view/journals/mwre/122/4/1520-0493_1994_122_0671_doatdm_2_0_co_2.xml, publisher: American Meteorological Society Section: Monthly Weather Review, 1994.

Gardner, A. S., Moholdt, G., Cogley, J. G., Wouters, B., Arendt, A. A., Wahr, J., Berthier, E., Hock, R., Pfeffer, W. T., Kaser, G., et al.: A reconciled estimate of glacier contributions to sea level rise: 2003 to 2009, science, 340, 852–857, 2013.

Goosse, H., Dalaiden, Q., Feba, F., Mezzina, B., and Fogt, R. L.: A drop in Antarctic sea ice extent at the end of the 1970s, Communications Earth & Environment, 5, 1–11, doi: 10.1038/s43247-024-01793-x, URL https://www.nature.com/articles/s43247-024-01793-x, publisher: Nature Publishing Group, 2024.

Gossart, A., Helsen, S., Lenaerts, J., Broucke, S. V., Van Lipzig, N., and Souverijns, N.: An evaluation of surface climatology in state-of-the-art reanalyses over the Antarctic Ice Sheet, Journal of Climate, 32, 6899–6915, 2019.

Grailet, J.-F., Hogan, R. J., Ghilain, N., Bolsée, D., Fettweis, X., and Grégoire, M.: Inclusion of the ECMWF ecRad radiation scheme (v1.5.0) in the MAR (v3.14), regional evaluation for Belgium, and assessment of surface shortwave spectral fluxes at Uccle, Geoscientific Model Development, 18, 1965–1988, doi: 10.5194/gmd-18-1965-2025, URL https://gmd.copernicus.org/articles/18/1965/2025/, publisher: Copernicus GmbH, 2025.

Granger, C. W.: Investigating causal relations by econometric models and cross-spectral methods, Econometrica: journal of the Econometric Society, pp. 424–438, 1969.

Hersbach, H., Bell, B., Berrisford, P., Hirahara, S., Horányi, A., Muñoz-Sabater, J., Nicolas, J., Peubey, C., Radu, R., Schepers, D., et al.: The ERA5 global reanalysis, Quarterly Journal of the Royal Meteorological Society, 146, 1999–2049, 2020a.

Hersbach, H., Bell, B., Berrisford, P., Hirahara, S., Horányi, A., Muñoz-Sabater, J., Nicolas, J., Peubey, C., Radu, R., Schepers, D., Simmons, A., Soci, C., Abdalla, S., Abellan, X., Balsamo, G., Bechtold, P., Biavati, G., Bidlot, J., Bonavita, M., De Chiara, G., Dahlgren, P., Dee, D., Diamantakis, M., Dragani, R., Flemming, J., Forbes, R., Fuentes, M., Geer, A., Haimberger, L., Healy, S., Hogan, R. J., Hólm, E., Janisková, M., Keeley, S., Laloyaux, P., Lopez, P., Lupu, C., Radnoti, G., de Rosnay, P., Rozum, I., Vamborg, F., Villaume, S., and Thépaut, J.-N.: The ERA5 global reanalysis, Quarterly Journal of the Royal Meteorological Society, 146, 1999–2049, doi: 10.1002/qj.3803, URL https://onlinelibrary.wiley.com/doi/abs/10.1002/qj.3803, _eprint: https://onlinelibrary.wiley.com/doi/pdf/10.1002/qj.3803, 2020b.

Hillebrand, F. L., Bremer, U. F., Arigony-Neto, J., da Rosa, C. N., Mendes Jr, C. W., Costi, J., de Freitas, M. W. D., and Schardong, F.: Comparison between atmospheric reanalysis models ERA5 and ERA-Interim at the North Antarctic Peninsula region, Annals of the American Association of Geographers, 111, 1147–1159, 2021.

Huai, B., Wang, Y., Ding, M., Zhang, J., and Dong, X.: An assessment of recent global atmospheric reanalyses for Antarctic near surface air temperature, Atmospheric Research, 226, 181–191, 2019.

Hugonnet, R., McNabb, R., Berthier, E., Menounos, B., Nuth, C., Girod, L., Farinotti, D., Huss, M., Dussaillant, I., Brun, F., et al.: Accelerated global glacier mass loss in the early twenty-first century, Nature, 592, 726–731, 2021.

Huot, P.-V., Kittel, C., Fichefet, T., Jourdain, N., and Fettweis, X.: Effects of ocean mesoscale eddies on atmosphere–sea ice–ocean interactions off Adélie Land, East Antarctica, Climate Dynamics, 59, 41–60, 2022.

IMBIE, T.: Mass balance of the Greenland Ice Sheet from 1992 to 2018, Nature, 579, 233–239, 2020.

IPCC: Climate Change 2023: Synthesis Report. Contribution of Working Groups I, II and III to the Sixth Assessment Report of the Intergovernmental Panel on Climate Change, IPCC, Geneva, Switzerland, doi: 10.59327/IPCC/AR6-9789291691647, 2023.

Isaksen, K., Nordli, Ø., Ivanov, B., Køltzow, M. A., Aaboe, S., Gjelten, H. M., Mezghani, A., Eastwood, S., Førland, E., Benestad, R. E., et al.: Exceptional warming over the Barents area, Scientific reports, 12, 1–18, 2022.

Jacobs, S. S., Jenkins, A., Giulivi, C. F., and Dutrieux, P.: Stronger ocean circulation and increased melting under Pine Island Glacier ice shelf, Nature geoscience, 4, 519–523, 2011.

Jourdain, N. C., Mathiot, P., Gallée, H., and Barnier, B.: Influence of coupling on atmosphere, sea ice and ocean regional models in the Ross Sea sector, Antarctica, Climate dynamics, 36, 1523–1543, 2011.

Kessler, E.: On the distribution and continuity of water substance in atmospheric circulations, in: On the distribution and continuity of water substance in atmospheric circulations, pp. 1–84, Springer, 1969.

King, M. D., Howat, I. M., Candela, S. G., Noh, M. J., Jeong, S., Noël, B. P., van den Broeke, M. R., Wouters, B., and Negrete, A.: Dynamic ice loss from the Greenland Ice Sheet driven by sustained glacier retreat, Communications Earth & Environment, 1, 1, 2020.

Kittel, C.: Present and future sensitivity of the Antarctic surface mass balance to oceanic and atmospheric forcings: insights with the regional climate model MAR, Universite de Liege (Belgium), 2021.

Kittel, C., Amory, C., Agosta, C., Delhasse, A., Doutreloup, S., Huot, P.-V., Wyard, C., Fichefet, T., and Fettweis, X.: Sensitivity of the current Antarctic surface mass balance to sea surface conditions using MAR, The Cryosphere, 12, 3827–3839, doi: 10.5194/tc-12-3827-2018, URL https://tc.copernicus.org/articles/12/3827/2018/, publisher: Copernicus GmbH, 2018.

Kittel, C., Amory, C., Agosta, C., Jourdain, N. C., Hofer, S., Delhasse, A., Doutreloup, S., Huot, P.-V., Lang, C., Fichefet, T., and Fettweis, X.: Diverging future surface mass balance between the Antarctic ice shelves and grounded ice sheet, The Cryosphere, 15, 1215–1236, doi: 10.5194/tc-15-1215-2021, URL https://tc.copernicus.org/articles/15/1215/2021/, publisher: Copernicus GmbH, 2021a.

Kittel, C., Amory, C., Agosta, C., Jourdain, N. C., Hofer, S., Delhasse, A., Doutreloup, S., Huot, P.-V., Lang, C., Fichefet, T., et al.: Diverging future surface mass balance between the Antarctic ice shelves and grounded ice sheet, The Cryosphere, 15, 1215–1236, 2021b.

Kolbe, M., Alavez, J. A. T., Mottram, R., Katurji, M., Bintanja, R., and van der Linden, E. C.: Atmospheric rivers and winter sea ice drive recent reversal in Antarctic ice mass loss, arXiv preprint arXiv:2510.03590, 2025.

Kromer, J. D. and Trusel, L. D.: Identifying the impacts of sea ice variability on the climate and surface mass balance of West Antarctica, Geophysical Research Letters, 50, e2023GL104 436, 2023.

Kuttippurath, J. and Nair, P. J.: The signs of Antarctic ozone hole recovery, Scientific reports, 7, 585, 2017.

Lambin, C., Fettweis, X., Kittel, C., Fonder, M., and Ernst, D.: Assessment of future wind speed and wind power changes over South Greenland using the MAR regional climate model, 2022.

Lan, X., Tans, P., and Thoning, K. W.: Trends in globally-averaged CO_2 determined from NOAA Global Monitoring Laboratory measurements, https://gml.noaa.gov, doi: 10.15138/9N0H-ZH07, national Oceanic and Atmospheric Administration (NOAA) Global Monitoring Laboratory, Boulder, Colorado, USA, 2023.

Lang, C., Fettweis, X., and Erpicum, M.: Stable climate and surface mass balance in Svalbard over 1979–2013 despite the Arctic warming, The Cryosphere, 9, 83–101, 2015.

Langematz, U. and Kunze, M.: An update on dynamical changes in the Arctic and Antarctic stratospheric polar vortices, Climate dynamics, 27, 647–660, 2006.

Lecomte, O., Fichefet, T., Vancoppenolle, M., Dominé, F., Massonnet, F., Mathiot, P., Morin, S., and Barriat, P.-Y.: On the formulation of snow thermal conductivity in large-scale sea ice models, Journal of Advances in Modeling Earth Systems, 5, 542–557, 2013.

Lefebre, F., Gallée, H., van Ypersele, J.-P., and Greuell, W.: Modeling of snow and ice melt at ETH Camp (West Greenland): A study of surface albedo, Journal of Geophysical Research: Atmospheres, 108, 2003.

Lenaerts, J. T., van Angelen, J. H., van den Broeke, M. R., Gardner, A. S., Wouters, B., and van Meijgaard, E.: Irreversible mass loss of Canadian Arctic Archipelago glaciers, Geophysical Research Letters, 40, 870–874, 2013.

Levermann, A., Clark, P. U., Marzeion, B., Milne, G. A., Pollard, D., Radic, V., and Robinson, A.: The multimillennial sea-level commitment of global warming, Proceedings of the National Academy of Sciences, 110, 13 745–13 750, 2013.

Levkov, L. and Rockel, B.: AN ICE CRYSTAL NUCLEATION SCHEME APPLYING BY 3-D SIMULATION OF CIRRUS CLOUDS, in: Nucleation and Atmospheric Aerosols: Proceedings of the Thirteenth International Conference on Nucleation and Atmospheric Aerosols, p. 237, A. DEEPAK Pub., 1992.

Li, J., Rodriguez-Morales, F., Fettweis, X., Ibikunle, O., Leuschen, C., Paden, J., Gomez-Garcia, D., and Arnold, E.: Snow stratigraphy observations from Operation IceBridge surveys in Alaska using S and C band airborne ultra-wideband FMCW (frequency-modulated continuous wave) radar, The Cryosphere, 17, 175–193, 2023.

Li, X., Rignot, E., Morlighem, M., Mouginot, J., and Scheuchl, B.: Grounding line retreat of Totten Glacier, east Antarctica, 1996 to 2013, Geophysical Research Letters, 42, 8049–8056, 2015.

Li, Z., Ding, Q., Steele, M., and Schweiger, A.: Recent upper Arctic Ocean warming expedited by summertime atmospheric processes, Nature communications, 13, 1–11, 2022.

Liang, X. S.: Unraveling the cause-effect relation between time series, Physical Review E, 90, 052 150, doi: 10.1103/PhysRevE.90.052150, URL https://link.aps.org/doi/10.1103/PhysRevE.90.052150, publisher: American Physical Society, 2014.

Liang, X. S.: Normalizing the causality between time series, Physical Review E, 92, 022 126, 2015.

Liang, X. S.: Information flow and causality as rigorous notions ab initio, Physical Review E, 94, 052 201, 2016.

Lin, Y.-L., Farley, R. D., and Orville, H. D.: Bulk parameterization of the snow field in a cloud model, Journal of Applied Meteorology and climatology, 22, 1065–1092, 1983.

Machguth, H., Thomsen, H. H., Weidick, A., Ahlstrøm, A. P., Abermann, J., Andersen, M. L., Andersen, S. B., Bjørk, A. A., Box, J. E., Braithwaite, R. J., et al.: Greenland surface mass-balance observations from the ice-sheet ablation area and local glaciers, Journal of Glaciology, 62, 861–887, 2016.

Man, K., Luterbacher, J., Holland, D. M., Yuan, N., Geng, L., Wang, Y., Liu, Y., Shi, G., Hou, Y., Cai, W., et al.: Century-long West Antarctic snow accumulation changes induced by tropical teleconnections, Science Advances, 11, eadr2821, 2025.

Mankoff, K. D., Fettweis, X., Langen, P. L., Stendel, M., Kjeldsen, K. K., Karlsson, N. B., Noël, B., Van Den Broeke, M. R., Solgaard, A., Colgan, W., et al.: Greenland ice sheet mass balance from 1840 through next week, Earth System Science Data, 13, 5001–5025, 2021.

Mann, G., Anderson, P., and Mobbs, S.: Profile measurements of blowing snow at Halley, Antarctica, Journal of Geophysical Research: Atmospheres, 105, 24 491–24 508, 2000.

Marbaix, P., Gallée, H., Brasseur, O., and van Ypersele, J.-P.: Lateral boundary conditions in regional climate models: a detailed study of the relaxation procedure, Monthly weather review, 131, 461–479, 2003.

Marshall, G. J. and Connolley, W. M.: Effect of changing Southern Hemisphere winter sea surface temperatures on Southern Annular Mode strength, Geophysical Research Letters, 33, 2006.

Marshall, G. J., Fogt, R. L., Turner, J., and Clem, K. R.: Can current reanalyses accurately portray changes in Southern Annular Mode structure prior to 1979?, Climate Dynamics, pp. 1–24, 2022.

Marshall, J. S. and Palmer, W. M. K.: The distribution of raindrops with size, Journal of Atmospheric Sciences, 5, 165–166, 1948.

Matthews, T., Hodgkins, R., Guðmundsson, S., Pálsson, F., and Björnsson, H.: Interdecadal variability in potential glacier surface melt energy at Vestari Hagafellsjökull (Langjökull, Iceland) and the role of synoptic circulation, International Journal of Climatology, 35, 3041–3057, 2015.

Maure, D., Kittel, C., Lambin, C., Delhasse, A., and Fettweis, X.: Spatially heterogeneous effect of climate warming on the Arctic land ice, The Cryosphere, 17, 4645–4659, doi: 10.5194/tc-17-4645-2023, URL https://tc.copernicus.org/articles/17/4645/2023/, publisher: Copernicus GmbH, 2023.

McDougall, T. J. and Barker, P. M.: Getting started with TEOS-10 and the Gibbs Seawater (GSW) oceanographic toolbox, Scor/iapso WG, 127, 1–28, 2011.

McMichael, C., Dasgupta, S., Ayeb-Karlsson, S., and Kelman, I.: A review of estimating population exposure to sea-level rise and the relevance for migration, Environmental Research Letters, 15, 123 005, 2020.

Medley, B. and Thomas, E.: Increased snowfall over the Antarctic Ice Sheet mitigated twentieth-century sea-level rise, Nature Climate Change, 9, 34–39, 2019a.

Medley, B. and Thomas, E. R.: Increased snowfall over the Antarctic Ice Sheet mitigated twentieth-century sea-level rise, Nature Climate Change, 9, 34–39, doi: 10.1038/s41558-018-0356-x, URL https://www.nature.com/articles/s41558-018-0356-x, publisher: Nature Publishing Group, 2019b.

Messager, C., Gallée, H., and Brasseur, O.: Precipitation sensitivity to regional SST in a regional climate simulation during the West African monsoon for two dry years, Climate Dynamics, 22, 249–266, 2004.

Meyers, M. P., DeMott, P. J., and Cotton, W. R.: New primary ice-nucleation parameterizations in an explicit cloud model, Journal of Applied Meteorology and Climatology, 31, 708–721, 1992.

Moon, T. A., Gardner, A. S., Csatho, B., Parmuzin, I., and Fahnestock, M. A.: Rapid reconfiguration of the Greenland Ice Sheet coastal margin, Journal of Geophysical Research: Earth Surface, 125, e2020JF005 585, 2020.

Mottram, R., Hansen, N., Kittel, C., van Wessem, J. M., Agosta, C., Amory, C., Boberg, F., van de Berg, W. J., Fettweis, X., Gossart, A., van Lipzig, N. P. M., van Meijgaard, E., Orr, A., Phillips, T., Webster, S., Simonsen, S. B., and Souverijns, N.: What is the surface mass balance of Antarctica? An intercomparison of regional climate model estimates, The Cryosphere, 15, 3751–3784, doi: 10.5194/tc-15-3751-2021, URL https://tc.copernicus.org/articles/15/3751/2021/, publisher: Copernicus GmbH, 2021.

Nakayama, Y., Greene, C. A., Paolo, F. S., Mensah, V., Zhang, H., Kashiwase, H., Simizu, D., Greenbaum, J. S., Blankenship, D. D., Abe-Ouchi, A., et al.: Antarctic slope current modulates ocean heat intrusions towards Totten Glacier, Geophysical Research Letters, 48, e2021GL094 149, 2021.

NEMO-Sea-Ice-Working-Group: Sea Ice modelling Integrated Initiative (SI^3) – The NEMO sea ice engine, 2011.

Nie, Y., Li, C., Vancoppenolle, M., Cheng, B., Boeira Dias, F., Lv, X., and Uotila, P.: Sensitivity of NEMO4. 0-SI 3 model parameters on sea ice budgets in the Southern Ocean, Geoscientific Model Development Discussions, 2022, 1–41, 2022.

Noël, B., Van De Berg, W. J., Lhermitte, S., Wouters, B., Schaffer, N., and van den Broeke, M. R.: Six decades of glacial mass loss in the Canadian Arctic Archipelago, Journal of Geophysical Research: Earth Surface, 123, 1430–1449, 2018.

Noël, B., Jakobs, C. L., Van Pelt, W., Lhermitte, S., Wouters, B., Kohler, J., Hagen, J. O., Luks, B., Reijmer, C., Van de Berg, W. J., et al.: Low elevation of Svalbard glaciers drives high mass loss variability, Nature Communications, 11, 4597, 2020.

Noël, B., Aðalgeirsdóttir, G., Pálsson, F., Wouters, B., Lhermitte, S., Haacker, J. M., and van den Broeke, M. R.: North Atlantic cooling is slowing down mass loss of Icelandic glaciers, Geophysical Research Letters, 49, e2021GL095 697, 2022.

Olive Abello, A., Mathiot, P., Jourdain, N. C., Kostov, Y., Holland, P. R., Gascoin, S., and Rousset, C.: Iceberg grounding enhances the release of freshwater on the Antarctic continental shelf, Journal of Geophysical Research: Oceans, 130, e2025JC022 857, 2025.

Orsi, A. H., Johnson, G. C., and Bullister, J. L.: Circulation, mixing, and production of Antarctic Bottom Water, Progress in Oceanography, 43, 55–109, 1999.

Østby, T. I., Schuler, T. V., Hagen, J. O., Hock, R., Kohler, J., and Reijmer, C. H.: Diagnosing the decline in climatic mass balance of glaciers in Svalbard over 1957–2014, The Cryosphere, 11, 191–215, 2017.

Otosaka, I. N., Horwath, M., Mottram, R., and Nowicki, S.: Mass balances of the Antarctic and Greenland Ice Sheets monitored from space, Surveys in Geophysics, 44, 1615–1652, 2023.

Overland, J. E. and Wang, M.: Resolving future Arctic/midlatitude weather connections, Earth's Future, 6, 1146–1152, 2018.

Overland, J. E., Dethloff, K., Francis, J. A., Hall, R. J., Hanna, E., Kim, S.-J., Screen, J. A., Shepherd, T. G., and Vihma, T.: Nonlinear response of mid-latitude weather to the changing Arctic, Nature Climate Change, 6, 992–999, 2016.

Palm, S. P., Yang, Y., Spinhirne, J. D., and Marshak, A.: Satellite remote sensing of blowing snow properties over Antarctica, Journal of Geophysical Research: Atmospheres, 116, 2011.

Parish, T. R. and Bromwich, D. H.: Reexamination of the near-surface airflow over the Antarctic continent and implications on atmospheric circulations at high southern latitudes, Monthly Weather Review, 135, 1961–1973, 2007.

Perovich, D., Meier, W., Tschudi, M., Hendricks, S., Petty, A., Divine, D., Farrell, S., Gerland, S., Haas, C., Kaleschke, L., et al.: Arctic report card 2020: Sea ice, 2020.

Petrov, O., Morozov, A., Shokalsky, S., Kashubin, S., Artemieva, I. M., Sobolev, N., Petrov, E., Ernst, R. E., Sergeev, S., and Smelror, M.: Crustal structure and tectonic model of the Arctic region, Earth-Science Reviews, 154, 29–71, 2016.

Pettitt, A. N.: A non-parametric approach to the change-point problem, Journal of the Royal Statistical Society: Series C (Applied Statistics), 28, 126–135, 1979.

Philippe, M., Tison, J.-L., Fjøsne, K., Hubbard, B., Kjær, H. A., Lenaerts, J. T., Sheldon, S. G., De Bondt, K., Claeys, P., and Pattyn, F.: Ice core evidence for a recent increase in snow accumulation in coastal Dronning Maud Land, East Antarctica, Cryosphere Discussions, 10, 2501–2516, 2016.

Pirlet, N., Fichefet, T., Vancoppenolle, M., Fraser, A. D., Mathiot, P., Rousset, C., Barthélemy, A., Barriat, P.-Y., Pelletier, C., Madec, G., et al.: Benefits of a landfast ice representation on simulated Antarctic sea ice and coastal polynya dynamics, Journal of Geophysical Research: Oceans, 130, e2024JC022 032, 2025.

Pithan, F. and Mauritsen, T.: Arctic amplification dominated by temperature feedbacks in contemporary climate models, Nature geoscience, 7, 181–184, 2014.

Polyakov, I. V., Ingvaldsen, R. B., Pnyushkov, A. V., Bhatt, U. S., Francis, J. A., Janout, M., Kwok, R., and Skagseth, Ø.: Fluctuating Atlantic inflows modulate Arctic atlantification, Science, 381, 972–979, 2023.

Prenni, A. J., Harrington, J. Y., Tjernström, M., DeMott, P. J., Avramov, A., Long, C. N., Kreidenweis, S. M., Olsson, P. Q., and Verlinde, J.: Can ice-nucleating aerosols affect Arctic seasonal climate?, Bulletin of the American Meteorological Society, 88, 541–550, 2007.

Previdi, M. and Polvani, L. M.: Impact of the Montreal Protocol on Antarctic surface mass balance and implications for global sea level rise, Journal of Climate, 30, 7247–7253, 2017.

Przybylak, R.: Variability of total and solid precipitation in the Canadian Arctic from 1950 to 1995, International Journal of Climatology: A Journal of the Royal Meteorological Society, 22, 395–420, 2002.

Radić, V. and Hock, R.: Regionally differentiated contribution of mountain glaciers and ice caps to future sea-level rise, Nature Geoscience, 4, 91–94, 2011.

Rajewicz, J. and Marshall, S. J.: Variability and trends in anticyclonic circulation over the Greenland ice sheet, 1948–2013, Geophysical Research Letters, 41, 2842–2850, 2014.

Rantanen, M., Karpechko, A. Y., Lipponen, A., Nordling, K., Hyvärinen, O., Ruosteenoja, K., Vihma, T., and Laaksonen, A.: The Arctic has warmed nearly four times faster than the globe since 1979, Communications Earth & Environment, 3, 1–10, 2022.

Ridder, K. D. and Schayes, G.: The IAGL land surface model, Journal of applied meteorology, 36, 167–182, 1997.

Rignot, E., Velicogna, I., van den Broeke, M. R., Monaghan, A., and Lenaerts, J. T.: Acceleration of the contribution of the Greenland and Antarctic ice sheets to sea level rise, Geophysical research letters, 38, 2011.

Rignot, E., Mouginot, J., Scheuchl, B., Van Den Broeke, M., Van Wessem, M. J., and Morlighem, M.: Four decades of Antarctic Ice Sheet mass balance from 1979–2017, Proceedings of the National Academy of Sciences, 116, 1095–1103, 2019.

Ritchie, H.: Who has contributed most to global CO2 emissions?, Our World in Data, https://ourworldindata.org/contributed-most-global-co2, 2019.

Schuler, T. V., Kohler, J., Elagina, N., Hagen, J. O. M., Hodson, A. J., Jania, J. A., Kääb, A. M., Luks, B., Małecki, J., Moholdt, G., et al.: Reconciling Svalbard glacier mass balance, Frontiers in Earth Science, p. 156, 2020.

Screen, J. A. and Simmonds, I.: The central role of diminishing sea ice in recent Arctic temperature amplification, Nature, 464, 1334–1337, 2010.

Seibert, P. and Morariu, B.: Improvements of upstream, semi-Lagrangian numerical advection schemes, Journal of Applied Meteorology and Climatology, 30, 117–125, 1991.

Serreze, M. C. and Meier, W. N.: The Arctic's sea ice cover: trends, variability, predictability, and comparisons to the Antarctic, Annals of the New York Academy of Sciences, 1436, 36–53, 2019.

Shannon, C. E.: A mathematical theory of communication, The Bell system technical journal, 27, 379–423, 1948.

Slivinski, L., Compo, G., Whitaker, J., Sardeshmukh, P., Giese, B., McColl, C., Brohan, P., Allan, R., Yin, X., Vose, R., Titchner, H., Kennedy, J., Spencer, L., Ashcroft, L., Bronnimann, S., Brunet, M., Camuffo, D., Cornes, R., Cram, T., Crouthamel, R.,

Dominguez-Castro, F., Freeman, J., Gergis, J., Hawkins, E., Jones, P., Jourdain, S., Kaplan, A., Kubota, H., Blancq, F., Lee, T.-C., Lorrey, A., Luterbacher, J., Maugeri, M., Mock, C., Moore, K., Przybylak, R., Pudmenzky, C., Reason, C., Slonosky, V., Smith, C., Tinz, B., Trewin, B., Valente, M., Wang, X., Wilkinson, C., Wood, K., and Wyszynski, P.: NOAA-CIRES-DOE Twentieth Century Reanalysis Version 3, doi: 10.5065/H93G-WS83, URL https://rda.ucar.edu, 2019a.

Slivinski, L. C., Compo, G. P., Whitaker, J. S., Sardeshmukh, P. D., Giese, B. S., McColl, C., Allan, R., Yin, X., Vose, R., Titchner, H., et al.: Towards a more reliable historical reanalysis: Improvements for version 3 of the Twentieth Century Reanalysis system, Quarterly Journal of the Royal Meteorological Society, 145, 2876–2908, 2019b.

Slivinski, L. C., Compo, G. P., Sardeshmukh, P. D., Whitaker, J. S., McColl, C., Allan, R. J., Brohan, P., Yin, X., Smith, C. A., Spencer, L. J., Vose, R. S., Rohrer, M., Conroy, R. P., Schuster, D. C., Kennedy, J. J., Ashcroft, L., Brönnimann, S., Brunet, M., Camuffo, D., Cornes, R., Cram, T. A., Domínguez-Castro, F., Freeman, J. E., Gergis, J., Hawkins, E., Jones, P. D., Kubota, H., Lee, T. C., Lorrey, A. M., Luterbacher, J., Mock, C. J., Przybylak, R. K., Pudmenzky, C., Slonosky, V. C., Tinz, B., Trewin, B., Wang, X. L., Wilkinson, C., Wood, K., and Wyszyński, P.: An Evaluation of the Performance of the Twentieth Century Reanalysis Version 3, Journal of Climate, 34, 1417–1438, doi: 10.1175/JCLI-D-20-0505.1, URL https://journals.ametsoc.org/view/journals/clim/34/4/JCLI-D-20-0505.1.xml, publisher: American Meteorological Society Section: Journal of Climate, 2021.

Sterl, A.: On the (in) homogeneity of reanalysis products, Journal of Climate, 17, 3866–3873, 2004.

Thomas, E. R., Marshall, G. J., and McConnell, J. R.: A doubling in snow accumulation in the western Antarctic Peninsula since 1850, Geophysical Research Letters, 35, doi: 10.1029/2007GL032529, URL https://onlinelibrary.wiley.com/doi/abs/10.1029/2007GL032529, _eprint: https://onlinelibrary.wiley.com/doi/pdf/10.1029/2007GL032529, 2008.

Thomas, E. R., van Wessem, J. M., Roberts, J., Isaksson, E., Schlosser, E., Fudge, T. J., Vallelonga, P., Medley, B., Lenaerts, J., Bertler, N., van den Broeke, M. R., Dixon, D. A., Frezzotti, M., Stenni, B., Curran, M., and Ekaykin, A. A.: Regional Antarctic snow accumulation over the past 1000 years, Climate of the Past, 13, 1491–1513, doi: 10.5194/cp-13-1491-2017, URL https://cp.copernicus.org/articles/13/1491/2017/, publisher: Copernicus GmbH, 2017.

Thompson, A. F., Stewart, A. L., Spence, P., and Heywood, K. J.: The Antarctic Slope Current in a changing climate, Reviews of Geophysics, 56, 741–770, 2018.

Tonboe, R., Lavelle, J., Pfeiffer, R.-H., and Howe, E.: Product user manual for osi saf global sea ice concentration, Danish Meteorological Institute: Copenhagen, Denmark, 2016.

Topál, D., Ding, Q., Ballinger, T. J., Hanna, E., Fettweis, X., Li, Z., and Pieczka, I.: Discrepancies between observations and climate models of large-scale wind-driven Greenland melt influence sea-level rise projections, Nature Communications, 13, 1–12, 2022.

Tschudi, M. A., Meier, W. N., and Stewart, J. S.: An enhancement to sea ice motion and age products at the National Snow and Ice Data Center (NSIDC), The Cryosphere, 14, 1519–1536, 2020.

van Dalum, C. T., van de Berg, W. J., van den Broeke, M. R., and van Tiggelen, M.: The surface mass balance and near-surface climate of the Antarctic ice sheet in RACMO2. 4p1, EGUsphere, 2025, 1–40, 2025.

van de Berg, W. J. and Medley, B.: Brief Communication: Upper-air relaxation in RACMO2 significantly improves modelled interannual surface mass balance variability in Antarctica, The Cryosphere, 10, 459–463, 2016.

Van Pelt, W., Pohjola, V., Pettersson, R., Marchenko, S., Kohler, J., Luks, B., Hagen, J. O., Schuler, T. V., Dunse, T., Noël, B., et al.: A long-term dataset of climatic mass balance, snow conditions, and runoff in Svalbard (1957–2018), The Cryosphere, 13, 2259–2280, 2019.

Vannitsem, S., Dalaiden, Q., and Goosse, H.: Testing for dynamical dependence: Application to the surface mass balance over Antarctica, Geophysical Research Letters, 46, 12 125–12 135, 2019.

Velicogna, I., Mohajerani, Y., A, G., Landerer, F., Mouginot, J., Noel, B., Rignot, E., Sutterley, T., van den Broeke, M., van Wessem, M., et al.: Continuity of ice sheet mass loss in Greenland and Antarctica from the GRACE and GRACE follow-on missions, Geophysical Research Letters, 47, e2020GL087 291, 2020.

Vignon, É., Traullé, O., and Berne, A.: On the fine vertical structure of the low troposphere over the coastal margins of East Antarctica, Atmospheric Chemistry and Physics, 19, 4659–4683, 2019.

Vignon, É., Roussel, M.-L., Gorodetskaya, I., Genthon, C., and Berne, A.: Present and future of rainfall in Antarctica, Geophysical Research Letters, 48, e2020GL092 281, 2021.

Wang, S., Liu, J., Cai, W., Yang, D., Kerzenmacher, T., Ding, S., and Cheng, X.: Strong impact of the rare three-year La Niña event on Antarctic surface climate changes in 2021–2023, npj Climate and Atmospheric Science, 8, 173, 2025.

Wang, W., Shen, Y., Chen, Q., and Wang, F.: Unprecedented mass gain over the Antarctic ice sheet between 2021 and 2022 caused by large precipitation anomalies, Environmental Research Letters, 18, 124 012, 2023.

Wang, Y., Ding, M., Reijmer, C. H., Smeets, P. C. J. P., Hou, S., and Xiao, C.: The AntSMB dataset: a comprehensive compilation of surface mass balance field observations over the Antarctic Ice Sheet, Earth System Science Data, 13, 3057–3074, doi: 10.5194/essd-13-3057-2021, URL https://essd.copernicus.org/articles/13/3057/2021/, publisher: Copernicus GmbH, 2021.

Williams, R. S., Marshall, G. J., Levine, X., Graff, L. S., Handorf, D., Johnston, N. M., Karpechko, A. Y., Orr, A., Van de Berg, W. J., Wijngaard, R. R., et al.: Future Antarctic climate: Storylines of midlatitude jet strengthening and shift emergent from CMIP6, Journal of Climate, 37, 2157–2178, 2024.

Appendix

A Additional elements for Chapter 3

Station	Station altitude [m asl]	MAR altitude [m asl]	Summer bias [°C]	Altitude correcte
Hopen	6	11	-0.63	-0.58
Sveagruva	9	244	-4.62	-2.27
Lufthavn	2	298	-5.06	-2.1
Ny-ålesund	8	180	-2.53	-0.81

Table S1: Temperature bias correction example from altitude difference between MAR pixel and AWSs using a fixed 1°C/100m gradient.

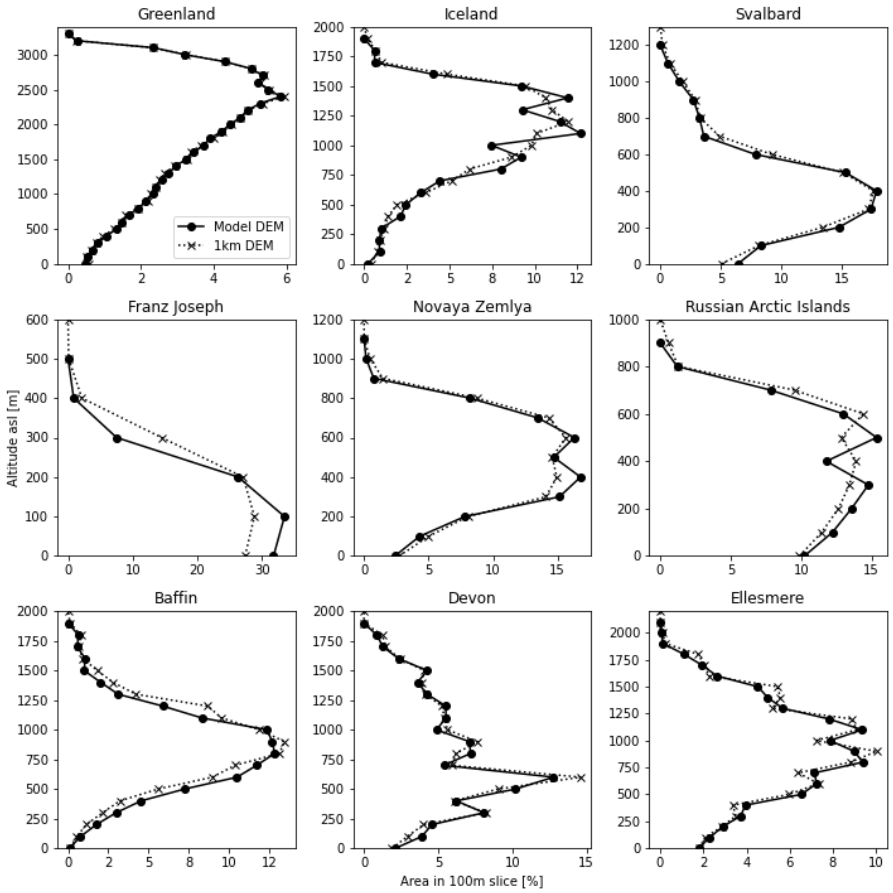

Figure A.1: Comparison of the hypsometry of the land ice from the model grids (6 km resolution, in dots, solid line) and of a 1km grid in the same georeferencing system (x marks, dotted line). Both DEMs come from ETOPO01.

Variable	Sub Domain	Mean Observed	Bias	CRMSE	r
P2m [hPa]	Greenland	1006.96	3.35	1.60	0.99
	Russia	1013.75	-4.35	2.15	0.98
	Svalbard	1008.87	0.51	2.45	0.98
	Iceland	1006.46	-5.13	0.95	1.00
	Canada	1005.68	-4.74	2.75	0.96
T2m [°C]	Greenland	-7.49	-1.24	3.07	0.95
	Russia	-10.74	-1.72	3.33	0.96
	Svalbard	-4.58	-2.48	3.59	0.92
	Iceland	4.13	-0.33	1.68	0.96
	Canada	-13.49	0.14	3.33	0.98

Table S2: Evaluation results for the pre-International Geophysical Year period (1950 - 1956)

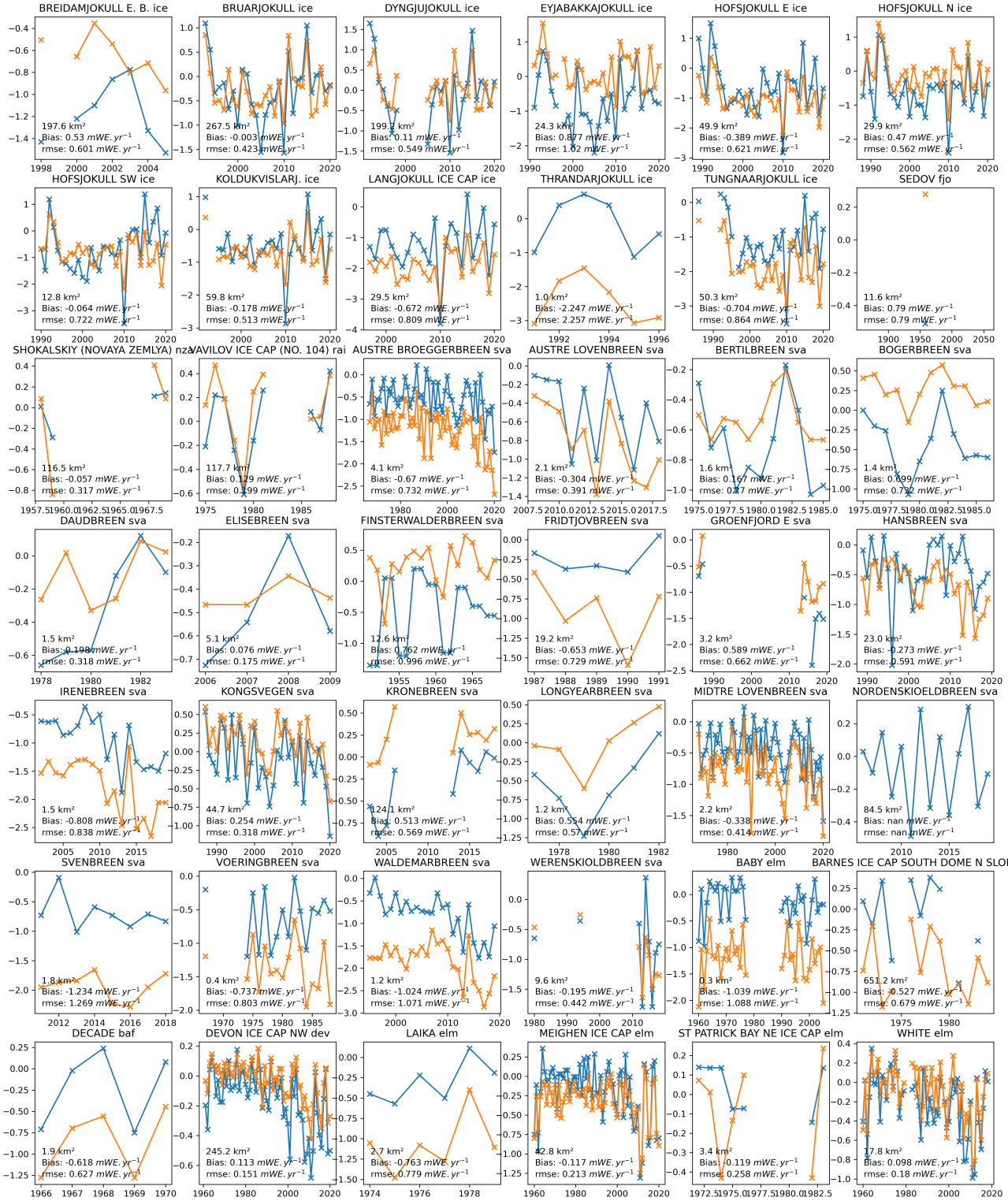

Figure A.2: Modelled and observed annual specific mass balance evolution for every relevant glacier of the WGMS dataset.The name of the glacier and its sub region is indicated in the title of each subplot.

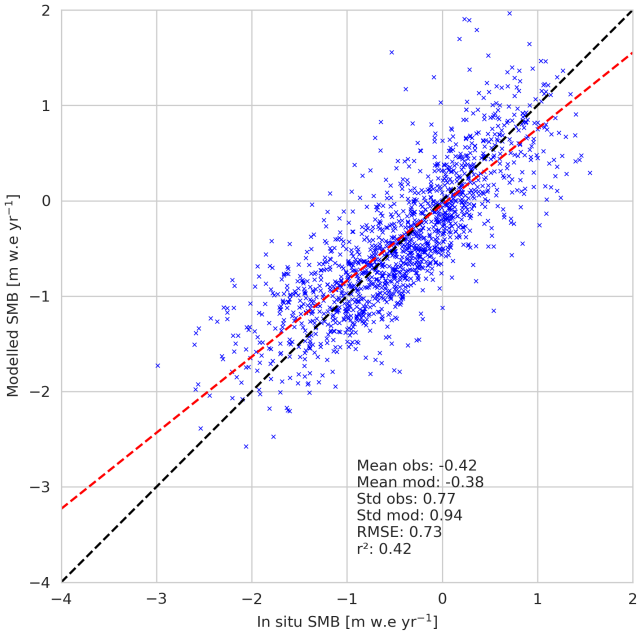

Figure A.3: Modeled versus observed SMB annual values using stake data from Noël et al. (2020). The modeled SMB was downscaled using a local SMB altitude gradient with the methodology described in Franco et al. (2012). The observed stake-averaged interannual-variability is 0.34 $mWEyr^{-1}$,the modeled one is 0.25 $mWEyr^{-1}$, and the average SMB correlation on a given stake is 0.69.

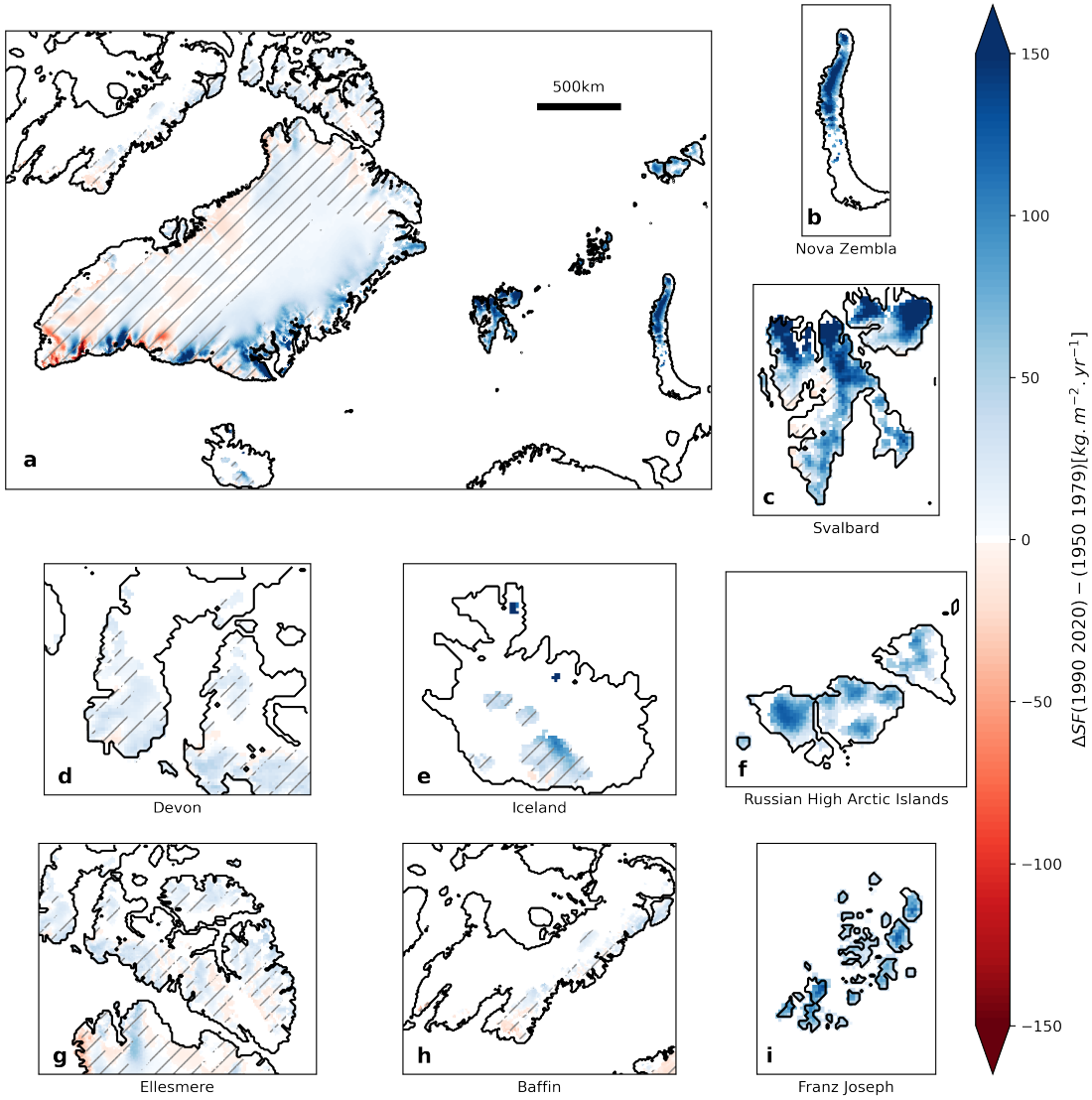

Figure A.4: Annual SF anomalies between the (1990-2020) and (1950-1979) periods over (a) the whole Arctic, (b) Nova Zembla, (c) Svalbard, (d) Devon, (e) Iceland, (f) Russian High Arctic Islands, (g) Ellesmere, (h) Baffin and (i) Franz Joseph land. Hashed areas denote where the anomaly has a low significance value regarding its variance (using Student's t-test with 90% p-value

B Additional elements for Chapter 4

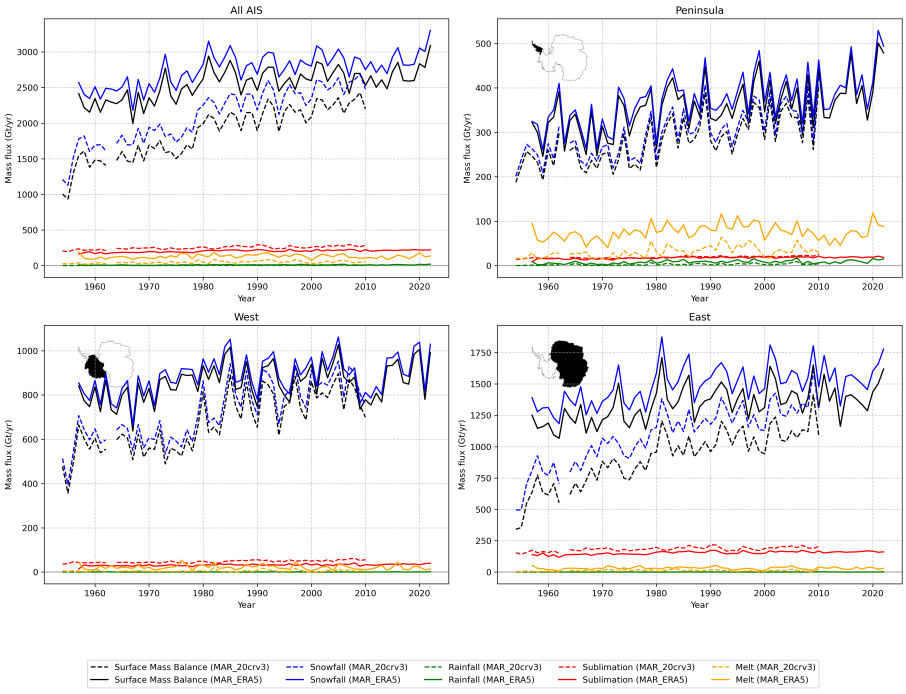

Figure B.1: Annual SMB components evolution for MAR_ERA5 and MAR_20CRv3, over All AIS (a), Peninsula (b), West Antarctica (c) and East Antarctica (d)

Trends ($Gt.yr^{-2}$)	East AIS	West AIS	Peninsula	All AIS
1958-1975	12.85	3.57	0.05	16.98
1975-1985	26.59	8.16	**7.4**	**44.58**
1985-2016	-0.03	-1.4	0.35	-0.91

Table S1: Linear trends in total annual SMB in both periods and around the break-point for all regions delimited in Fig.4.1. In bold are highlighted the significant values (p-value $<$ 0.05) under Wald t-test with a null trends assumption.

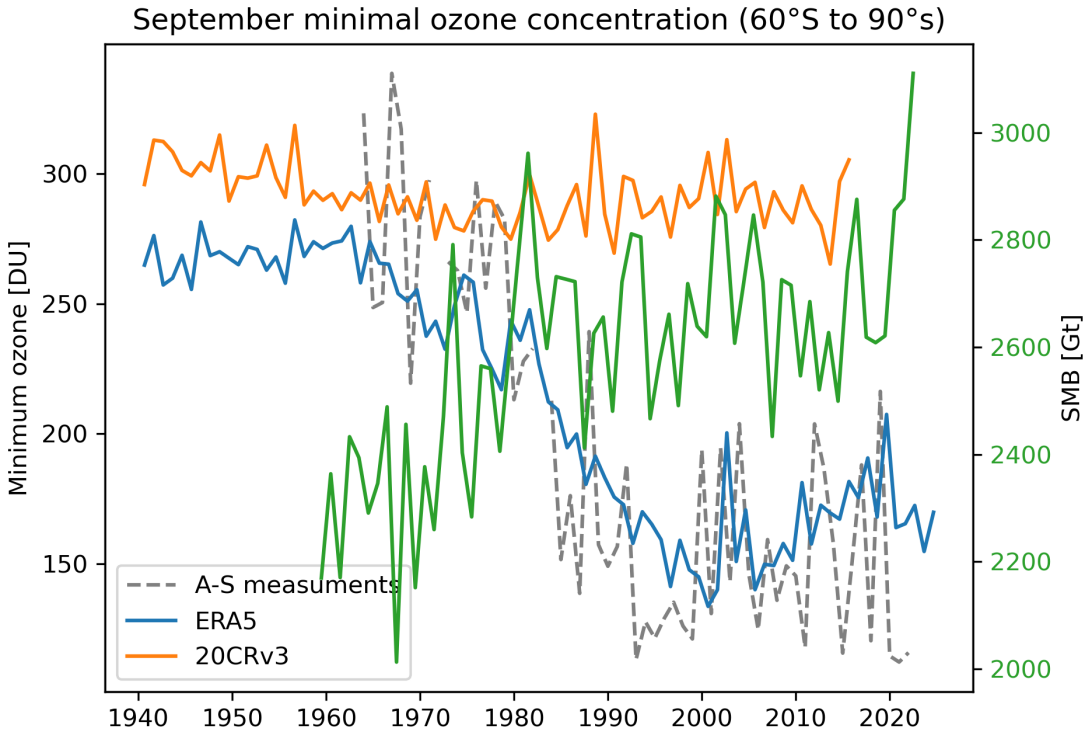

Figure B.2: September minimal ozone concentration in the air column below 60°S in ERA5 (blue) and 20CRv3 (orange) against measurments at Amunsden-Scott base (grey - dashed). Against is plotted the annual AIS SMB from MAR_ERA5 (green - right axis).

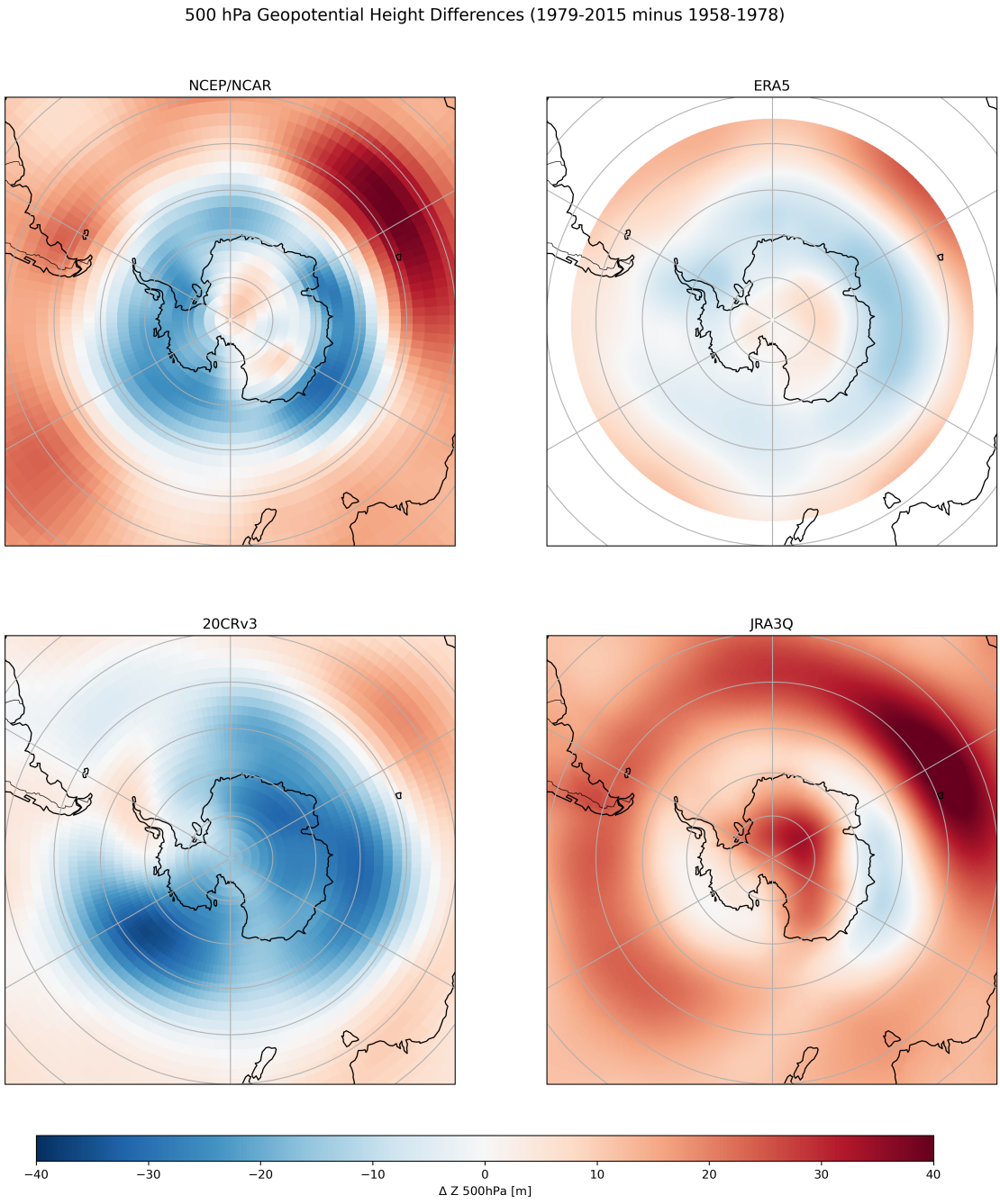

Figure B.3: 500hPa geopotential height difference between 1980-2015 and 1958-1979, in NCEP (top left), ERA5 (top right), 20CRv3 (bottom left) and JRA3q (bottom right).

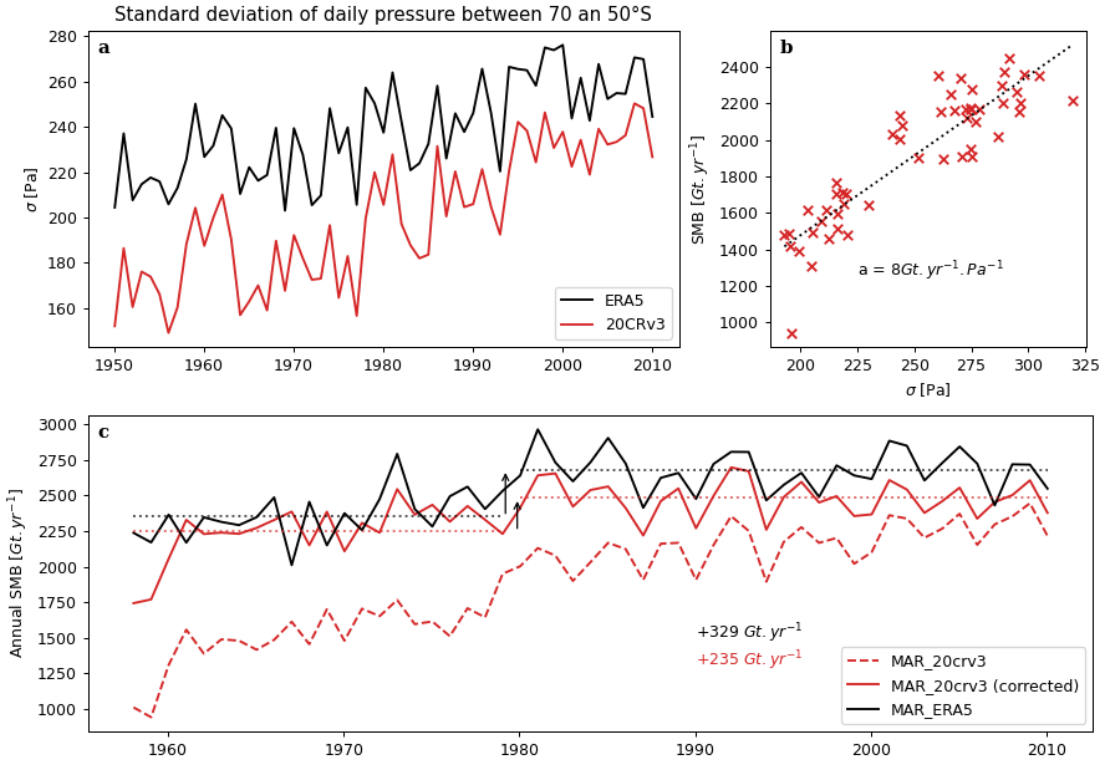

Figure B.4: Daily standard deviation of surface pressure evolution spatially averaged between 50 and 70°S for ERA5 (blue) and 20CRv3 (orange).

Hindcast	Period	Variable	Bias	RMSE	CRMSE	r	n
ERA5	1980-2023	SP	7.48	9.38	3.33	0.86	8474
ERA5	1958-1979	SP	6.88	9.03	3.42	0.86	5373
ERA5	1980-2023	T2m	0.17	2.14	1.19	0.84	8690
ERA5	1958-1979	T2m	0.42	2.48	1.52	0.70	5374
20crv3	1980-2023	SP	5.28	8.79	3.01	0.86	8299
20crv3	1958-1979	SP	5.30	8.39	3.07	0.86	5373
20crv3	1980-2023	T2m	1.01	4.79	1.82	0.72	8515
20crv3	1958-1979	T2m	0.74	4.58	2.04	0.58	5374
NCEP	1980-2023	SP	4.26	7.52	2.61	0.86	8474
NCEP	1958-1979	SP	2.47	8.27	3.87	0.68	5373
NCEP	1980-2023	T2m	-31.40	31.91	5.53	0.01	8690
NCEP	1958-1979	T2m	-31.49	32.02	5.64	0.01	5374
JRA3q	1980-2023	SP	87.55	89.81	5.83	0.56	8474
JRA3q	1958-1979	SP	83.78	88.42	7.30	0.40	5373
JRA3q	1980-2023	T2m	0.33	8.31	3.08	0.80	8690
JRA3q	1958-1979	T2m	0.72	9.14	3.38	0.79	5374

Table S2: Surface temperature and pressure evaluation of 4 different hindcast products for the two periods considered (before and after the satellite introduction). n stands for the number of observation points used.

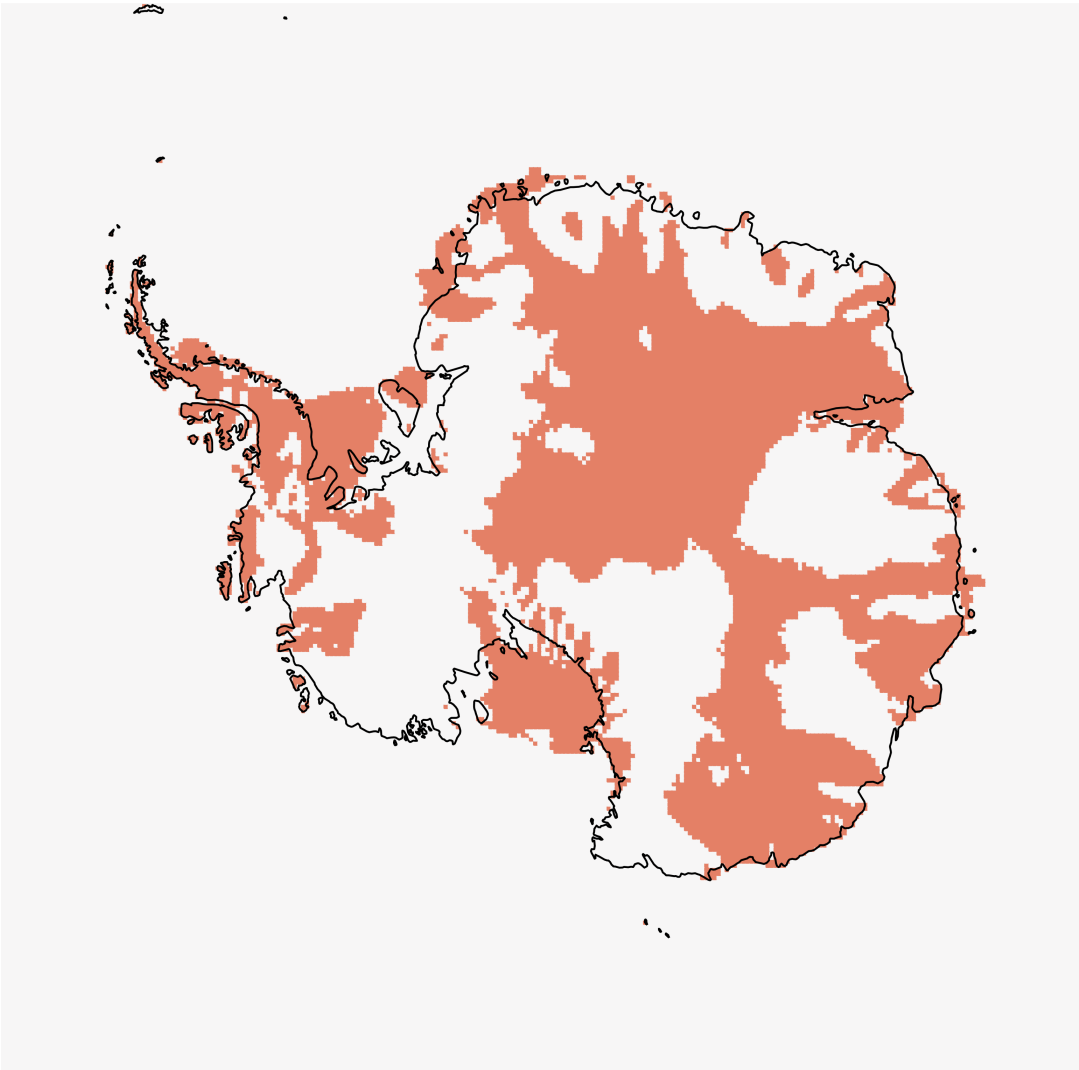

Figure B.5: 1-year lag Granger-causality between october minimal ozone concentration measurements at Amundsen-Scott and annual SMB. The area in red is where the test p-value is lower than 0.05.

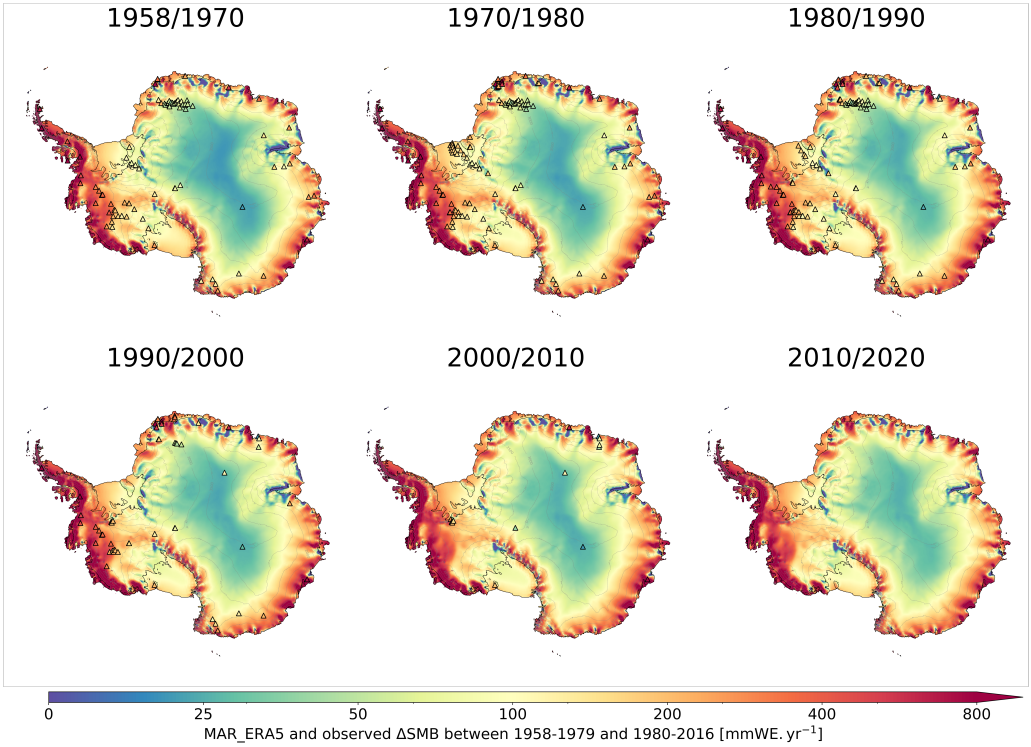

Figure B.6: Averaged annual SMB field against available ice-core measurements for all decades between 1958 and 2020.

C Additional elements for Chapter 5

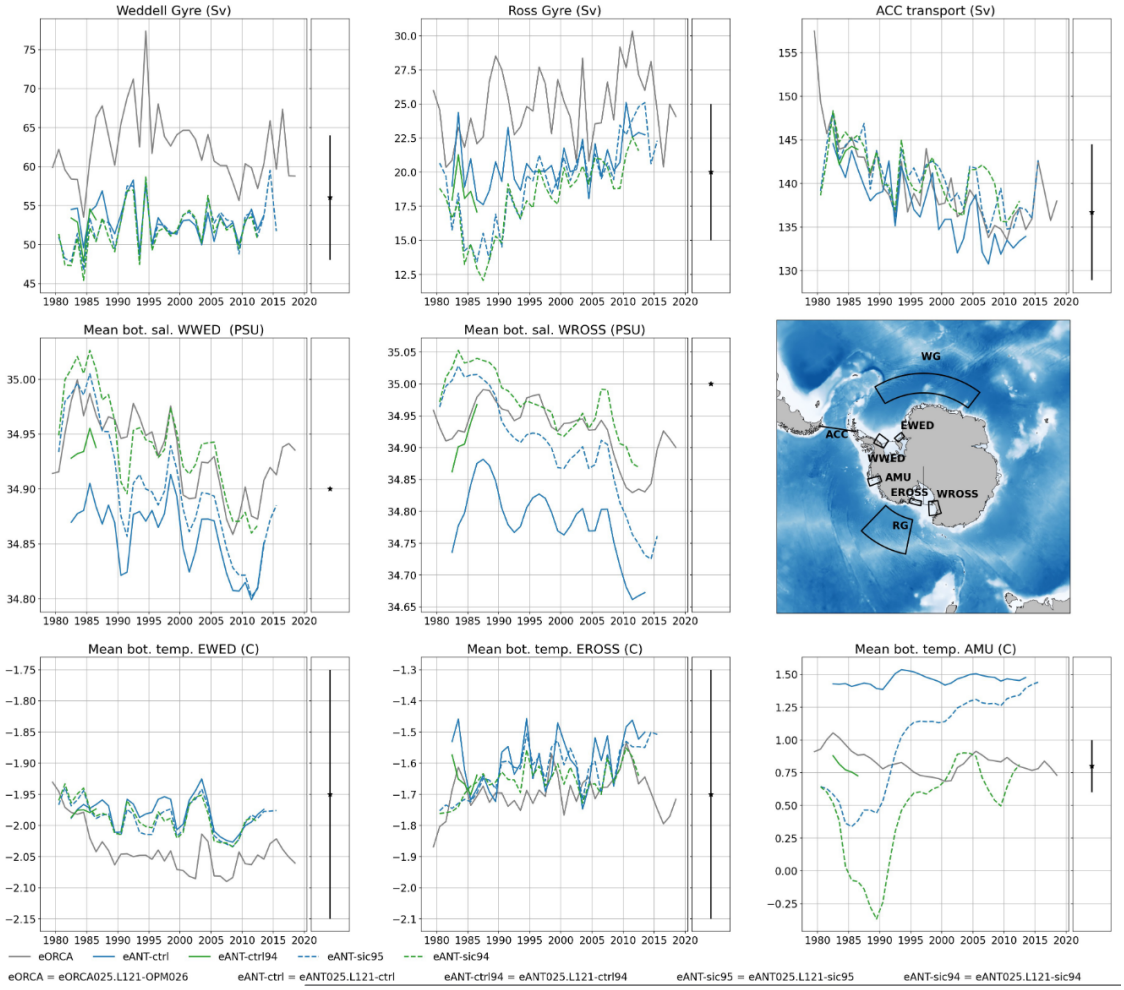

Figure C.1: Validation of the regional NEMO domain used in the coupling (blue,solid) against reference eORCA simulation (grey), using VALSO workflow from P.Mathiot.

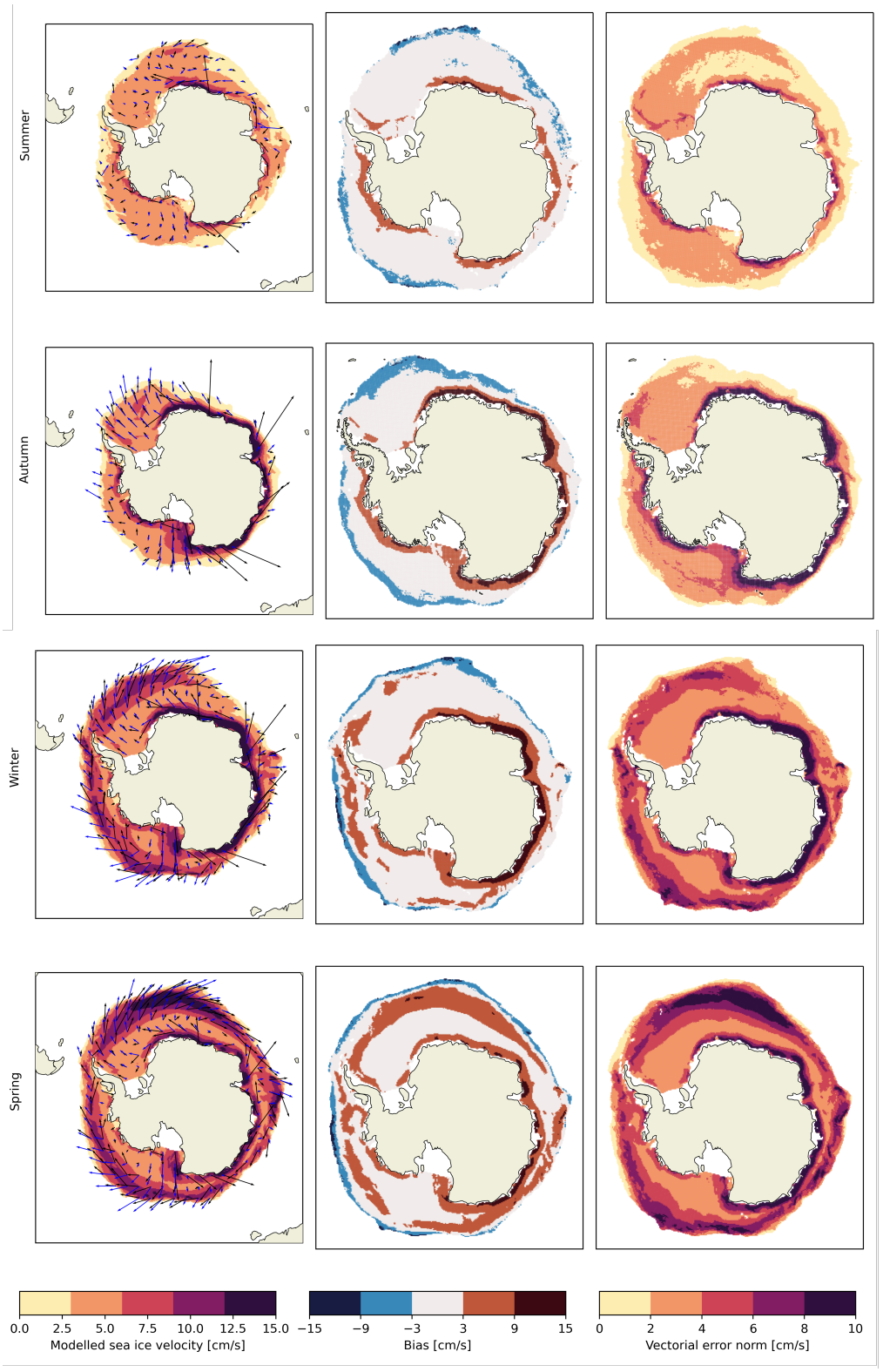

Figure C.2: Modeled average sea-ice velocity (left), bias (middle) and vectorial error (right) compared to NSIDC observations for all 4 seasons. Black arrows show NEMO velocity and blue arrow show observations. The vectorial error is computed as $\|\vec{V_{obs}} - \vec{V_{mod}}\|$

D On MAR and its definite article / Sur (le) MAR et son article défini

Depuis l'invention du language, l'attribution des noms aux objets et aux concepts n'est bien souvent que le fruit de l'usage répété par un groupe d'individus d'une même locution ou écriture. Ainsi, une langue évolue autant qu'évolue le peuple qui la parle. Dans ce contexte, il n'est pas rare de voir émerger des débats d'usage lors de l'irruption dans une langue de nouveaux mots ou expressions; l'usage majoritaire qui fait la règle n'étant pas, au commencement, bien identifiable. Pour remédier à certaines de ces confusions, et afin d'homogénéiser les différents usages au sein d'une même langue, il est coutume que soit instauré des "rêgles", d'ortographe, de syntaxe, de conjugaison ou de prononciation. Cela passe parfois par un système d'éducation, qui les définit pour ses élèves et ce faisant, implicitement pour le reste de la population; ou, comme l'Académie française pour le français, par une instituion officielle chargée d'édicter des règles pour tous [1].

Sans cette homogénéisation et sans une règle garante de l'unité, une langue risque alors de s'éparpiller aux différents patois locaux, et à terme favoriser l'éloignement de peuples qui, à l'origine, se comprenaient.

C'est dans ce contexte que vit le débat portant sur la pronontiation et/ou l'écriture d'un article défini devant "MAR", sigle de "Modèle Atmosphérique Régional", outil bien connu des géographes - de belgique et d'ailleurs. Doit-on dire et/ou écrire "le MAR" ou "MAR" lors de son évocation dans une phrase? Est-ce que "utiliser le MAR rend fou" ou bien est-ce que "faire fonctionner _ MAR n'est pas une mince affaire" ? Aussi, la communauté scientifique de ses utilisateurs n'étant pas uniquement francophone (bien qu'elle soit majoritaire), ce débat à t-il également sa place dans la langue de Shakespeare?

Au demeurant, il est facile d'identifier certains acteurs "militants" (conscients ou non) dans ce débat. et d'autres hésitants, perdus dans l'"usage correct" qu'ils devraient faire de cet acronyme. On peut prendre pour héraut légitime de la vision "non-articléenne" C. Kittel, qui ne ménage pas ses oeuvres pour faire comprendre au monde sa vision; tandis que X. Fettweis se pose lui, en défenseur naturel - bien que moins cavalier - de la pensée qu'on appellera "articlo-définie", "du MAR" donc. On ne saurait lire dans ce texte la vision de son auteur qui, bien qu'ayant un avis propre, s'efforce de ne pas le faire jouer ici.

Dans un premier temps, il convient de rappeler la règle grammaticale qui prévaut lors de l'usage d'acronymes quels qu'il soient en français. Il s'agit bien ici d'acronymes tels

[1] Cette dernière servant surtout à garantir la légitimité et la domination culturelle des classes bourgeoises sachantes face à la plèble incapable par exemple d'apprendre parfaitement la règle de l'accord du participe passé avec le COD si celui-ci est placé devant l'auxilliaire. C'est une histoire de distinction dont l'auteur se gardera bien d'exprimer son entier avis.

que “l’OTAN”,”l’ONU”, à différencier des sigles qui se prononcent eux lettre par lettres, tels que “FNRS” ou ‘EDF”. La règle est donc, quasi systématiquement, d’appliquer un article défini devant les sigles et acronymes - accordés avec le premier mot de ce dernier. Ainsi, on dira “la SNCB est ponctuelle”, “le FNRS m’accorde toutes mes bourses” ou “L’ULG à des beaux bâtiments”. Dans ce contexte, il est évident que pour le cas qui nous intéresse, il n’y a à première vue pas lieu de faire une exeption. On devrait alors dire tout normalement que “le MAR produit des résultats époustouflants”. Une exeption est a noter toutefois, lorsque les sigles sont employés dans un contexte abbrégé, télégraphié tels que des légendes de graphiques, ceux-ci peuvent perdrent naturellement leurs articles.

On pourrait alors se demander ce qu’il en est lors de la lexicalisation - complète ou partielle - du sigle; c’est à dire lorsque celui-ci passe d’une abbréviation (de Modèle Atmosphérique Régional) à un mot courant, qui sert à le définir (ainsi, on ne lit plus jamais “Action de Recherche Petite Echelle Grande Echelle”, mais bien toujours ARPEGE, comme le nom réel du modèle). C’est évidemment un mécanisme à l’oeuvre pour (le) MAR. Cela ne change alors strictement rien. L’article défini prévaut toujours, et est-même plus important encore, puisque le mot est a présent réellement défini comme un nom à part entière. Hors de question de dire “SNCF est à l’heure”.

Ces dernières considérations tendent alors à remettre en question l’école Kittellienne de l’emploi de l’article défini. Or, le contexte scientifique d’emploi du mot “MAR” impose qu’il soit bien souvent inséré dans une phrase écrite dans la langue de Shakespeare. Il nous faut donc maintenant aborder la règle qui y prévaut. La règle, lorsqu’il s’agit de l’emploi d’un sigle ou d’un acronyme en anglais, reste la même qu’en Français. Ainsi, on devrait écrire “the MAR” dans toutes les phrases, lorsque l’on utilise l’acronyme pour simplifier l’écriture (en lieu et place de “the Modèle Atmosphérique Régional” qui - avouons le - est tout de même très moche à l’emploi, bien que correct). Par exemple, nos collègues américains du NOAA (RIP) pourraient suposément écrire “After Trump election, the FBI came into our offices to look for hidden woke artifacts”.

Ce n’est pas tout à fait la fin de l’histoire ni la victoire des Fettweissiens. En effet, lors de la lexicalisation d’un sigle en anglais, la règle qui prévaut change complètement (contrairement à ce que nous avons vu précédemment en Français). Lorsqu’un acronyme ou sigle n’est plus employé comme raccourci pratique, mais bien comme un nom à part entière, plus question d’article. On dira bien “MAR was thoroughly commented and documented” ou “Magic numbers inside MAR are a real delight”. Il est a noter cependant que l’anglais n’est pas une langue rigide (et ne possède pas d’institution telle que l’Académie Française - cf *). Ainsi, cette règle, et celle de l’usage d’un article pour un acronyme, reste fluide et possible selon certains usages.

En conclusion, il semble que après toutes ces expertises grammaticales sorte deux réponses concrètes: L’emploi "articlo-définie" en français par l’école Fettweissienne pour

“le MAR” découle d’une appréciation stricte et rigoureuse de la façon dont doivent être traités les acronymes en français. C’est une vision traditionnelle plus en lien avec les réelles contraintes de la langue. L’approche Kittellienne de la suppression de l’article, sûrement plus moderne, est une forme d’anglicisme de la règle qui prévaut lors des lexicalisations en anglais. Elle a alors le mérite d’être fluide et similaire dans les deux langues d’usage pour des scientifiques Wallons ou Français. Il conviendrait, pour explorer plus en détail ces deux emplois, de se pencher sur l’appréciation de la “beauté” de l’une ou l’autre des deux écoles. Un angle sociologique qui permettrait d’appréhender la façon dont sont perçu l’emploi ou non de cet article défini, “MAR ou le MAR”, au regard des différents environnements culturels, sociaux et des habitus de chaque individu.